The Rift Valley Fever Virus Replicative Cycle

by

Mary Elise Piper

A dissertation submitted in partial fulfillment
of the requirements for the degree of
Doctor of Philosophy
(Cellular and Molecular Biology)
in The University of Michigan
2010

Doctoral Committee:

Assistant Professor Sonja R. Gerrard, Chair
Professor Michael J. Imperiale
Professor Janet L. Smith
Professor Michele S. Swanson
Associate Professor David Miller

Table of Contents

List of Figures

List of Tables

Abstract

The Rift Valley fever virus (RVFV) is responsible for numerous, explosive epizootics throughout Africa and the Arabian Peninsula. The virus causes disease predominantly in humans and livestock, with sheep and cattle being particularly susceptible. In humans, the disease generally manifests as a flu-like illness; however, in a small percentage of cases, severe symptoms develop, such as encephalitis and hemorrhagic fever disease. In these severe cases, mortality rates are high. Livestock often succumb to the viral infection, and case-fatality rates are particularly high among young animals. Outbreaks are devastating to the public health and regional economies, and the development of antiviral therapies is difficult due to the limited understanding of the RVFV replicative cycle.

We have developed a system for the generation of Rift Valley fever virus-like particles (RVF-VLPs). The RVF-VLPs are antigenically and morphologically indistinguishable from virulent RVFV virus, but can only perform a single round of infection. Using the virus-like particle system for RVFV, in combination with biochemical and crystallization techniques, we have elucidated the roles of the viral proteins in multiple steps of the viral replicative cycle. Specifically, we describe crucial interactions necessary for replication and transcription, elucidate the structure of the nucleocapsid protein, identify the envelope glycoprotein, Gn, as necessary and sufficient

for the recruitment and packaging of the RdRp and encapsidated genome into virus particles, determine that the encapsidated genome triggers the efficient release of virus, and ascertain the limitations governing RVFV reassortment with other phleboviruses. Based on our results, we suggest targets for the development of therapeutics directed against RVFV and other phleboviruses.

Chapter 1

Introduction

Negative-sense RNA viruses

RNA viruses are ubiquitous in nature and have developed parasitic relationships with most organisms, from bacteria to plants to humans. The co-evolution of RNA viruses with their hosts requires the viruses to constantly evolve in response to changes in host defense or to better thrive in a particular environment. The negative-sense, segmented RNA viruses are particularly adept at rapidly responding to selective pressures, utilizing processes of antigenic drift and antigenic shift.

Negative-sense RNA viruses encompass an array of human pathogens, including influenza A, Ebola, rabies, Andes, and Rift Valley fever viruses. These viruses may contain either an unsegmented or segmented RNA genome. The unsegmented RNA viruses belong to the order *Mononegavirales*, and include the rabies (*Rhabdoviridae*), measles (*Paramyxoviridae*), Ebola (*Filoviridae*), and borna disease (*Bornaviridae*) viruses (Fig. 1.1). Virus families outside the *Mononegavirales* order have varying numbers of genomic segments, and include the influenza A (*Orthomyxoviridae*), Rift Valley fever (*Bunyaviridae*), and Andes (*Arenaviridae*) viruses, which have eight, three, and two genomic segments, respectively (Fig. 1.1). The viruses of the *Bunyaviridae* and *Arenaviridae* families contain genomic segments of negative-sense and ambisense polarity (Fig. 1.2). In contrast to positive-sense RNA viruses, which contain genomes that are essentially mRNA and can be translated upon infection of host cells, negative-

sense RNA virus genomes must be transcribed by a viral polymerase prior to translation (Fig. 1.2). The ambisense genomic segments encode viral genes encoded in the negative-sense RNA, as well as in the RNA complementary (cRNA) to the negative-sense genome (Fig. 1.2). The cRNA is generated as an intermediate during replication.

The segmented, negative-sense RNA viruses have a unique capability for rapidly responding to selective pressures through a process known as antigenic shift, or reassortment. When two related viruses co-infect the same cell, progeny can be produced that have packaged genomic segments from both parental viruses, forming a novel virus. The progeny virus may be more pathogenic or have a greater fitness in a particular environment (Fig. 1.3). Segmented RNA viruses can rapidly evolve to new environments or hosts through reassortment, and the reassortment of viruses belonging to the *Orthomyxoviridae* and *Bunyaviridae* families has been previously documented. The virus strain responsible for the global outbreak of the influenza A virus (*Orthomyxoviridae*) H1N1 in 2009 originated from multiple reassortment events between human, avian, and swine influenza A virus strains (1, 2). As a result of the reassortment events, the influenza A virus could replicate in a range of hosts.

Reassortment of viruses within the *Bunyaviridae* family has been observed among different strains of the same virus (3-9), as well as between different viruses within the same genus (5, 10-18). In the *Orthobunyavirus* genus (*Bunyaviridae* family), Ngari virus is known to cause hemorrhagic fever disease and was isolated from regions throughout Kenya and Somalia (10, 19). Upon sequencing of the viral genome, it was found to contain two segments from the Bunyamwera virus, and one segment from the Batai virus (11, 17, 19). The Bunyamwera virus typically causes a febrile disease, while the Batai

virus had not been previously documented as causing human disease (11). The reassorted progeny virus was found to cause hemorrhagic fever disease in humans, exhibiting a similar, yet more severe pathogenesis compared to the documented cases of the Bunyamwera virus (10).

Natural and experimental evidence suggests that different viruses in the genera *Orthobunyavirus* and *Hantavirus* of the *Bunyaviridae* family can reassort (5, 10-16, 18). Within the *Bunyaviridae* family, there is little information on the interactions between the viral proteins necessary for replication/transcription, assembly, and cellular release. A better understanding of the viral replicative cycle for bunyaviruses would aid in predicting which bunyaviruses may be capable of reassorting. The public health threat posed by the reassortment of highly pathogenic viruses in the *Bunyaviridae* family is significant, and could extend the geographical range, host or vector species susceptibility, and/or pathogenesis of the viruses. Discovery of the viral interactions restricting bunyavirus reassortment is critical for the public health preparation of future global epidemics.

Rift Valley fever virus

The Rift Valley fever virus (RVFV) is one of the more pathogenic viruses within the *Bunyaviridae* family (*Phlebovirus* genus) (20), capable of causing enormous epizootics throughout Africa, with human symptoms ranging from fever and malaise to encephalitis and hemorrhagic fever. The severe pathogenesis associated with RVFV, the wide range of mosquito vectors capable of transmitting the virus (21-28), the ability of viruses of other genera of the *Bunyaviridae* family to reassort, and the presence of other highly-related viruses in nearby regions increase the importance of understanding the

mechanisms of RVFV replication and transcription, assembly, and cellular release for the identification of RVFV therapeutic targets, as well as for determining the potential for viral reassortment. There are no FDA-approved therapeutics or prophylactics available, and little is known about the replication cycle of RVFV.

Epidemiology

RVFV is an aerosol- and mosquito-borne virus endemic to sub-Saharan Africa. RVFV causes disease in both livestock and humans, with sheep and cattle being particularly susceptible (29). In livestock, the virus can cause high rates of mortality, especially among young animals, and near 100% abortion rates (30). In humans, the disease generally manifests as a flu-like illness with fever and fatigue, but in a small number of cases the disease progresses to more severe manifestations, such as retinitis, hepatitis, encephalitis, and hemorrhagic fever disease (29, 31, 32). Mortality rates are nearly 50% among hemorrhagic fever cases (31). Due to the explosive nature of the RVFV epizootics, the high number of infected individuals can result in hundreds of fatalities. In the 1978-79 RVFV outbreak in Egypt, between 20,000 - 200,000 people were predicted to have been infected, generating more than 600 fatalities (30).

Emergence and dissemination of RVFV throughout Africa and Arabian Penninsula

RVFV was first isolated in 1930 from the Great Rift Valley in Kenya from infected lambs. Since its identification, serological sampling has demonstrated the presence of RVFV throughout most of Africa, including Madagascar (4). Phylogenetic analysis of the various RVFV strains throughout Africa suggests that the progenitor strain of RVFV arrived in the late 1800s, around the same time as African colonization and the arrival of European domesticated animals (4). European animals appear more susceptible

to RVFV infection than the African species of livestock, and their arrival may have increased the magnitude of the epizootics (4). Phylogenetic analyses also suggest that individual RVFV strains have traveled great distances, likely through the transport of the mosquito vector or infected host species (4).

In 1977, the first outbreak of RVFV in Egypt resulted in extensive human and animal infection, and it is believed to have been caused by the border-crossing of infected animals from Kenya (33). The emergence of RVFV epizootics in West Africa and the Arabian Peninsula was also associated with human activities. In 1987, the first RVFV outbreak in West Africa was associated with dam construction, which produced favorable breeding grounds for mosquitos (34). In 2000, RVFV spread outside the African continent to the Arabian Peninsula, apparently due to trade of infected cattle from eastern Africa (4). The restriction of the virus to the African continent appears to be mainly due to its geographical/physical isolation from the rest of the world.

Transmission

The mosquito is the vector for RVFV, and epizootics occur during times of heavy rainfall. Normally dry inland depressions known as damboes flood during periods of intense rainfall creating favorable conditions for mosquito breeding. The *Aedes* subspecies of mosquito is the primary vector for the virus, and it can transmit the virus transovarially to its eggs (35). The virus has been found to persist in the periods between epizootics in infected mosquito eggs, possibly representing the viral reservoir (35). During periods of heavy rainfall, the infected young hatch and feed on nearby animals, including domesticated sheep and cattle. Amplification of the virus occurs with the hatching of the *Culex* and other subspecies of mosquito, which feed on the RVFV-

infected animals (30). The *Culex* mosquitos can further aid in transmission of the virus by continued feeding. Human infections occur either through direct transmission from mosquito or through contact with infected tissues or aerosol during the maintenance or slaughter of infected animals (6). Due to its ability to be transmitted through aerosol, RVFV could also be used as an agent for biological warfare or bioterrorism. For example, the US biological warfare program weaponized RVFV prior to termination of the effort in 1969 (36).

Upon transmission, the virus is proposed to travel to the lymphatic system, then enter the bloodstream for dissemination throughout the body (35). In infected animals, the virus affects most internal organs, including liver, spleen, and brain (35, 37, 38), and death is often associated with necrosis of the liver (39). Some studies suggest the liver is the primary target for RVFV; however, the high volume of blood that circulates through the liver may simply deliver more virus to this organ.

The vectors for RVFV transmission are found throughout the world, and the introduction of RVFV into previously unaffected areas has resulted in large epizootics. World trade, global warming, and human activities, such as deforestation and the construction of dams and roads, increase the likelihood that RVFV will spread from Africa and the Arabian Peninsula in the future. RVFV is devastating to the public health and the economy in affected areas, and the capacity to spread to unaffected regions of the world highlights the necessity in understanding the replicative cycle of the virus. Through gaining a better understanding of the viral replication, new prophylactic and therapeutic targets can be identified.

Replicative cycle

The replicative cycle of RVFV initiates with the entry of the virus into host cells. Similar to all bunyaviruses, RVFV is spherical, enveloped, and contains three negative-sense (or ambisense) RNA genomic segments, termed the large (L), medium (M), and small (S) segments (Fig. 1.4) (40). Upon cellular entry, RVFV releases the encapsidated genome into the cytoplasm, where replication and transcription occurs. The 3' and 5' termini contain the untranslated regions (UTRs) of the viral genomic segments, and the terminal complementary nucleic acids are proposed to base-pair and generate a panhandle structure (Fig. 1.4) (41). The transcriptional promoters and terminators for the RNA-dependent RNA polymerase (RdRp) reside within the UTRs, with the exception of the S segment, which is ambisense and terminates transcription in the intergenic region (42).

The S, M, and L segments encode the nucleocapsid protein (N), envelope glycoproteins (Gn/Gc), and the RdRp, respectively (Fig. 1.4) (40). The M and S segments also encode nonstructural proteins, NSm and NSs (40). NSm appears to exhibit anti-apoptotic activity (43), while NSs inhibits the host immune response through interactions with TFIIH and SAP30 and downregulation of PKR expression (44-46). NSs and NSm are not required for viral replication in cell culture (47, 48). After transcription of the viral genes, Gn/Gc is translated as a polyprotein on the endoplasmic reticulum (ER), while the RdRp and N, which do not contain signal peptides, are presumably translated on free ribosomes in the cytoplasm (40). Gn/Gc is cleaved by signal peptidase in the ER into the Gn and Gc glycoproteins, which are glycosylated as they mature through the secretory system (49). Gn localizes to the Golgi apparatus independently, and complex formation between Gn and Gc results in the masking of the Gc ER retention signal and co-translocation of Gc to the Golgi apparatus (50). RdRp and

N localize to the cytoplasm, and must be recruited to the Golgi apparatus for assembly. Since bunyaviruses do not encode a matrix protein, it is hypothesized that the cytoplasmic tails of the envelope glycoproteins are involved in their recruitment. Following assembly, the virus buds into the lumen of the Golgi apparatus, and virus is released from the cell when virus-containing Golgi-derived vesicles fuse with the plasma membrane (40). The stimulus for virus budding into the Golgi is unknown, as are the viral components necessary for virus release.

Through our investigations with RVFV, we have elucidated various steps in the RVFV replicative cycle. We describe critical interactions necessary for replication and transcription, detail the viral protein-protein interactions involved in the recruitment and packaging of the RdRp and encapsidated genome into virus particles, determine the viral components necessary for efficient release of virus, and ascertain the limitations governing RVFV reassortment with other phleboviruses. Based on our results, we suggest targets for the development of therapeutics directed against RVFV and other phleboviruses.

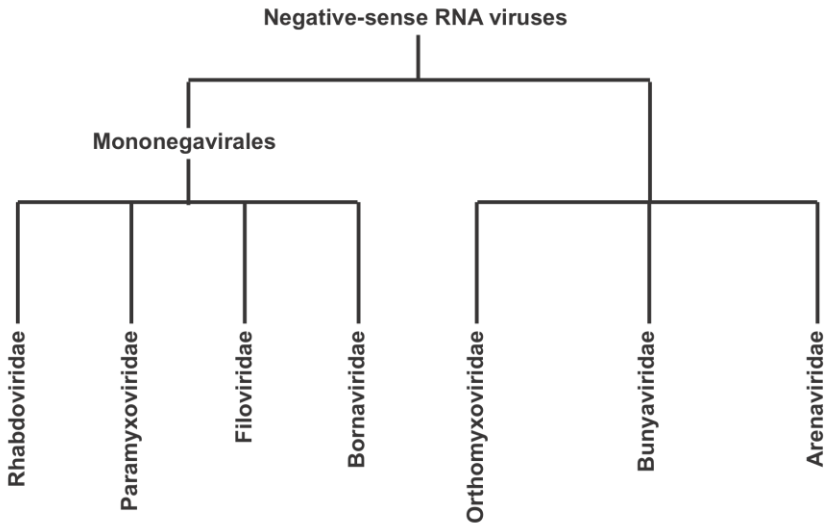

Figure 1.1. Classification of negative-sense RNA viruses.
Negative-sense RNA viruses are comprised of viruses with segmented or unsegmented genomes. Virus families of the Mononegavirales order have unsegmented genomes, while virus families outside of this order contain segmented genomes.

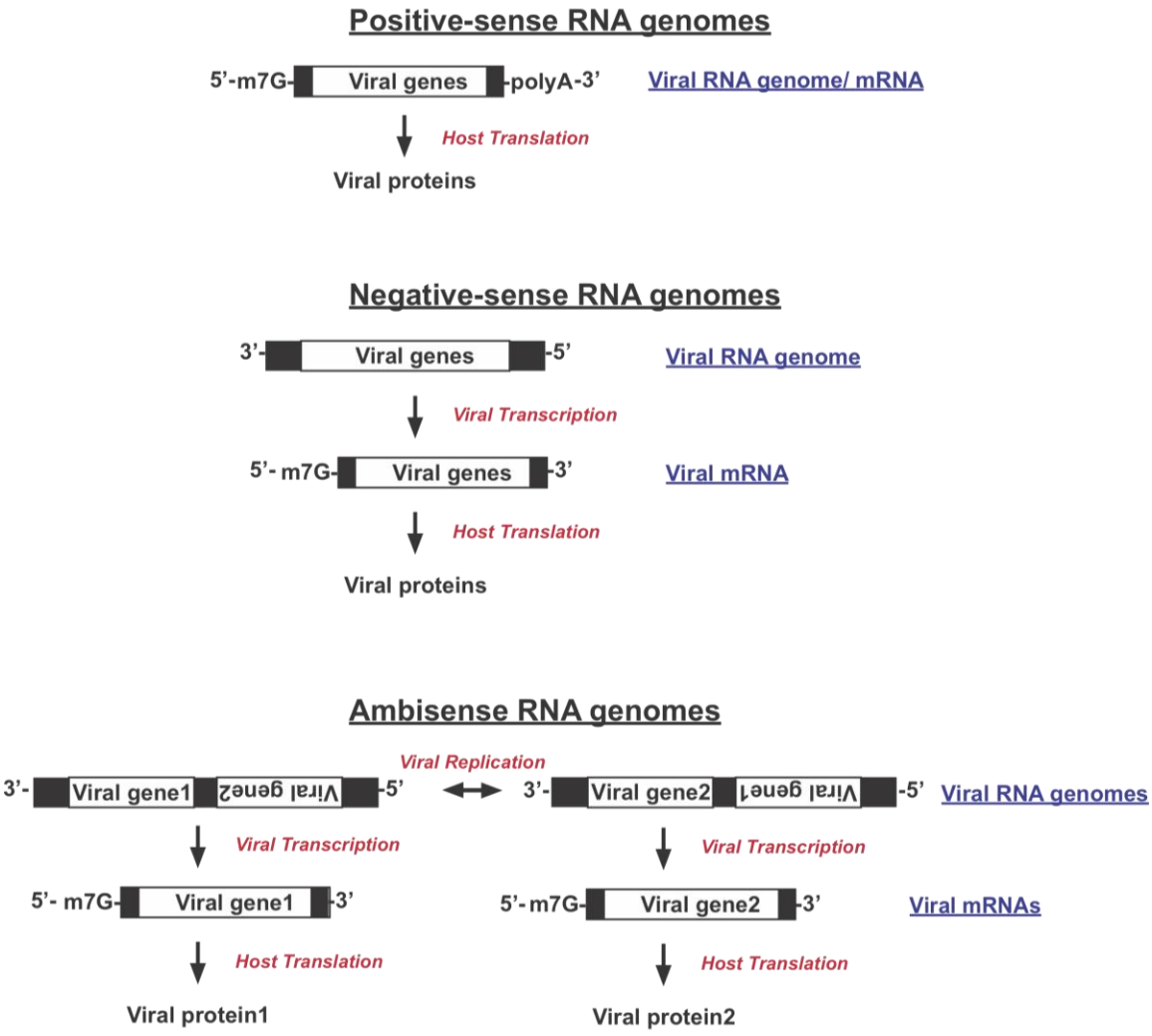

Figure 1.2. Replication and transcription strategies of single-strand RNA viruses.
In contrast to positive-sense RNA genomes, which are essentially mRNA and can be translated directly upon infection of host cells, negative-sense RNA virus genomes must be transcribed by the viral RdRp into mRNA prior to translation. Viruses of the negative-sense RNA virus families, *Bunyaviridae* and *Arenaviridae*, also contain ambisense RNA genomic segments, which encode viral genes in both the viral sense and complementary sense RNA. Therefore, one gene can be transcribed directly from the viral RNA, while the other gene cannot be transcribed until the complementary RNA is generated as an intermediate during viral replication of the genome. The black rectangles represent the untranslated regions (UTRs) of the genomic segments. RNA viruses are diverse, and although the genomes in this figure are depicted as having m7G caps or polyA tails, the features of the genomic segments and mRNA vary by virus family.

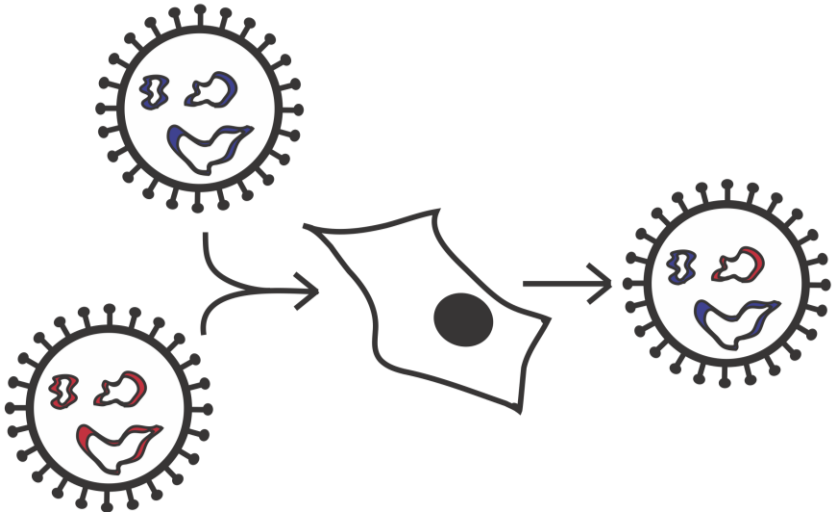

Figure 1.3. Reassortment of segmented negative-sense RNA viruses.
Co-infection of a cell with two segmented RNA viruses can result in the production of particles that contain segments from both parental viruses.

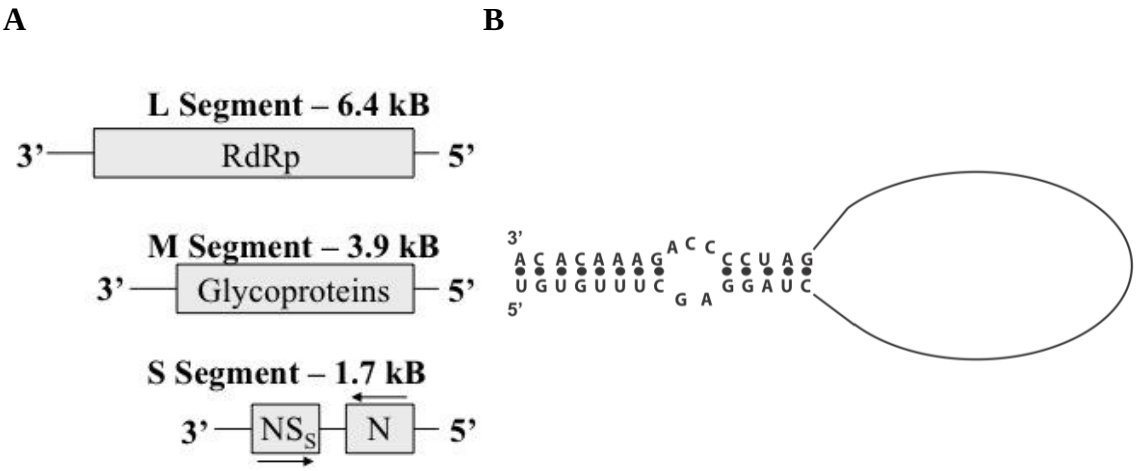

Figure 1.4. Schematic of RVFV genome.
(A) The RVFV genome is divided into the large (L), medium (M), and small (S) segments. The L and M segments are negative-sense and encode the RdRp and envelope glycoproteins, respectively. The S segment is ambisense, encoding the NSs and N. (**B)** The 3' and 5' termini of the RVFV genomic segments are comprised of complementary nucleotides that are predicted to base-pair, forming a panhandle structure. The termini contain the promoters necessary for replication and transcription, as well as packaging of the genomic segments into viral particles. The eight terminal residues are conserved within the *Phlebovirus* genus.

Chapter 2

A Novel System for Identification of Inhibitors of Rift Valley Fever Virus Replication

Introduction

The Rift Valley fever virus (RVFV) is a vector- and aerosol-borne virus endemic to sub-Saharan Africa. RVFV can cause disease in humans and in common livestock species, such as sheep and cattle. Pregnant animals exhibit a high incidence of abortion and young animals frequently succumb to infection (40). People typically develop a flu-like illness; however, more severe manifestations, such as hemorrhagic fever or encephalitis, occur in a small percentage of cases. The hemorrhagic and encephalitic forms of disease exhibit high case-fatality rates (29, 31, 32). Competent vectors of RVFV are found worldwide (21-24, 26-28, 51), and release of the virus into a new region would be damaging for both the economy and public health. In 2000, the first documented outbreak of the virus outside of the African continent occurred on the Arabian Peninsula, and the virus was determined to be of East African origin (52, 53). The presence of the virus outside of Africa demonstrates the ability of the virus to spread to previously unaffected regions of the world. Thus, geographic isolation appears to be mainly responsible for the containment of the virus to African regions. No licensed vaccines or therapeutic treatments are available; our RVF-VLP system will aid in the screening of small molecule inhibitors for the development of novel therapeutics.

RVFV is an enveloped virus belonging to the *Phlebovirus* genus of the *Bunyaviridae* family. RVFV contains a negative-sense RNA genome that is divided into three segments, termed the small (S), medium (M), and large (L) segments. The S segment encodes the nucleocapsid protein (N), which encapsidates the viral RNA genome, and a nonstructural protein, NSs, which is involved in inhibition of the host

innate-immune response (40). The M segment encodes the envelope glycoproteins, Gn and Gc, and a nonstructural protein, termed NSm, while the L segment encodes an RNA-dependent RNA polymerase (RdRp). The nonstructural proteins, NSs and NSm, are not required for viral replication in cell culture (47, 48, 54). Transcription and replication of the viral genome is initiated through the recognition of promoter sequences in the 5' and 3' terminal untranslated regions (UTRs) of each genomic segment (55, 56). These processes occur in the cytoplasm and require both RdRp and N (40, 57). The RdRp and N are translated in the cytoplasm, while the envelope glycoproteins enter the secretory system. Gn and Gc form a complex and localize in steady-state to the Golgi apparatus due to a signal found on Gn (49, 50, 58). The assembled virus buds into the lumen of the Golgi apparatus, and virions are released from the cell when elements of the Golgi fuse with the plasma membrane.

We have developed a T7 RNA polymerase (T7 RNAP)-dependent system for the production of infectious RVFV-like particles (RVF-VLPs) that obviates the need for high-level biosafety containment and allows for generation of viral particles that are antigenically indistinguishable from authentic RVFV. RVF-VLPs can deliver a minigenome to target cells, and expression of RdRp and N in target cells is not necessary for generation of significant reporter activity. Minigenome activity is inhibited by the same chemical compounds that inhibit authentic RVFV replication. RVF-VLPs are efficiently produced in our system, which should facilitate future studies aimed at examination of virus assembly and screening for small molecule inhibitors of viral entry and replication.

Results

System for Production of RVF-VLPs from Cloned cDNAs

We utilized a set of plasmids similar to that described for rescue of the virulent ZH-501 strain of RVFV as the basis of our RVF-VLP system (Table 2.1) (54). To assess production of RVF-VLPs, a minigenome based on the S segment was generated such that the NSs open reading frame was replaced with a gene encoding a reporter molecule, such as GFP or renilla luciferase (RLuc) (Fig. 2.1). Additionally, the vector backbone of all transcription plasmids was changed to one with transcriptional silencers flanking the

cloning site (see Methods section). The new vector dramatically reduced the background expression of the reporter gene (data not shown). An additional transcription plasmid was constructed that lacked 237 nucleotides of the N gene in order to investigate the contribution of N and minigenome independently in the generation and infectivity of RVF-VLPs (Fig. 2.1). Immunofluorescence microscopy (Fig. 2.2) and immunoblot (data not shown) using a polyclonal antibody recognizing full-length N failed to detect N expression. These S segment-based plasmids will henceforth be referred to as minigenome plasmids.

A schematic detailing our method for RVF-VLP production and analysis is shown in Fig. 2.3. The minigenome along with expression plasmids for N, RdRp, and Gn/Gc are transfected into BSR-T7/5 cells (Fig. 2.3). The BSR-T7/5 cells constitutively express T7 RNAP, which drives production of the primary minigenome transcript. Expression of the reporter from the minigenome in transfected cells requires co-expression of RdRp and N. Co-expression of Gn/Gc results in the production of RVF-VLPs containing the minigenome (Fig. 2.3). The RVF-VLPs are released from the cells into the media and are then used to infect target cells (Fig. 2.3). Replication of the minigenome and expression of RLuc or GFP in RVF-VLP-infected target cells relies on packaging of the encapsidated minigenome and RdRp. The RVF-VLPs do not contain the L or M genomic segments. Additionally, the S segment-based minigenome lacks the NSs gene and, in some experiments, the N gene. Therefore, RdRp, Gn/Gc, and, in some cases, N cannot be synthesized in infected target cells, and thus further production of RVF-VLPs is prevented.

Production of Infectious RVF-VLPs.

We investigated the ability of the recombinant structural proteins, N, RdRp and Gn/Gc, to replicate and transcribe the minigenome in transfected BSR-T7/5 cells. Replication of the minigenome requires expression of N and RdRp, but not Gn/Gc (57). Cells transfected with minigenome and pN, but not pRdRp and pGn/Gc, were unable to transcribe the minigenome reporter (Fig. 2.4, EV/EV), and the RLuc activity in these samples was considered background. The addition of pRdRp resulted in RLuc activity at levels greater than 1,500-fold background levels (Fig. 2.4, RdRp/EV). Though Gn/Gc is not required for replication of the minigenome, Gn/Gc expression further increased the

production of RLuc in transfected cells to levels greater than 40,000-fold background (Fig. 2.4, RdRp/Gn/Gc). The increase in RLuc expression could be due to an effect of Gn/Gc on RdRp activity or due to RVF-VLP-infection of other cells in the monolayer.

RVF-VLPs released into the media from the transfected cells (Fig. 2.4) were used to infect various target cells, and RLuc expression in the RVF-VLP-infected target cells was measured. Cells receiving media from cells transfected with minigenome, pN, and pRdRp (RdRp/EV) did not generate RLuc expression greater than background for any timepoint or cell type investigated (Fig. 2.5). By contrast, target cells receiving media from cells transfected with minigenome, pN, pRdRp, and pGn/Gc (RdRp,Gn/Gc) produced RLuc activity substantially above background for all timepoints and cell types (Fig. 2.5). Therefore, infectious RVF-VLP production is dependent on expression of Gn/Gc.

The production of RVF-VLPs peaked at 48 h post-transfection; however, considerable amounts of RVF-VLPs were released at 72 h post-transfection (Fig. 2.5). RLuc activity in RVF-VLP-infected target cells did not require expression in *trans* of the T7 RNAP or RdRp and N. RVF-VLP-infection of Vero E6 cells, which do not express the T7 RNAP or any viral proteins, produced RLuc levels that were over 200-fold background (Fig. 2.5). However, the addition of support plasmids did increase RLuc activity in BSR-T7/5 and Vero E6 cells. For instance, at the 48 h timepoint, expression of RdRp and N in BSR-T7/5 cells increased RLuc activity greater than 15-fold, and expression of RdRp in Vero E6 cells increased RLuc activity 1.8-fold (Fig. 2.5).

RVF-VLPs are Efficiently Produced

Using the green fluorescent protein (GFP) version of the minigenome, we investigated whether the increase in RLuc activity in transfected cells due to expression of Gn/Gc (Fig. 2.4) was caused by RVF-VLP infection of cells in the transfected cell monolayer. BSR-T7/5 cells transfected with the GFP minigenome, pN, and either empty vector (EV/EV), pRdRp and empty vector (RdRp/EV) or pRdRp and pGn/Gc (RdRp/Gn/Gc) were visualized by fluorescence microscopy (Fig. 2.6A). As expected, no GFP signal was detected in cells that lacked RdRp and Gn/Gc (Fig. 2.6A, EV/EV). However, in cells that expressed RdRp (RdRp/EV) or RdRp and Gn/Gc (RdRp/Gn/Gc), GFP expression was evident (Fig. 2.6A). Although the signal intensity increased over

time in cells that lacked Gn/Gc, the percentage of cells expressing GFP did not increase (Fig. 2.6A). With addition of the glycoproteins (RdRp/Gn/Gc), the intensity of GFP fluorescence as well as the percentage of cells expressing GFP increased over time (Fig. 2.6A). Therefore, it appears that the increase in RLuc activity observed in the experiment shown in Figure 2.4 is mainly due to spread of RVF-VLPs in the transfected cell monolayer.

The media harvested from the transfected cells (Fig. 2.6A) at 24, 48, or 72 h post-transfection was placed onto target cells, and GFP expression was visualized by fluorescence microscopy (Fig. 2.6B). Target cells receiving harvested media from cells lacking Gn/Gc did not produce any GFP, while target cells receiving media from cells expressing Gn/Gc did exhibit GFP expression. The number of cells expressing GFP and the intensity of GFP expression was greatest for cells infected with RVF-VLPs (RdRp/Gn/Gc) harvested 48 h post-transfection. However, RVF-VLP production appeared to exhibit high yields at 72 h post-transfection, mimicking the RLuc results shown in Figure 2.5. The majority of the cells in the monolayer appeared to express GFP after RVF-VLP (RdRp/Gn/Gc) infection, demonstrating that RVF-VLPs were efficiently produced.

RVF-VLPs are Antigenically Indistinguishable from Authentic RVFV

To determine whether RVF-VLPs and virulent RVFV are antigenically indistinguishable, RVF-VLPs were investigated for their ability to be neutralized by RVFV neutralizing antibodies. BSR-T7/5 cells were transfected with minigenome, pN, pRdRp, and pGn/Gc. The media containing RVF-VLPs was harvested and clarified, and then incubated with antibodies recognizing RVFV or not incubated with antibody (Mock). The media was then transferred to BSR-T7/5 target cells, and RLuc activity was measured at 24 h post-infection. The level of RLuc activity in cells infected by RVF-VLPs receiving the Mock treatment represents 100% infectivity (Fig. 2.7). Incubation of the RVF-VLPs with neutralizing polyclonal antibodies to RVFV nearly completely neutralized the RVF-VLPs and resulted in minigenome activity levels that were only 1% of the Mock treatment (Fig. 2.7). Incubation with neutralizing monoclonal antibodies recognizing the envelope glycoproteins (59), which are exposed on the surface of the RVF-VLPs, neutralized the RVF-VLPs dramatically, allowing only 6% activity (Fig.

2.7). By contrast, monoclonal antibodies recognizing N, which is not exposed on the surface of the RVF-VLPs, did not significantly reduce infectivity of the RVF-VLPs (Fig. 2.7). These antibodies were evaluated on the same strain of RVFV (ZH-501) that was used to generate our VLP system (data not shown), and the same trends were observed. Our results suggest that the RVF-VLPs are antigenically similar to virulent RVFV.

RVF-VLPs are Efficiently Harvested by High-Speed Centrifugation

To assay cellular release of particles and to determine the protein content of RVF-VLPs, we devised a method for harvesting the RVF-VLPs in order to assay cellular release of particles and to determine the protein content of RVF-VLPs. BSR-T7/5 cells were transfected with minigenome, pN, pRdRp, and either pGn/Gc or empty vector. At 48 h post-transfection, the media from transfected cells was harvested, clarified, and RVF-VLPs were pelleted by ultracentrifugation. The concentrated RVF-VLPs in the pellet were either resuspended in the supernatant (Fig. 2.8; Pellet + Supernatant) or the supernatant was decanted (Figure 2.8; Supernatant), and the pellet was resuspended in equivalent amount of fresh media (Fig. 2.8; Pellet). These samples were used to infect BSR-T7/5 cells that expressed RdRp and N. At 24 h post-infection, the cells were harvested, and RLuc activity was measured. RLuc activity in BSR-T7/5 cells that were infected with the passage containing both the supernatant and pellet fractions represents 100% infectivity. Nearly 80% of the infectivity was present in the pellet, while only 3% of the infectivity was in the supernatant. Presumably, the decrease in RLuc activity between the “Pellet and Supernatant” and “Pellet” samples is due to RVF-VLP loss when the media was decanted.

RVF-VLPs Behave Similar to Authentic RVFV with Respect to Small Molecule Inhibitors

To determine the feasablity of the RVF-VLPs to function in place of virulent RVFV for the screening of RVFV small molecule inhibitors, we tested a panel of small molecule inhibitors for activity against RVF-VLPs and RVFV. Two of these compounds, ribavirin (60-63) and actinomycin D (64), had previously been tested for activity against RVFV and thus serve as positive controls. Ribavirin is a broad spectrum antiviral that is believed to inhibit viral replication directly acting on the RdRp or indirectly through inhibition of a cellular enzyme necessary for biosynthesis of guanine nucleotides or

through the accumulation of mutations and induction of error catastrophe (65-67). Actinomycin D was investigated due to its ability to inhibit cellular DNA-dependent RNA polymerases but not viral RNA-dependent RNA polymerases (68). Guanidine and mycophenolic acid were tested because they have been shown to have activity against other RNA viruses. Guanidine is active against the RdRp of poliovirus and many other positive-sense RNA viruses (69) and has been also been shown to inhibit the RdRp of a dsRNA virus (70). Mycophenolic acid acts on the same cellular enzyme as ribavirin (66, 71). And finally, monensin and ammonium chloride block the acidification of endocytic organelles (72). The acidic organelles are required for membrane fusion for many viruses that enter host cells through receptor-mediated endocytosis.

The inhibitors were added to the cultures at the time of infection with either RVF-VLPs or RVFV. Infected cells were harvested at 22 h post-infection and minigenome activity or expression of N was assayed, respectively. As expected, ribavirin was found to be a potent inhibitor of RVF-VLPs (Table 2.2) and RVFV (Fig. 2.9). Mycophenolic acid was also a strong inhibitor (Table 2.2, Fig. 2.9), suggesting that inhibition of guanine nucleotide biosynthesis is sufficient for inhibition of viral replication. The endocytic inhibitors, ammonium chloride and monensin, inhibited both RVF-VLPs (Table 2.2) and RVFV (Fig. 2.9), suggesting that the virus enters cells through receptor-mediated endocytosis. Guanidine did not strongly inhibit either RVF-VLPs (Table 2.2) or RVFV (Fig. 2.9). Actinomycin D blocked activity of RVF-VLPs (Table 2.2) but did not inhibit RVFV (Fig. 2.9). Recently, Ikegami *et al.* discovered the combination of RVFV (MP12 strain) replication and host transcriptional repression, either by actinomycin D or RVFV NSs, was sufficient to induce the activation of protein kinase R (PKR) (46). PKR inhibits translation of host and viral proteins, but can be targeted for degradation by RVFV NSs (46, 64). The RVF-VLPs do not express NSs, so the induction of PKR by actinomycin D cannot be down-regulated.

Discussion

In this paper we report on the development of a T7-dependent system for production of RVF-VLPs and its application for the high-throughput screening for antivirals against RVFV. We generated RVF-VLPs through the expression of a minigenome and four viral structural proteins; Gn, Gc, N and RdRp. Although these

particles lack the full complement of genomic segments, they behave in a similar fashion to authentic RVFV in the four respects tested in this study. (1) RVF-VLPs are able to package a minigenome based on the S segment and deliver it to naive target cells. (2) RVF-VLPs are secreted from the cell and can be concentrated from the media by centrifugation. (3) RVF-VLPs are inhibited from infection of a naive monolayer by antibody neutralization using the same set of antibodies that neutralize RVFV. (4) Chemical inhibitors of RVFV replication also inhibit RVF-VLPs indicating that the minigenome activity is an appropriate surrogate for viral replication.

Plasmid-based genetic and RVF-VLP systems are powerful tools for studying the replicative cycle of viruses. We have modified the design of the T7 RNAP-driven plasmid-based rescue system for the virulent ZH-501 RVFV strain (54) to produce RVF-VLPs capable of performing only a single round of infection. In our design, expression plasmids encoding the open-reading frames of the structural proteins were expressed along with a minigenome. The expression plasmids do not contain the 5' and 3' UTRs that have been demonstrated to be required for packaging of the genome (55, 56). Thus, the RNAs produced from these plasmids cannot be packaged and these RVF-VLPs are capable of only a single round of replication. Using our system, we efficiently generated infectious RVF-VLPs.

Detection of minigenome activity in target cells was robust and did not require expression of any RVFV proteins or T7 RNAP. Therefore, RVF-VLPs can be used to deliver minigenome to cells that are not efficiently transfected, such as mosquito cells. Minigenome activity in RVF-VLP-infected target cells was reduced to near background levels by ribavirin, mycophenolic acid, ammonium chloride and monesin, all of which were also shown to be active against RVFV. Mycophenolic acid, ammonium chloride and monensin had not been tested previously for activity against RVFV. The results obtained with ammonium chloride and monensin suggest that RVFV enters cells through receptor-mediated endocytosis. Our results are the first to examine endocytic entry by RVFV in the context of authentic RVFV infection. However, previous studies exploring the ability of the RVF envelope glycoproteins to form syncitia using either baculovirus or alphavirus-driven expression systems have previously found syncitia formation to be pH dependent (73, 74). Interestingly, we saw a differential effect with actinomycin D, in that

this compound inhibits RVF-VLPs but not RVFV. Recently it has been shown that NSs from either MP12 (vaccine) or ZH-548 (virulent) strains is capable of degrading PKR (46, 64). Thus, it is likely that the differential effect we see with actinomycin D is because RVF-VLPs do not express NSs. However we cannot rule out the possibility that the differential effect of actinomycin D is the result of an inherent difference between how infected cells respond to RVFV versus RVF-VLPs.

Taken together our results strongly suggest that RVF-VLPs can serve as effective screening tools for identification of antivirals with activity against RVFV. The RVF-VLPs obviate the need for operating under select agent guidelines and biosafety level 3 conditions for agricultural hazards (BSL-3Ag), which would be necessary if using virulent RVFV. Our replicon assay produced activity levels 1,500-fold over background, while our signal-to-noise values for the minigenome delivered by RVF-VLPs were found to be as high as 7,800. Therefore, we have highly sensitive assays for both replication/transcription and RVF-VLP infectivity. Additionally, the RVF-VLPs express RLuc; thus, they provide a method of determining inhibition in a format that can be scaled to high-throughput levels. Furthermore, while the vaccine strain of RVFV (MP12) is cytopathic and can be used for high-throughput screening under BSL2 conditions, RVF-VLPs have the advantage of allowing for screening for small molecules that inhibit discrete viral processes and the ability to identify molecules that increase replication. For instance, RVF-VLPs can be used to screen specifically for effects on replication or entry into cells, thus making it easier to identify the target of inhibitory or enhancing molecules identified in a screen. Additionally, our RVF-VLPs are based on a virulent strain of RVFV, thus eliminating the potential of attenuating mutations influencing the activity of compounds.

We are using the RVF-VLP system to study various steps in the RVFV replicative cycle, including entry, replication, assembly, and budding. The RVF-VLP system can be used to identify the viral proteins and genome elements necessary for the production of infectious RVF-VLPs, as well as to elucidate the role of individual protein domains. Since expression of N or RdRp in target cells is not required for detection of RVF-VLP infection, we can identify protein-protein and protein-RNA interactions that are essential to virus assembly through analyzing mutagenesis of all the viral structural proteins.

Identification of critical protein domains will allow us to not only screen, but also design, small molecule inhibitors targeting these important regions for the development of specific therapeutics.

Materials and Methods

Plasmids

The construction of pTrRVFV-SΔNSs::GFP, pSTrRVFV-ΔNSmM, pN-Amp, and pGn/Gc have been described elsewhere (50, 54). pSTrRVFV-SΔNSs::hRLuc was derived from pTrRVFV-SΔNSs::GFP in several steps. First, the GFP gene was released by digestion with EcoRV, followed by ligation with a humanized renilla luciferase gene (RLuc) that was flanked by EcoRV sites. The resulting plasmid was then subcloned into pSMART HC Kan (Lucigen). pSTrRVFV-SΔNΔNSs::hRLuc was derived from pSTrRVFV-SΔNSs::hRLuc by removing the 237 nucleotide SmaI fragment. pRdRp-Amp (pSRG309) is derived from the L segment plasmid, pTrRVFV-L (50). In brief, the RdRp ORF was amplified from pTrRVFV-L with primers that contained SalI (5') and NotI (3') sites. The resulting PCR product was then cloned into the SalI/NotI site of pIRES (Clontech) and the IRES was subsequently removed by digest of the plasmid with XhoI and SalI. The expression plasmids pN and pRdRp were constructed by cloning the open reading frames for N and RdRp into pVAX1 (Invitrogen) using HindIII/EcoRI and BamHI/NotI sites, respectively.

Cells and Virus

Vero E6 and BSR-T7/5 cells were generous gifts from Dr. C. Fulhorst (University of Texas Medical Branch, Galveston) and Dr. K. Conzelmann (Max-von Pettenkofer-Institut, Munchen, Germany), respectively. BSR-T7/5 cells were subsequently cloned by limiting dilution and the resulting clonal lines were tested using the RVFV minigenome that expresses RLuc. Lines that produced high levels of RLuc from the minigenome were expanded. The C3 clone of the BSR T7/5 line was used for all experiments. The BSR-T7/5 and Vero E6 cells were grown in Dulbecco's Modified Eagle Medium (Invitrogen) supplemented with 10% FCS and sodium pyruvate. The T7 RNAP transgene in the BSR-T7/5 cells was selected for using 1 mg/mL Geneticin (Invitrogen). The Vero E6 cells that

stably express the RVFV RdRp (Vero E6-RdRp) were generated by transfection of Vero E6 cells with pSRG309 and pcDNA-Hygromycin (Invitrogen), then selection of hygromycin resistant cells with 200 μg/mL hygromycin (Invitrogen). The ZH548-MP12 vaccine strain of RVFV used for all experiments involving infectious virus and was obtained from Dr. R. Tesh (World Reference Center of Emerging Viruses and Arboviruses).

Antibodies

Hybridomas that secrete neutralizing monoclonal antibodies that recognize Gn and Gc (R1-4B6-1-2, R1-4D4-1-1 and R5-3G2-1A) and monoclonal antibodies recognizing N (R1-P6-F6-6-2-2, R1-P6-F6-10-1-1, R1-P5-A6-12-2-2, RV-V-1B9-1-1, R3-1D8-1-2 and RV5-V6E4-1-1) were a generous gift of Dr. G. Ludwig (USAMRIID). Polyclonal antibodies that were generated against RVFV in mice were a generous gift of Dr. P. Rollin (CDC). Full-length N was expressed with an N-terminal histidine tag and purified under denaturing conditions on a Ni-NTA agarose column (Qiagen Inc.). The N antibody was generated in rabbits using purified protein as antigen (Harlan Laboratories). The secondary antibody used in immunofluorescence experiments was Alexa Fluor 488 goat anti-rabbit (Molecular Probes).

Virus-Like Particle Production

BSR-T7/5 cells were plated at 1 x 10^5 cells/well in 12-well culture plates. After 24 h, cells were transfected using 2 μL/μg TransIT LT1 (Mirus Corporation) and plasmids in the ratio 0.25 μg minigenome: 0.50 μg pN: 0.75 μg pRdRp: 0.50 μg pGn/Gc. Media on transfected cells was replaced every 24 h. Media containing RVF-VLPs was typically harvested at 48 or 72 h post-transfection, clarified by low speed centrifugation (300 rcf for 10 min at 4˚C) and then diluted prior to being used to infect target cells. For some experiments target cells were transfected with pRdRp and pN 24 h prior to infection. Target cells were harvested at 24 h post-infection, and were analyzed by either fluorescence microscopy or RLuc assay (Promega). For some experiments, RVF-VLPs were concentrated. In those cases, clarified media was centrifuged at 82,700 rcf for 4 h at 4˚C. The supernatant was removed and the pellet was resuspended in complete media.

RVFV Inhibitor Screen

Concentrated stocks of inhibitors were prepared either in water and filter sterilized (ribavirin, ammonium chloride, guanidine) or 100% ethanol (monensin, mycophenolic acid, actinomycin D). The inhibitors were obtained from Sigma-Aldrich (monensin, actinomycin D, guanidine), Calbiochem (mycophenolic acid), VWR (ammonium chloride) and RPI Corporation (ribavirin). RVF-VLPs and the ZH548-MP12 vaccine strain of RVFV (at an MOI of 1) were diluted 1:1 with 2X concentration of inhibitors in complete media. After 22 hours incubation, the inhibitors were removed and cells were analyzed for RLuc expression (RVF-VLPs) or immunofluorescence microscopy (RVFV-infected).

Immunofluorescence Microscopy

Cells were plated on glass coverslips and were fixed using freshly prepared 4% paraformaldehyde (Sigma-Aldrich) for 30 minutes. The paraformaldehyde was removed and cells were washed with PBS containing 1% BSA (PBS/BSA). The cells were permeabilized with PBS/BSA containing 0.1% Triton-X100 (Shelton Scientific, Inc.) for 30 minutes, then washed with PBS/BSA before adding the primary antibody. The primary antibody in all experiments was rabbit anti-N. The cells were washed again, and the secondary antibody goat anti-rabbit A488 (Molecular Probes) was added and incubated in the dark for 1 h. Finally, the cells were washed thoroughly and mounted onto glass slides using Prolong Antifade Gold with DAPI (Molecular Probes). The fluorescence was visualized using an Olympus BX-51 microscope in the University of Michigan Microscopy and Image Analysis Laboratory.

Table 2.1. Plasmids used in this study.

Plasmid name	Description	Ref
pTrRVFV-SΔNSs::GFP	S segment-based minigenome plasmid. The NSs gene has been replaced with GFP. Primary transcription is mediated by T7 RNAP. Vector backbone derived from pSP64 (Promega).	(54)
pRdRp	RdRp ORF cloned into pVAX1 (Invitrogen). Contains T7 RNAP and CMV promoters.	This study
pRdRp-Amp (pSRG309)	RdRp ORF cloned into pIRES (Clontech). Contains T7 RNAP and CMV promoters.	This study
pN	N ORF cloned into pVAX1 (Invitrogen). Contains T7 RNAP and CMV promoters.	This study
pSTrRVFV-SΔNSs::hRLuc	S segment-based minigenome plasmid. The NSs gene has been replaced with hRLuc. Primary transcription is mediated by T7 RNAP. Vector backbone is pSMART HC Kan (Lucigen).	This study
pSTrRVFV-SΔNΔNSs::hRLuc	Derived from pSTrRVFV-SΔNSs::hRLuc, the SmaI fragment within the N gene has been removed.	This study
pGn/Gc	Gn/Gc polyprotein ORF cloned into pcDNA1.1	(50)

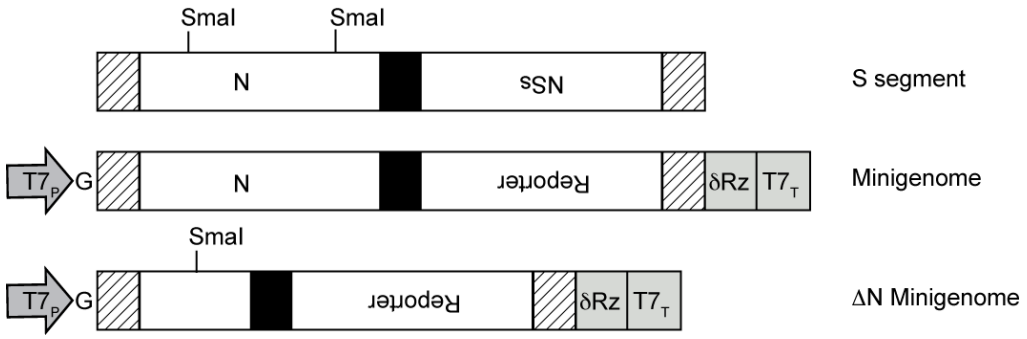

Figure 2.1. Schematic of RVFV S segment-based minigenome and procedure for generation and analysis of RVF-VLPs.

The minigenome plasmids are derived from the S-segment. The minigenome is flanked by a T7 promoter (T7P) and hepatitis delta ribozyme (δRz) and T7 terminator (T7T). T7 RNA polymerase (RNAP) initiates transcription at the final G residue in the promoter and terminates at the T7T site. Following transcription, the δRz excises itself to generate an authentic viral 3' terminus. The 5' and 3' UTRs are indicated by hashed marks and the intergenic region is indicated in black. The S segment is ambisense, and the genes illustrated upside-down indicate that they are encoded in the complementary RNA. Therefore, following T7 RNAP transcription, the Reporter gene can be transcribed through the co-expression of pRdRp and pN.

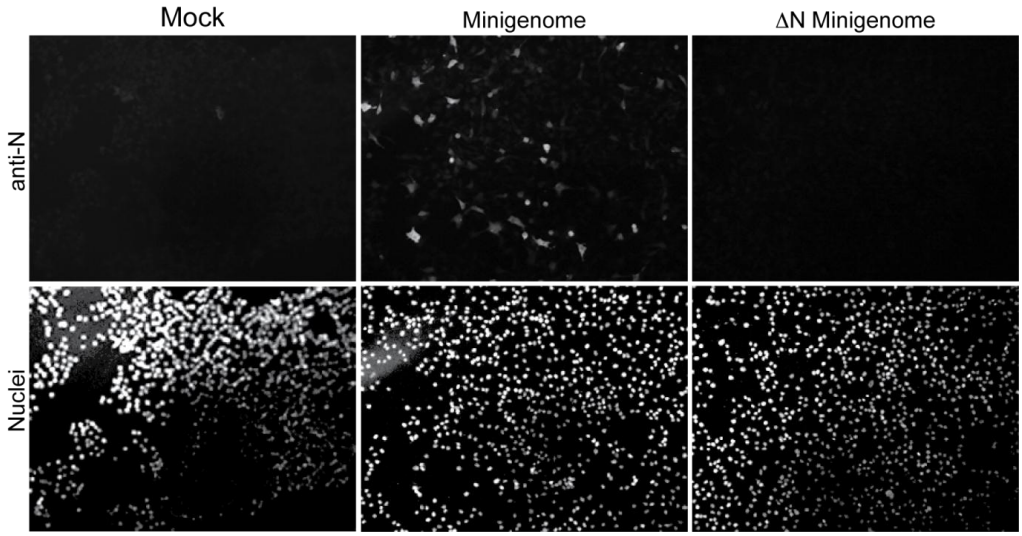

Figure 2.2. Internal deletion in N ORF prevents expression from ΔN minigenome.
BSR-T7/5 cells were either transfected with empty vector (Mock) or transfected with minigenome or ΔN minigenome. Cells were fixed 24 h post-transfection and incubated with rabbit anti-N polyclonal antibody, followed by Alexa Fluor 488 mouse anti-rabbit secondary antibody. Slides were mounted in Prolong antifade with DAPI.

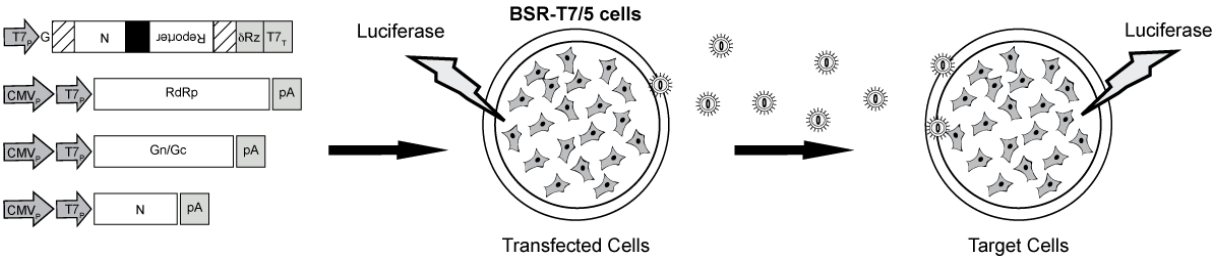

Figure 2.3. Schematic of RVF-VLP production.
Minigenome along with expression plasmids for N, RdRp, and Gn/Gc are transfected into BSR-T7/5 cells. The expression constructs have the open reading frames downstream of T7 (T7P) and CMV promoters (CMVP) and are followed by polyadenylation signals (pA), generating high-level constitutive expression of the genes. The minigenome is first transcribed by T7 RNAP followed by replication and transcription of the RNA by the RdRp and N. Transcription of the reporter gene on the minigenome results in production of the reporter molecule (RLuc or GFP). Expression of Gn and Gc results in packaging of the minigenome into RVF-VLPs that can be harvested and used to infect target cells. In target cells the minigenome is transcribed by the packaged RdRp, resulting in expression of the reporter molecule.

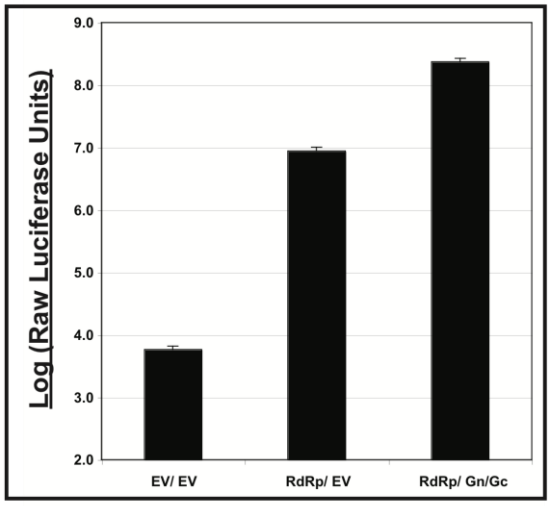

Figure 2.4. Gn/Gc increases RLuc expression in transfected cells.
BSR-T7/5 cells were transfected with the RLuc minigenome, pN and either empty vector (EV/EV), pRdRp and empty vector (RdRp/EV), or pRdRp and pGn/Gc (RdRp/Gn/Gc) and analyzed at the indicated times for expression of RLuc.

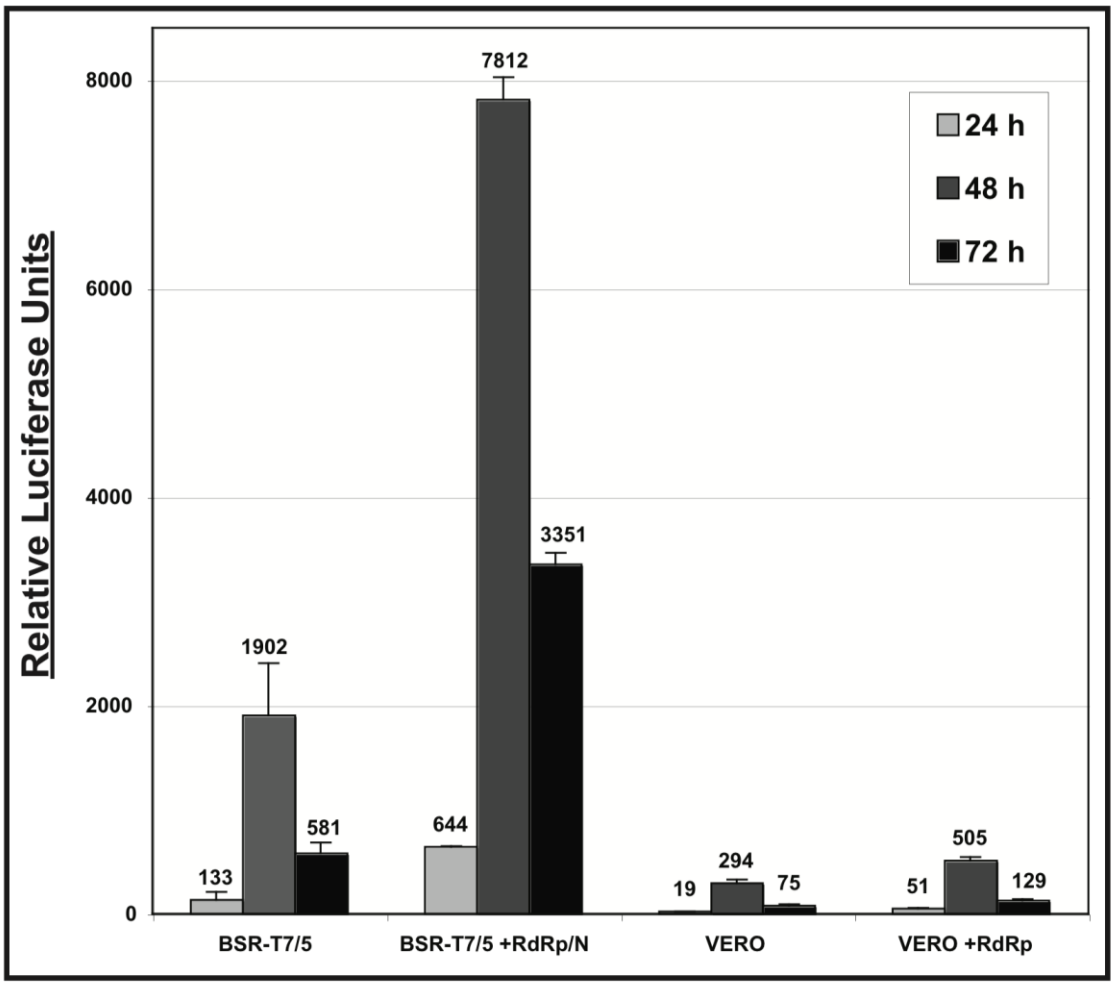

Figure 2.5. RdRp expression in trans enhances RLuc expression in target cells.
Media from cell monolayers shown in Figure 2.1 was harvested at the indicated times and used to infect untransfected BSR-T7/5 cells, BSR-T7/5 cells that expressed RdRp and N, untransfected Vero cells, or Vero cells stably transfected with RdRp. The RLuc values are expressed relative to conditions lacking the envelope glycoproteins.

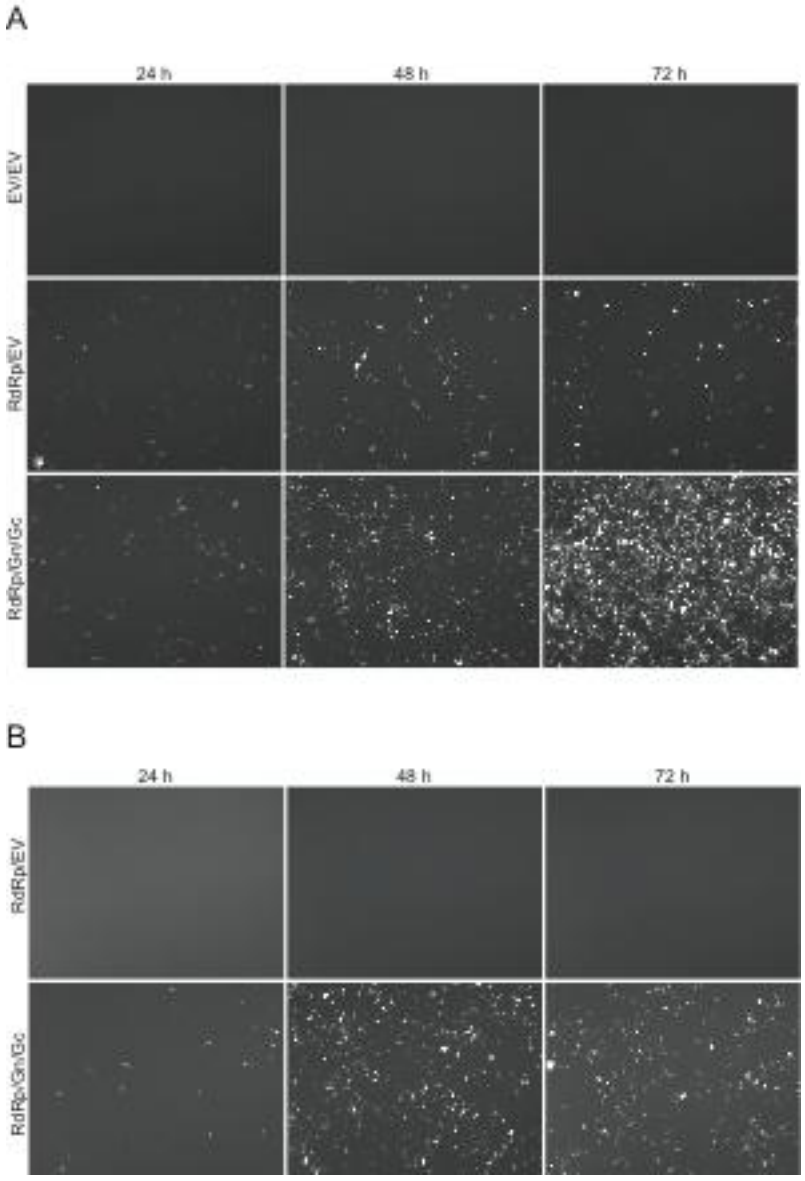

Figure 2.6. Infectious RVF-VLPs are efficiently released.
(A) Cells were transfected with the GFP minigenome, pN and either empty vector (EV/EV), pRdRp and empty vector (RdRp/EV), or pRdRp and pGn/Gc (RdRp/Gn/Gc) and analyzed at the indicated times for expression of GFP. (**B)** Media from cell monolayers shown in (A) was harvested at the indicated times and used to infect BSR-T7/5 cells that expressed RdRp and N.

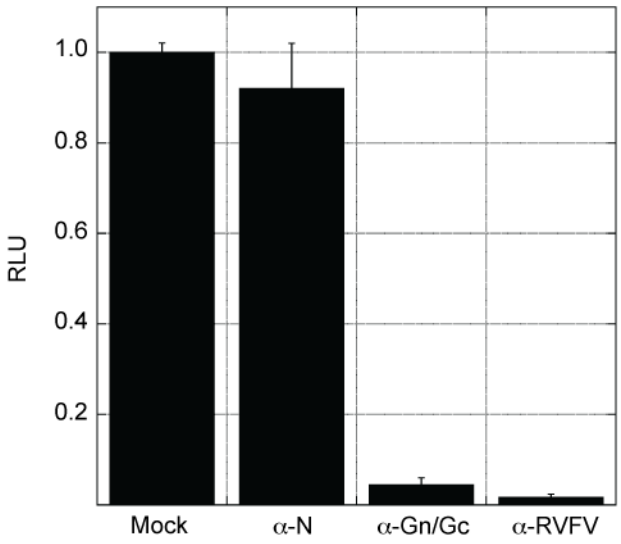

Figure 2.7. RVF-VLPs are neutralized by the same antibodies that neutralize RVFV.
RVF-VLPs were generated and subjected to a 30 min incubation at room temperature with no antibody (Mock), monoclonal anti-N, neutralizing anti-Gn and anti-Gc monoclonals or a polyclonal anti-RVFV antibody prior to application on target cells. The antibody concentration effective for neutralization was determined on authentic RVFV. The target cells were harvested at 24 h post-infection, and the RLuc activity levels were measured. RLuc values (RLU) are expressed relative to the no antibody control. Shown is the data for a representative experiment performed in triplicate with standard deviation bars.

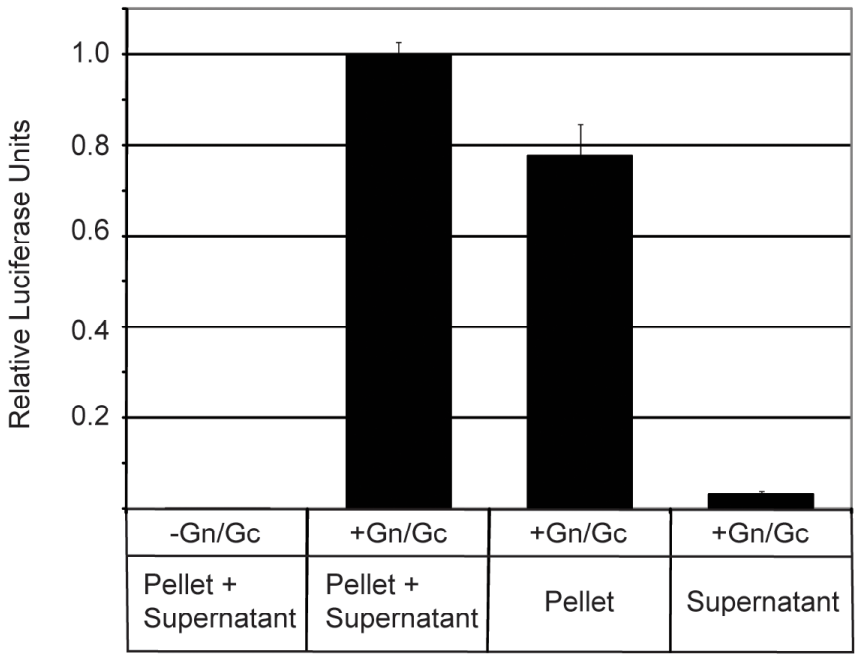

Figure 2.8. RVF-VLPs can be harvested using high-speed centrifugation.
Clarified media from transfected cells was subjected to high-speed centrifugation as described in the materials and methods. The "Supernatant","Pellet" or "Pellet + Supernatant" were used to infect target cells. RLuc activity was measured at 24 h post-infection and is expressed in relative RLuc units. Shown is the data for a representative experiment performed in quadruplicate, the error bars reflect the standard deviation.

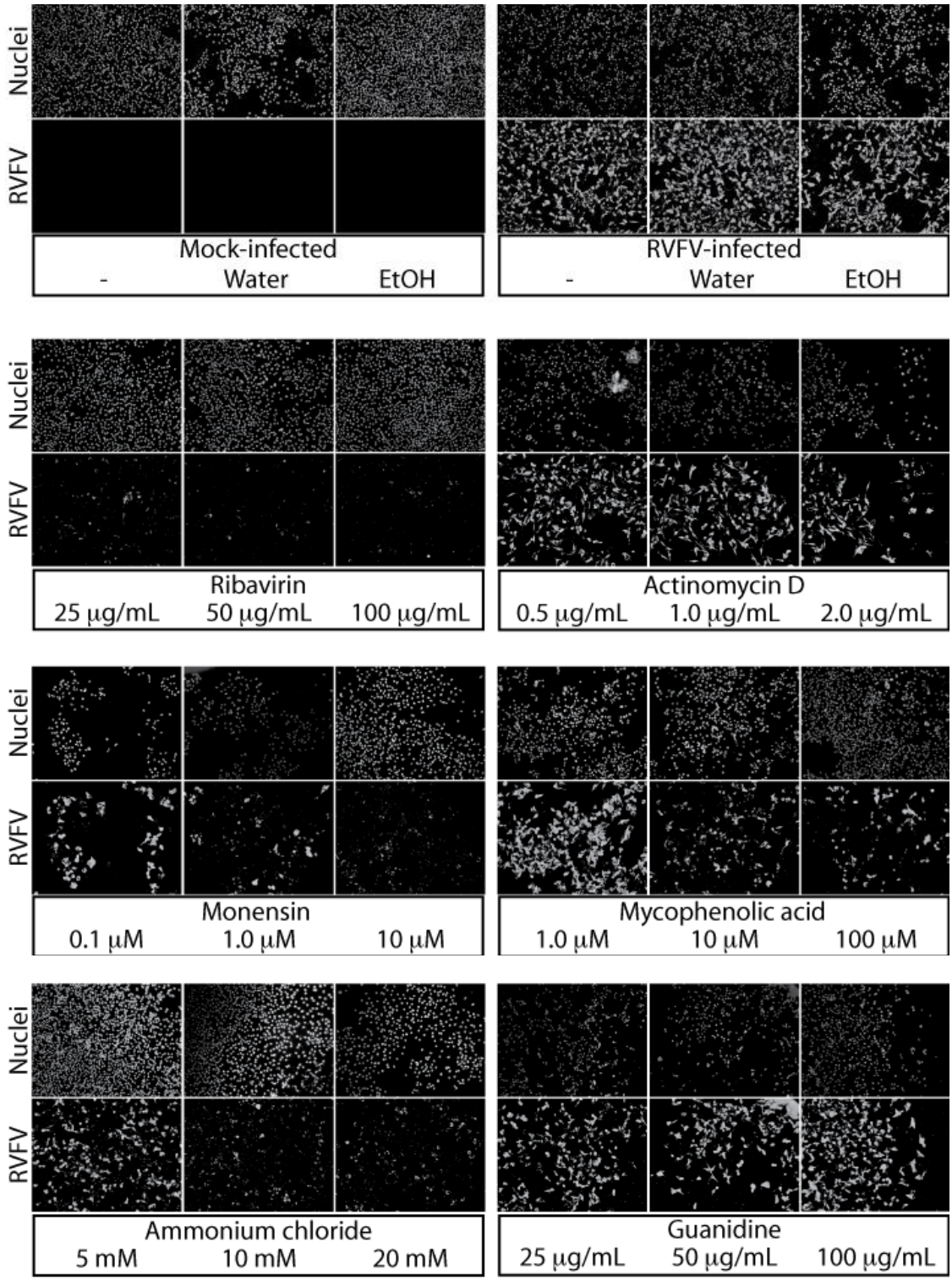

Figure 2.9. Effect of small molecule inhibitors on RVFV replication.
Inhibitors were added at the indicated concentrations at the time of infection with the ZH548-MP12 vaccine strain of RVFV at an MOI of 1. At 22 h post-infection, cells were fixed and stained with rabbit anti-N followed by anti-rabbit Alexa 488. The nuclei were visualized with DAPI.

Inhibitor	Concentration	% Activity
Mock (water)	-	100
Ammonium chloride	5 mM	9.7
	10 mM	1.3
	20 mM	0.5
Guanidine	25 μg/mL	45.8
	50 μg/mL	19.2
	100 μg/mL	22.4
Ribavirin	25 μg/mL	12.8
	50 μg/mL	6.2
	100 μg/mL	4.3
Mock (ethanol)	-	100
Actinomycin D	0.5 μg/mL	13.2
	1.0 μg/mL	6.4
	2.0 μg/mL	5.2
Monensin	0.1 μM	58.2
	1.0 μM	2.1
	10.0 μM	0.2
Mycophenolic acid	1.0 μM	48.6
	10.0 μM	8.9
	100.0 μM	5.8

Table 2.2. Effect of chemical inhibitors on RVF-VLP delivered minigenome activity.
Inhibitors were added at the indicated concentrations at the time of infection with the ZH548-MP12 vaccine strain of RVFV at an MOI of 1. At 22 h post-infection, cells were harvested and analyzed for RLuc activity.

Chapter 3

Structure of the Rift Valley Fever Virus Nucleocapsid Protein Reveals a New Architecture for RNA Encapsidation

Introduction

RNA viruses are responsible for a myriad of human and animal diseases, including measles, polio, rabies, the common cold, dengue fever, and Rift Valley fever. Despite tremendous diversity among RNA viruses, all must package a protected RNA genome into virus particles. RNA viruses protect their genome in one of two ways, providing either a protein shell or a protein coat for the genome (75). The process is generally known by the term encapsidation, however functionally and structurally encapsidation takes a variety of forms. Most positive-sense RNA and double-stranded RNA viruses place their genome within a protein shell, known as a capsid. By contrast, the negative-sense RNA viruses encapsidate their genome by coating the length of the RNA with a nucleocapsid protein (N). Although capsid and N all bind RNA, the resulting RNA-protein complexes differ, and it is not possible to make generalizations about the proteins involved in encapsidation across all RNA virus families.

Rift Valley fever is a mosquito- and aerosol-borne disease of livestock and humans in sub-Saharan Africa, and is caused by Rift Valley fever virus (RVFV). Rift Valley fever in domestic ruminants results in abortion and high rates of mortality, especially among young animals (29, 32). In humans, Rift Valley fever is typically a self-limited febrile illness, although severe disease, such as hemorrhagic fever and encephalitis, occurs in a small percentage of cases (29, 31, 32). RVFV has a membrane envelope and a genome comprised of three negative-sense RNA segments, termed small (S), medium (M) and large (L) (40). It belongs to the *Phlebovirus* genus in the *Bunyaviridae* family. As with all negative-sense RNA viruses, the genome is bound, or encapsidated, by N. The N of RVFV is a 27-kDa protein encoded by the S segment.

Bunyavirus N binds single-stranded RNA (ssRNA) non-specifically (76-78), although some N may have a preference for specific viral RNA sequences (78-83). Studies on some animal viruses within the *Bunyaviridae* family found that encapsidated RNA is resistant to disruption by high salt and RNase treatment (78, 80, 82).

Despite the common property of tight, non-specific binding to single-stranded RNA, homology of N within the *Bunyaviridae* family is not apparent from sequence data, as N from different genera appear unrelated. However, within a genus, the N are clearly homologous. When RVFV N is compared across the *Phlebovirus* genus, the amino acid identity generally ranges from 50% to 59%, and is 36% for Uukuniemi virus, the most divergent clade within the *Phlebovirus* genus. The high degree of sequence identity indicates that the phlebovirus N have similar structures and likely bind RNA in a similar fashion. Additionally, the phlebovirus N are distantly related to the N of the *Tenuivirus*, a genus of negative-sense RNA viral plant pathogens with worldwide distribution (84). Otherwise, by sequence analysis, the phlebovirus N appear unrelated to N of other negative-sense RNA viruses.

Encapsidation of RVFV genomic RNA, as with all negative-sense RNA viruses, plays an essential role in multiple steps within the replicative cycle including transcription and replication by the RNA-directed RNA polymerase (RdRp)(57, 85), and packaging of genome into virions (40). RVFV N is thought to interact with the viral RdRp because N is essential to replication and transcription (40). N also plays a role in virus assembly through interactions with the viral envelope glycoproteins (G_N and G_C) (86). Structural information is essential to understanding how N participates in these critical processes.

Crystal structures are available for N from several negative-sense RNA viruses, including influenza A virus (FLUVA (87)), rabies virus (RABV (88)), human respiratory syncytial virus (HRSV (89)), vesicular stomatitis virus (VSV (90)) and Borna disease virus (BDV (91)). For some of these, ribonucleoprotein (RNP) complexes have been visualized by crystallography or electron microscopy (FLUVA (92), RABV (88), HRSV (89), VSV (90)). The RNP complexes are high-order ring structures in which loops or chain termini of N make specific contacts with neighboring N subunits, leading to a condensed structure for the encapsidated genome. In contrast to these viruses,

encapsidated bunyavirus genomes have a non-condensed, macro-circular form, based on low-resolution images (93, 94). None of the structurally characterized N is from the *Bunyaviridae* family and none has detectable homology with the phlebovirus N.

Here we report the characterization and crystal structure of recombinant RVFV N. The protein was purified under denaturing conditions. The re-folded N forms RNA complexes similarly to N from virus-infected cells. The 1.93-Å crystal structure of RVFV N reveals a novel protein fold that differs substantially from N of other negative-sense RNA viruses. A dimeric association of N subunits appears critical to its function. A conserved electropositive surface is proposed as the site of RNA binding.

Results

Protein oligomeric state in solution

Purification of recombinant N (recN) under native conditions, including exhaustive ribonuclease treatment, resulted in a discrete complex of the protein and *E. coli* nucleic acid as determined by the ratio of absorbances at 260 nm and 280 nm. Attempts to separate the protein from nucleic acid under native conditions using high salt concentrations and pH extremes were unsuccessful. The complex had an apparent mass of 99 kDa by size exclusion chromatography, which is similar to the 109-kDa species observed for the recombinant 27-kDa N of bunyamwera virus, from the *Orthobunyavirus* genus of the *Bunyaviridae* family (76). Nucleic acid was extracted from the recombinant RVFV N by denaturation and then treated with either DNase or RNase. The purified nucleic acid was sensitive only to RNase treatment, demonstrating that N was bound to RNA (Fig. 3.1A). The majority of the RNA purified was 30-35 nucleotides with minor species of ~60 and ~90 nucleotides (Fig. 3.1B, asterisks). The formation of a nonspecific ribonucleoprotein (RNP) complex between recombinant RNA-binding proteins and *E. coli* RNA is not uncommon (76, 89, 95). Indeed crystal structures of RABV (88), VSV (90) and HRSV (89) RNPs were solved from RNPs bound to *E. coli* RNA, however no crystals were obtained using the recombinant RVFV RNPs. We therefore used denaturation to obtain RNA-free recN. After purification from RNA and refolding, the protein eluted from a size-exclusion column primarily as a monomer, with about 10% apparently as a dimer under chromatographic conditions (Fig. 3.2).

Authentic virus RNPs and purified recombinant N bound to RNA form similar multimeric complexes

We tested whether the refolded recN could interact with RNA similarly to N in viral RNPs. Purified viral RNPs, refolded recN, and refolded recN with added RNA (recN-RNA) were subjected to cross-linking using the homo-bifunctional amine-reactive cross-linker, dithiobis[succinimidyl propionate] (DSP), and then separated by electrophoresis under denaturing conditions (Fig. 3.3). In the absence of cross-linker (Fig. 3.3A, lane 1; Fig. 3.3B, lanes 4 and 9), recN migrated as a monomer, regardless of the presence of RNA. When viral RNPs were cross-linked with increasing amounts of DSP, the monomer band decreased in intensity and four higher molecular weight complexes appeared (Fig. 3.3A, lanes 2 and 3). The number of N within the dominant cross-linked species was estimated to be 2, 4, 6, and 10 based on an apparent molecular weight per monomer of 25 kDa. When RNA-free, re-folded recN was cross-linked with increasing concentrations of DSP, only two species were observed (Fig. 3.3B, lanes 5-8). The higher molecular weight species was estimated to contain two N (Fig. 3.3B, lane 5). The cross-linked dimer and its low concentration relative to the monomer are consistent with the predominant monomeric and minor dimeric species observed by size exclusion chromatography for refolded recN (Fig. 3.2). In contrast, when recN-RNA was cross-linked with DSP, many species of higher molecular weight were observed (Fig. 3.3B, lanes 10-13). The number of N within the dominant cross-linked species created from recN-RNA (Fig. 3.3B, lane 11) was estimated to be 2, 4, 6, and 10. The sizes of the high molecular weight N complexes were similar regardless of whether the cross-linked sample contained viral RNP or reconstituted recN-RNA. Thus, refolded recN behaves similarly to viral N in its ability to bind RNA and to form multimeric complexes. Interestingly, the cross-linked species formed by both viral RNPs and recN-RNA appear primarily as multiples of 2, suggesting that N binds RNA as a dimer.

Overall structure

Recombinant, RNA-free RVFV N was crystallized and the structure was solved by multiwavelength anomalous diffraction from the selenomethionyl (SeMet) protein (Table 3.1). The crystals contained four N polypeptides in the asymmetric unit of space group *P*1, affording four independent views of the structure. The four copies of the N

polypeptide are nearly identical with root-mean-square-deviations (RMSD) of 0.46 Å for 238 Cα atoms. The refined structure is complete with the exception of residues 16-19 and 28-30. In these regions, each of the four polypeptides lacks density for one, four or seven amino acids.

RVFV N has a compact, helical fold consisting of N-terminal and C-terminal lobes of approximately equal size, connected by a linker helix (α7, residues 112-121) (Fig. 3.4). Both the N-lobe (α1-α6, residues 1-111) and the C-lobe (α8-α12, residues 122-245) have a central helix (α3 and α9) surrounded by four or five other helices. Despite these similarities, the topologies differ and the N- and C-lobes cannot be superimposed. We examined the structural database for proteins with folds similar to RVFV N. Remarkably, the folds of both the N- and C-lobes appear to be novel. No structure similar to either lobe was identified in searches with the servers Dali (96) and VAST (97).

The crystallized protein includes the full natural sequence (Met1-Ala245) without additional residues. Both chain termini are well ordered (Fig. 3.5). Met1 makes intra- and intermolecular contacts with hydrophobic residues in helix α1 (residues 3-10). The C-terminal α-carboxyl of Ala245 forms a salt bridge with the Arg178 side chain. Neither of the chain termini nor any loops protrude from the protein.

RVFV N crystallized as a symmetric dimer (Fig. 3.6A). We conclude that this is a natural dimer because the crystal contains two independent copies of the dimer, which are nearly identical (RSMD of 0.48 Å for 476 C α atoms), and because we observed dimers of RNA-free N in solution (Fig. 3.2, 3.3). As expected for a natural dimer, the subunit interface is hydrophobic and lacks buried water. The small interface (502 $Å^2$ buried surface area per monomer) is consistent with the low proportion of dimeric relative to monomeric species of RNA-free N observed by gel filtration (Fig. 3.2). The dimeric species is expected to predominate in crystals where the protein concentration is higher than in solution. The dimer is formed by contacts of residues in helices α 1, α 7 and α 8. The side chain of Trp125 (α 7- α 8 loop) is buried in the dimer interface where it contacts the side chains of Met1, Gln5, Ile9 and Trp125 in the second monomer (Fig.

3.6). Ala12, Val120, Val121, Glu124 and Thr131 also form inter-subunit van der Waals contacts.

Comparison with N of other negative-sense RNA viruses

Given the rapid rate of virus divergence, we anticipated that the phlebovirus N might resemble the N of other negative-sense RNA viruses even though the sequences are dissimilar. Two different folds for N have been reported, one for FLUVA (87) in the family *Orthomyxoviridae*, and the other for four viruses in the order *Mononegavirales* (RABV (88), VSV (90), HRSV (89) and BDV (91)). However, the phlebovirus N fold differs from both these other N folds. Thus at least three different folds exist for N of the negative-sense RNA viruses. Intriguingly, all three folds are predominantly helical and are bi-lobed. However, the phlebovirus N has a more compact structure. RNA binds in a deep, positively charged cleft between the two lobes of N from both the *Mononegavirales* and FLUVA N (88-92). Phlebovirus N lacks a cleft between the N- and C-lobes (Fig. 3.4). Another important difference is the lack of protrusions in phlebovirus N. The N- and C-termini of N of the *Mononegavirales* protrude from the subunit, as does an extended loop in the N of FLUVA. These protrusions contact other N subunits and are important to the structure of the RNP (88-92).

Conservation of Phlebovirus N

Sequences of N from phleboviruses are highly conserved (Fig. 3.7), with at least 41% pairwise sequence identity among 30 representative phleboviruses (excluding the divergent Uukuniemi clade, whose N is 35% identical to RVFV N). The 66 invariant residues map primarily to the core of the structure, suggesting that they are important for conservation of the overall fold (Fig. 3.8A). Residues in the dimer interface are not strictly conserved. However, the dimer contact appears to be present in all phlebovirus N because compensatory sequence changes accommodate the size and hydophobicity of the residue corresponding to Trp125. For example, if the residue at position 125 (Trp in RVFV N) is aromatic, then the residue at position 12 (Ala in RVFV N) has a small side chain such as glycine, serine or alanine (Fig. 3.7). However, if the residue at position 125 has a smaller side chain such as serine, then the residue at position 12 is correspondingly larger (leucine). The structure and sequence alignment are consistent with published

mutagenesis data suggesting that the N-terminus of RVFV N is required for dimer formation (98). However, the conserved residues tested in the previous study (Tyr4, Phe11) are not in the dimer interface. Instead they point away from the dimer interface towards the inside of the monomer where they form stabilizing contacts in the hydrophobic core of the protein. The observed loss of function of Tyr4Gly and Phe11Gly (98) is likely due to destabilization of helix α1 (residues 3-10) and, indirectly, the dimer interface.

Trp125 in the dimer interface and C-terminal salt bridge are required for N function

The structure suggests that Trp125 is critical for dimer formation because of the hydrophobic contacts it makes with Met1, Ile9 and Trp125 of the opposing N monomer. Additionally, a salt bridge between the C-terminal carboxyl group of Ala245 and the Arg178 side chain, which is Arg or Lys in all phlebovirus N, may be important for overall structural integrity. To test these predictions, three mutant N alleles were generated, Trp125Ala, Arg178Gln and Arg178Glu, and the function of these alleles was analyzed in a cell-based RdRp transcription assay. In the transcription assay, RdRp and N are expressed from separate plasmids. When RdRp and N were both present and functional, a luciferase mRNA from a recombinant S segment is transcribed (Chapter 2). The Trp125Ala allele was severely compromised and activity was only 4% of the wild type allele (Table 3.2). This result suggests that dimer formation is essential for activity, presumably because N binds RNA as a dimer. If the salt bridge of Arg178 with the C-terminus is critical, then the Arg178Gln allele should retain more function than the Arg178Glu allele, and this was the observed result (Table 3.2). The activity of the Arg178Gln and Arg178Glu alleles was 25% and 7% of wild type, respectively. All alleles expressed protein at a level similar to wild type and all appeared capable of forming higher molecular weight complexes with RNA (Fig. 3.9). Presumably, the defect lies in either the efficiency of binding RNA or possibly in the stability of N dimers.

RNA binding

Consistent with the high affinity for RNA, RVFV N is positively charged with a calculated isoelectric point of 9.1. We considered whether there is an obvious RNA-

binding surface on the RVFV N dimer. A map of the electrostatic surface potential revealed two positive patches that are candidate RNA binding sites (Fig. 3.10A). One positive patch crosses the dimer axis on a convex surface we designate "front". A cleft at the dimer interface on the "back" of the dimer lacks a positive patch. A second patch maps to one "side" of each monomer, resulting in positive patches on both sides of the dimer.

As N from related phleboviruses share high sequence identity, they are likely to bind RNA similarly. We generated structure-based homology models for four N that represent clades within the *Phlebovirus* genus, calculated the electrostatic surface potentials (Fig. 3.11), and also mapped conservation onto the RVFN surface (Fig. 3.10B). The positive patch on the convex front surface of the RVFV N dimer is not conserved across the *Phlebovirus* genus and is negatively charged in some phlebovirus N (Fig. 3.11). In contrast, a positive patch is present on the sides of all the modeled phlebovirus N. Thus, RNA may bind in the positively charged surfaces on opposite sides of the N dimer. The most strongly conserved surface on *Phlebovirus* N is at the "top" and "bottom" of the dimer. The conserved surface is a hydrophobic pocket formed by a loop between residues 27-35 and the C-terminal half of α10 along with the 5 succeeding amino acids (residues 198-210) (Figs. 3.10B and 3.11), which include the most mobile regions of the N structure (Fig. 3.8B). The combination of mobility, conservation and hydrophobicity suggest that this site may be involved in a conserved protein-protein interaction.

Discussion

The structure of RVFV N is the first for a nucleocapsid protein from any virus in the *Bunyaviridae* family. The structure reveals a new protein fold and an addition to nature's repertoire of RNA-binding proteins. The sequence of RVFV N is 36-59% identical to those of other phleboviruses, and aligns largely without internal gaps. Such high sequence identity assures that the new fold observed for RVFV N exists in all phlebovirus N, and also suggests that all phlebovirus N bind RNA similarly.

This work establishes a fundamental dimeric form of RVFV N. In RNPs extracted from the virus, the dimer was observed in a ladder of cross-linked species of N (Fig. 3.3). The dimer was also observed in the recombinant and refolded N by cross-

linking in presence of RNA to a similar ladder of species (Fig. 3.3B), by cross-linking to a dimeric species in absence of RNA (Fig.3.3B), by gel filtration (Fig. 3.2), and in the crystal structure (Fig. 3.6). The functional significance of the dimer was corroborated by site-directed mutagenesis of Trp125 in the center of the dimer interface (Fig. 3.6). Substitution of Trp125 by Ala severely compromised transcription by the RdRp. Although it did not alter the level of N in cells or affect the formation of cross-linked species *in vitro* (Table 3.2, Fig. 3.9), the Trp125 mutation may affect the stability of N dimers. Taken together, the data indicate that the N dimer is critical to RdRp transcription, that it may be the fundamental unit of nucleocapsid assembly, and that it forms higher-order species in the presence of RNA.

The minimal higher-order species is the RNase-resistant multimer of apparent molecular weight 99 kDa (Fig. 3.2). This species may be a dimer of dimers, or it may be one dimer with a hydrodynamic radius expanded by RNA. It is similar to the reported 109-kDa recombinant RNP from Bunyamwera virus, which was predicted to be a tetramer of N (27 kDa) bound to ~48 RNA nucleotides (76). Bunyamwera virus and RVFV belong to different genera within family *Bunyaviridae* and their N are not obviously similar at the amino acid level. Nevertheless the existence of similar multimeric species suggests that the bunyavirus N may fold and bind RNA similarly.

An electropositive surface on RVFV N was identified as a potential RNA interaction site because it appears to be positively charged in N from all phlebovirus clades. The surface is on the "side" of the N monomer and maps to both sides of the dimer by symmetry (Figs. 3.10 and 3.11). This is consistent with a model in which RNA wraps around the N dimer in nucleosome fashion. Neither the position of the conserved electropositive surface on opposite sides of the N dimer nor the electrostatic potential of other surfaces suggests an obvious structure for a stable RNA complex with two N dimers, but certainly does not rule out such a possibility. In whatever manner N binds RNA, it is expected to engage the phosphate backbone because the multimer is so highly RNase resistant. All negative-sense RNA viruses form RNPs in order to protect and package their genome. Many of these RNPs are RNase-resistant structures formed by oligomers of N associated with RNA that resemble beads on a string and in some cases assemble into higher-order structures with helical symmetry (40). Our results indicate

that phlebovirus RNP has a fundamentally different higher-order structure than has been observed for RNPs from other negative-sense viruses.

The structures of RNPs from four negative-sense RNA viruses from the *Paramyxoviridae, Rhabdoviridae*, and *Orthomyxoviridae* families have been reported (88-90, 92). In all cases, RNA binds nonspecifically in an electropositive cleft between the lobes of the N subunit. The RNPs have a similar architecture in which RNA binds around either the outside or inside of a ring of 9-11 N subunits. In all cases, protrusions from the N subunits make specific contacts with adjacent N subunits to maintain the ring structure. For HRSV, each N subunit also interacts with other N subunits in the preceding or following turns of the helical nucleocapsid (89).

The RNP of *Phleboviruses*, and perhaps all bunyaviruses, clearly has a different organizing principal than the RNPs of theviruses of the *Mononegavirales* order and *Orthomyxoviridae* family. Early electron microscopy studies suggested that the RNPs from bunyaviruses form large macro-circles (93, 94), probably due to pairing of 10-15 complementary bases at the 3' and 5' ends of each genomic segment (99). Although the lack of obvious superhelical periodicity in bunyavirus RNPs could be an artifact of the negative staining used in these experiments, it is consistent with the crystal structure of *Phlebovirus* N. The *Phlebovirus* N monomer lacks a cleft between lobes, and there is no electropositive cleft between subunits of the dimer (Fig. 3.11). More important, the highly compact *Phlebovirus* N structure has no protruding hooks that could link it to other N molecules in a super-structure like the rings of 9-11 subunits observed for the *Mononegavirales* order and *Orthomyxoviridae* family. Indeed, we observed no such super-structure for recombinant RVFV N in solution, unlike the recombinant rings purified for N from HRSV (89) and FLUVA (92). Thus, we suggest a simple string-of-beads architecture for phlebovirus RNP, based on the preponderance of data.

The most strongly conserved surface of phlebovirus N is a hydrophobic pocket at the top and bottom of the dimer (Fig. 3.8A and 3.10). The conservation in this region suggests it has an important function that is common to phleboviruses, and the hydrophobicity of the surface suggests that it is not involved in RNA binding. Therefore we propose that this is the site of a conserved protein-protein interaction. It is possible that an unidentified host protein interacts with this site on N. Among potential viral

protein partners, the RdRp is an obvious possibility because N is required for transcription and replication by the RdRp (40). However, several lines of evidence suggest that an envelope glycoprotein may be the target of the conserved hydrophobic pocket on N.

Packaging of RNPs into virions occurs at a site of virus assembly on the Golgi membrane (100, 101) and is thought to involve contact between N and the cytosolic region(s) of one or both of the envelope glycoproteins (G_N and G_C). The G_N cytoplasmic tail was shown recently to recruit the encapsidated genome to the Golgi membrane prior to virion assembly (86, 102) (Chapter 4). Moreover, the encapsidated genome of RVFV interacts with a 30-residue domain on the C-terminal cytoplasmic tail of G_N immediately downstream of the transmembrane domain (Chapter 4). Since the recruitment of the genome is expected to be similar in all phleboviruses, the conserved hydrophobic pocket of N is a candidate G_N binding site. This hypothesis is consistent with the ability of bunyaviruses to undergo reassortment of genomic segments both in nature and *in vitro* (13-15). The progeny of a reassortment event have genomic segments that derive from more than one parental virus. Thus, there must be a certain amount of promiscuity in the interaction of N with genomic RNAs from heterologous viruses and in protein-protein interactions necessary for assembling virions. All characterized reassortant bunyaviruses isolated in nature are M segment reassortants (10, 12, 17), demonstrating that the envelope glycoproteins, which are encoded by the M segment, are capable of interacting with heterologous RNPs. The hydrophobic character of the G_N-tail interaction domain, as well as certain Pro and Trp residues within it, are conserved amongst phleboviruses (50) and could function in protein-protein interactions with N in both pure and reassortant viruses. Thus the conserved pocket in N may be an interacting surface for the cytoplasmic tail of G_N. Whether the conserved pocket of N interacts with the G_N cytoplasmic tail, with the RdRp or with a host protein, it has potential as a drug target because it is conserved in phleboviruses.

The structure and characterization of *Phlebovirus* N reveal a new paradigm for encapsidation of the genomes of negative-sense RNA viruses, provide a platform for further studies of virus pathogenicity, and suggest a potential site for development of effective antiviral therapeutics.

Materials and Methods

Plasmids

All plasmids were generated using standard molecular cloning techniques and were confirmed by sequencing. pTrRVFV-SΔNSs::GFP, pRdRp-Amp and pN-Amp have been described previously (50, 54). To generate the protein expression construct for N, the gene was amplified using Phusion polymerase (New England Biolabs), pTrRVFV-SΔNSs::GFP as template, and primers 5'-GACGTGGGTCTCGAGGTATGGACAACTATCAAGAGCTTG-3' and 5'-CTCGAGTTAGGCTGCTGTCTTGTAAGCCTG-3'. The PCR product was cloned into pCRII-Blunt-TOPO (Invitrogen). Digestion with BsaI and XhoI liberated the N ORF, which was subsequently ligated into pSUMO (Life sensors, Inc.), thus producing pIPER1. For the RdRp transcription assay, the plasmids pN and pRdRp were constructed by subcloning the open reading frames from pN-Amp and pRdRp-Amp into pVAX1 (Invitrogen) using the HindIII/EcoRI and BamHI/NotI sites, respectively. pSTrRVFV-SΔNSs::hRLuc was derived from pTrRVFV-SΔNSs::GFP in several steps. First, the GFP gene was released by digestion with EcoRV, followed by ligation with a Renilla luciferase gene that was flanked with EcoRV sites. The resulting plasmid was then subcloned into pSMART HC Kan (Lucigen). pSTrRVFV-SΔNΔNSs::hRLuc was derived from pSTrRVFV-SΔNSs::hRLuc by removing the 237 nucleotide SmaI fragment from the N gene. The RVFV N mutants, W125A, R178Q, and R178E, were generated using Phusion polymerase, pN as template, and primer pairs 5'-GTCTTGAGTGAGGCGCTTCCTGTCACTG-3' and 5'-CAGTGACAGGAAGCGCCTCACTCAAGAC-3', 5'-CTGCAGTTCTCCCAGGTCATCAACCCA-3' and 5'-TGGGTTGATGACCTGGGAGAACTGCAG-3', and 5'-CTGCAGTTCTCCGAGGTCATCAACCCA -3' and 5'-TGGGTTGATGACCTCGGAGAACTGCAG-3', respectively.

Cells and virus

BSR-T7/5 cells expressing the T7 RNA polymerase were a generous gift of Dr. K. Conzelmann (Max-von Pettenkofer-Institut, Munchen, Germany). BSR-T7/5 cells

were subsequently cloned by limiting-dilution, and the resulting clonal lines were screened using the RVFV transcription assay. The C3 clone of the BSR T7/5 line was used for all experiments. The cells were grown in Dulbecco's Modified Eagle Medium (Invitrogen) supplemented with 10% fetal calf serum, and 1 mg/mL geneticin. RVFV ZH548 MP12 vaccine strain was a generous gift of Dr. R. Tesh (World Reference Center of Emerging Viruses and Arboviruses).

Production and purification of recombinant N

pIPER1 was transformed into E. coli strain BL21 AI (Invitrogen) containing the pRARE2 plasmid (Novagen) (103) and grown in 1 L of TB media (12 g tryptone, 24 g yeast extract, 2.31 g KH_2PO_4(monobasic), 12.5 g K_2HPO_4 (dibasic), 40 mL glycerol) containing 35 µg/mL chloramphenicol and 50 µg/mL kanamycin at 37˚C until OD_{600}=1.0. The temperature was reduced to 20˚C, and expression was induced after 1 hr by addition of 4 mL 50% w/v arabinose and isopropyl-β-D-thiogalactopyranose (IPTG) to a final concentration of 0.4 mM. The cultures were incubated 12 hr at 20˚C and cells were harvested by centrifugation. All purification steps were carried out at 4˚C unless otherwise noted.

Initial attempts to purify the recombinant protein under native conditions resulted in protein bound to heterologous E. coli RNA, so the protein was purified under denaturing conditions and refolded (95). Briefly, cell pellets were resuspended in 35 mL lysis buffer (50 mM Na-phosphate pH 7.8, 1 M NaCl, 20 mM imidazole, 5% glycerol), lysed by sonication, and centrifuged at 27,000 x g for 45 minutes. The supernatant was loaded onto a 5-mL HiTrap chelating column (GE Healthcare) pre-equilibrated with lysis buffer. After a wash with 10 column volumes of lysis buffer, the protein was unfolded with a linear gradient of 0-8 M urea in lysis buffer over 5 column volumes. After a wash with 5 column volumes of lysis buffer with 8 M urea, the protein was refolded with a linear gradient of 8-0 M urea in lysis buffer over 10 column volumes followed by a wash with 10 column volumes of lysis buffer. The protein was eluted with a linear gradient of 20-500 mM imidazole in lysis buffer. Fractions containing SUMO-N, as determined by 12% SDS-PAGE, were pooled and dialyzed 1 hr against 1 L dialysis buffer (50 mM Na-phosphate pH 7.8, 1 M NaCl, 5% glycerol). SUMO-protease was added to a final concentration of 1:1000 (protease:protein) and dialysis was continued with fresh buffer

for 16 hr. The expression plasmid for SUMO protease was a kind gift of C. Lima, Memorial Sloan-Kettering Cancer Center (104). The proteolysis mixture was loaded on a 5-mL HiTrap column pre-equilibrated with lysis buffer, and cleaved protein was washed from the column with lysis buffer. N was concentrated using Centriprep-10 (Millipore), and subjected to size exclusion chromatography by a HiLoad 16/60 Superdex 75 gel filtration column (Amersham) pre-equilibrated with storage buffer (20 mM TRIS pH 7.8, 0.5 M NaCl, 10% glycerol). The fractions corresponding to the N monomer peak were pooled and concentrated to 13 mg/mL using Centriprep-10. Purified protein was flash-frozen in liquid N_2 and stored at -80˚C. Typical 1-L cultures yielded 20 mg of purified, refolded N.

To produce the selenomethioninyl (SeMet) variant of N, 50-mL cultures were grown in rich media and cells were harvested and added to SelenoMet Medium Base supplemented with SelenoMet Nutrient Mix (Athena Enzyme Systems) and 100 mg/L of D,L-SeMet to give an initial OD_{600} of 0.3. Cultures were grown to OD_{600}=0.5, incubated 1 hr at 20˚C, and induced with 0.4 mM IPTG. SeMet N was purified identically to the wild type.

Crystallization

Prior to crystallization, N was dialyzed against crystallization buffer (20 mM Tris pH 7.8, 250 mM NaCl). N was crystallized at 4˚C by hanging drop vapor diffusion from a 1:1 mixture of protein (10 mg/mL N in crystallization buffer) and well solution (26% PEG 3350, Na/K phosphate pH 5.5). Optimal crystals were obtained after 2 weeks. The crystals were cryo-protected by soaking in well solution with the addition of 10% glycerol, harvested into loops, and frozen by plunging into liquid N_2.

Crystallography

Diffraction data were collected at 100 K on GM/CA-CAT beamline 23ID-D (native) and 23ID-B (SeMet) at the Advanced Photon Source (APS), Argonne National Laboratory (Argonne, IL).

Although the crystals appeared single, all diffracted in two lattices, which complicated data processing. The SeMet data were processed using HKL2000 (105), with which images could be indexed on the stronger lattice by using only data beyond 4-

Å spacings for initial indexing. Data from crystals of wild type N were processed with iMOSFLM (106), which was able to index with no exclusions. SOLVE (107) and RESOLVE (108) were used for initial phasing using a two-wavelength MAD data set from one crystal of SeMet protein. 36 of the 48 Se sites were located and used for MAD phasing (phasing-power = 0.9, initial FOM = 0.35), followed by density modification phase refinement with four-fold averaging and automated modeling (60% of main chain) in phenix (109). Modeling was completed manually using COOT (110) and refinement was performed using REFMAC5 (111) of the CCP4 suite (112). The structure was solved from triclinic crystals with four N polypeptides in the asymmetric units. The final model is complete except for residues 17 in chain A, 18 in chain B, 16-19 in chain C, and 16-19 and 28-30 in chain D. All residues are in favored regions of the Ramachandran plot except for Ile209 in all four chains, which is well supported by density. The structure was validated using MolProbity (113), PyMOL was used for generating figures and for molecular superpositions (114), sequence alignments were done using ClustalW (115), the apbs plugin in PyMOL was used to calculate electrostatic surface potential (116), and ESPript (117) was used for secondary structure assignment. Structure based homology models were generates using the MMM server (118) and optimized using YASARA (http://www.yasara.org). Conservation scores were calculated by the ConSurf server (119).

RNP preparation

Encapsidated genomes or ribonucleoparticles (RNPs) were purified from Vero E6 cells infected with RVFV MP-12 strain. Cells and supernatants were harvested when cells started to show cytopathic effect and frozen at -80˚C. The cell slurry was thawed on ice and octyl-β-D-glucopyranoside was added to a final concentration of 1%, and the mixture was incubated on ice for 1 h. Insoluble material was removed by centrifugation at 1,100g for 15 min at 4˚C. The supernatant was then centrifuged at 53,000g in an SW28 rotor for 8 h at 4˚C. The pellet was resuspended in 1X TNE (10 mM Tris, pH 7.5, 100 mM NaCl, 1 mM EDTA) with 5% sucrose. The soluble material was then layered on top of a 30-50% CsCl gradient that was then subjected to centrifugation at 53,000 x g in an SW28 rotor for 16 h at 4˚C. Fractions were taken from the bottom of the gradient and

analysed for the presence of N by ELISA. Fractions containing N were pooled and analyzed by SDS-PAGE followed by colloidal Coomassie staining.

Antibodies

The N antibody was generated in rabbits using purified and denatured N as antigen (Harlan Laboratories). The horseradish peroxidase conjugated anti-rabbit antibody was obtained from Amersham.

Cross-linking

For cross-linking, a reconstituted RNP (N-RNA) was generated by incubating refolded recombinant N (recN) with a 25-nucleotide polyU RNA oligomer for 30 minutes at a ratio of 6:1 recN:RNA. The sample was then run on an S200 size exclusion column to separate N-RNA from RNA-free recN. The recN and N-RNA were dialyzed against PBS to remove the Tris storage buffer prior to incubation with DSP. Purified recN, N-RNA, or purified viral RNPs (vRNP) were cross-linked by incubating 30 μg of recN at a concentration of 1 mg/mL, or purified vRNPs with 0.0, 1.0, 5.0, 10.0 or 20.0 μM dithiobis[succinimidyl propionate] (Pierce) for 15 minutes at room temperature. The cross-linking was quenched by addition of Tris pH 6.7 to a final concentration of 100 mM. Protein complexes were analyzed by SDS-PAGE followed by either colloidal Coomassie stain or western blot using a polyclonal rabbit anti-N antibody.

RVFV transcription assay

BSR-T7/5 cells were plated at $1x10^5$ cells/well in 12-well culture plates. After 24 h, cells were transfected using 2 μL/μg TransIT LT1 (Mirus Corporation) and plasmids in the ratio 0.25 μg pSTrRVFV-SΔNΔNSs:hRLuc: 0.50 μg pN: 0.75 μg pRdRp. At 48 h post-transfection, the cells were harvested and analyzed by luciferase assay and western blot.

A

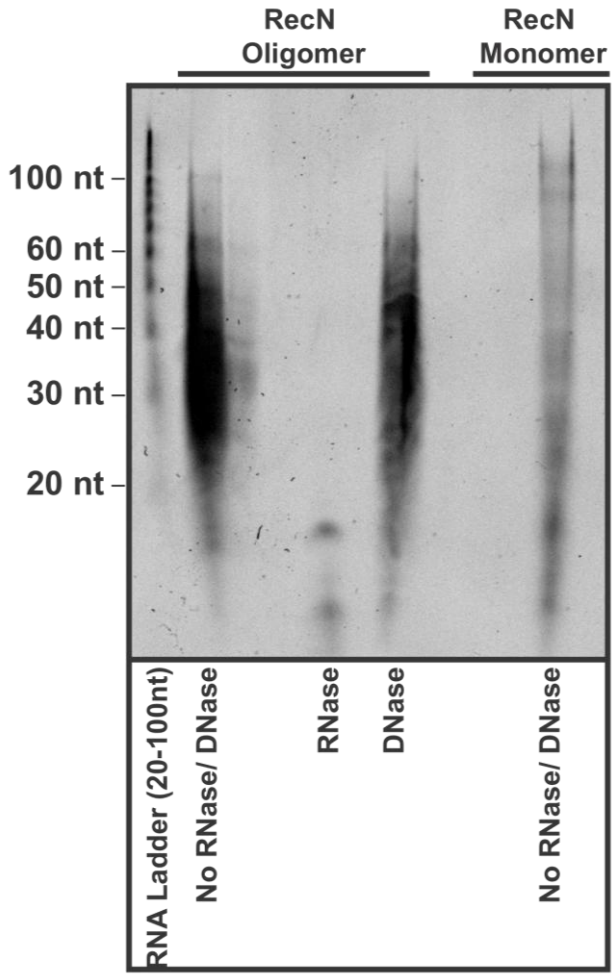
RecN
Oligomer
RecN
Monomer
100 nt
60 nt
50 nt
40 nt
30 nt
20 nt
RNA Ladder (20-100nt)
No RNase/ DNase
RNase
DNase
No RNase/ DNase

B

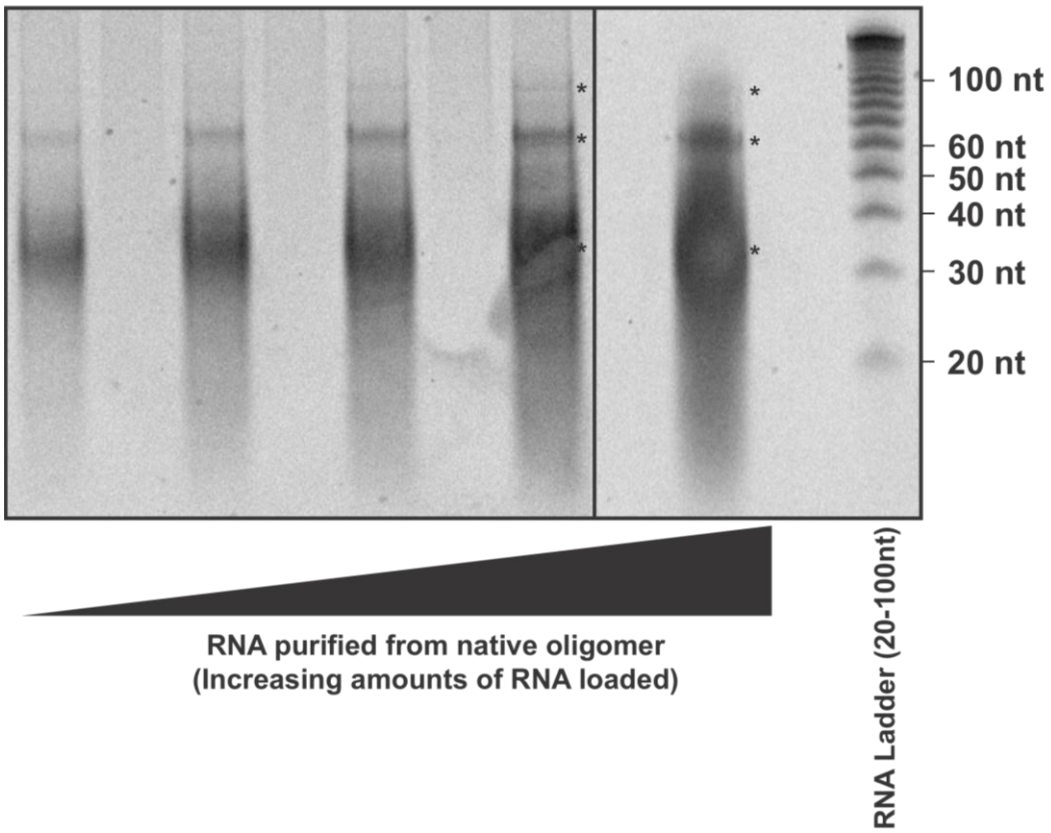

Figure 3.1. RecN binds non-specifically to E. coli RNA.
(A) RecN was purified under native conditions with extensive RNase A treatment, and eluted from the size-exclusion column predominantly as an oligomer (apparent molecular weight of 99 kDa) with a small fraction of monomer. The RNA was extracted from recN oligomer and recN monomer then treated with RNase or DNase. The purified RNA was separated on a denaturing urea-polyacrylamide gel and visualized using SYBR Green. **(B)** Increasing amounts of RNA purified as in (A) from 80 μg of the recN oligomer were separated on a denaturing urea-polyacrylamide gel and visualized using SYBR Green. The amounts loaded correspond to 2.5, 5.0, 10, 20, and 40% of total RNA purified. Dominant RNA species are indicated with asterisks (*). *(Contributed by M. Piper)*

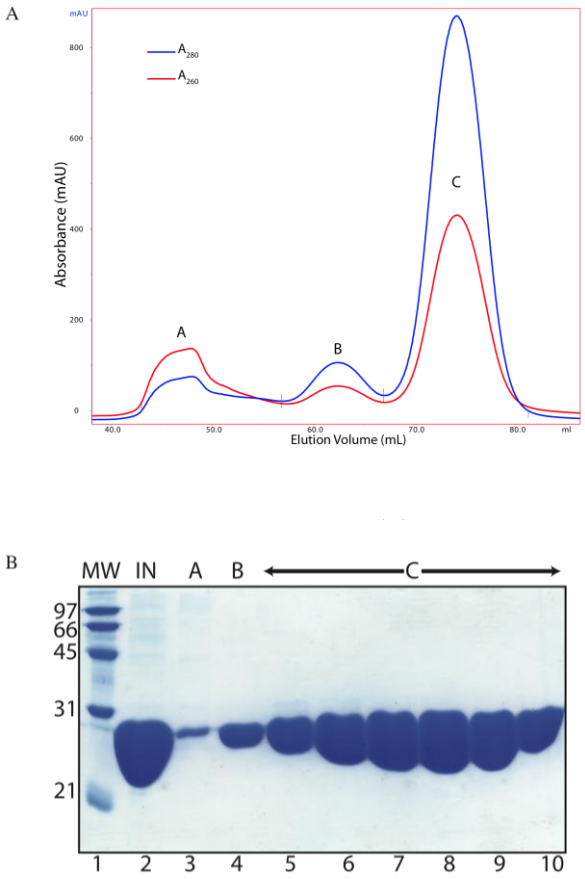

Figure 3.2. RVFV N purification under denaturing conditions.
(A) S75 gel filtration chromatogram of refolded RVFV N. The red and blue traces represent absorption at 260 nm and 280 nm, respectively. Peak A is in the void volume, peak B is the N dimer and peak C is the N monomer. Even after denaturation, some N is still bound to RNA and elutes as an oligomer. **(B)** SDS-PAGE of fractions from the chromatogram shown in (A). Lane 1: molecular weight markers, lane 2: input sample, lane3: peak A fraction, lane 4: peak B fraction, and lanes 5-10: peak C fractions. *(Contributed by D. Raymond).*

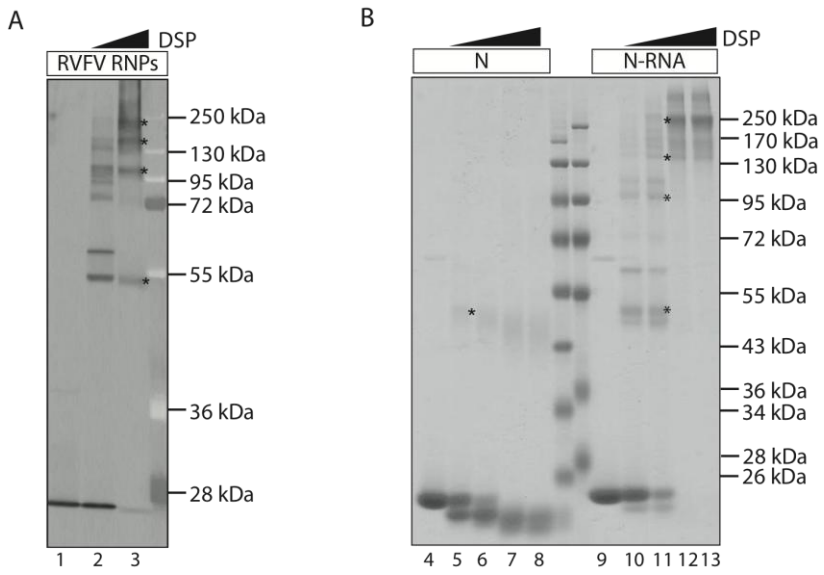

Figure 3.3. Similar multimer complexes of authentic virus RNPs and purified recombinant N bound to RNA.

(A) Viral RNP. Purified RVFV RNPs were cross-linked with 0.0, 5.0, or 20.0 mM DSP and analyzed by immuno-blot. Asterisks indicate predominant cross-linked species. Molecular weight markers are in the rightmost lane. **(B)** Recombinant N. N or N bound to U25 ssRNA (N-RNA) was cross-linked using 0.0, 1.0, 5.0, 10.0, or 20.0 mM DSP, separated by SDS-PAGE, and visualized with colloidal Coomassie stain. The dominant cross-linked species are indicated by asterisks (*). *(Contributed by M. Piper)*

Table 3.1. Diffraction data and Refinement Statistics
(Contributed by D. Raymond)

	SeMet		Native
Diffraction data			
Space group	*P*1		*P*1
Unit cell lengths (Å) a, b, c	67.0, 69.5 80.5		67.1 69.6 80.6
Unit cell angles (°) α, β, γ	82.6, 70.2, 61.4		78.4 69.7 60.9
X-ray source	APS 23 ID-D		APS 23 ID-B
Wavelength (Å)	0.9794	0.9796	1.0333
d_{min} (Å)	2.44(2.53-2.44)[a]	2.44(2.53-2.44)	1.93(2.03-1.93)
Unique reflections	44,975	44,817	87,736
R_{merge}[b] %	0.16 (0.38)	0.15 (0.45)	0.08 (0.43)
Avg I/σ_I	10.1 (4.2)	14.2 (2.8)	9.6 (3.1)
Completeness (%)	96.6 (81.7)	97.0 (86.6)	97.1 (95.7)
Average redundancy	3.9 (3.8)	3.9 (3.8)	4.0 (3.9)
Refinement			
Data range (Å)	50.0 - 2.44		50.0 - 1.93
Reflections	41,208		83,342
R/R_{free}[c]	0.221/0.279		0.211/0.254
RMSD bond lengths (Å)	0.008		0.013
RMSD bond angles (°)	1.091		1.293
Avg. protein B-factor (Å^2)	32.5		29.9
Avg. solvent B-factor (Å^2)	37.4		35.0
Ramachandran agreement[d]			
Allowed (%)	98.0		99.6
Disallowed (%)	2.0		0.4
Protein atoms	6969		7565
Water molecules	191		616
Glycerol	0		4

[a]Values in parenthesis are for the outermost shell of data.

[b]$R_{merge} = \sum|I_i - \langle I \rangle| / \sum I_i$, where I_i is the intensity of the i^{th} observation and $\langle I \rangle$ is the mean intensity. Sums are taken over all reflections. R_{merge} values include anomalous scattering

[c]$R = \sum||F_o| - |F_c|| / \sum|F_o|$. R_{free} is calculated for a random 5% subset of the data that was excluded from refinement.

[d]Calculated with MolProbity[1].

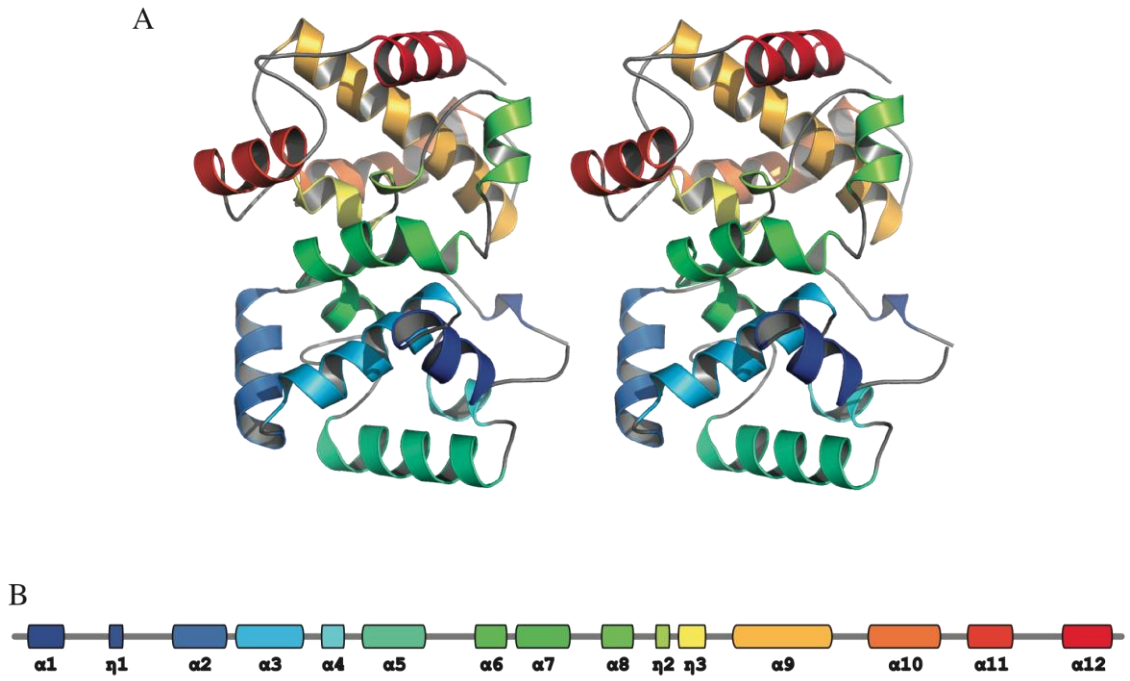

Figure 3.4. Structure of RVFV N monomer
(A) Polypeptide fold. The stereo ribbon diagram is colored as a rainbow from blue at the N terminus to red at the C terminus with loops in grey. Helix α7, (horizontal) in the center of the image, links the N-lobe at the bottom and the C-lobe at the top. **(B)** Diagram of helical secondary structure in the RVFN polypeptide. Colors are matched to (A). *(Contributed by D. Raymond)*

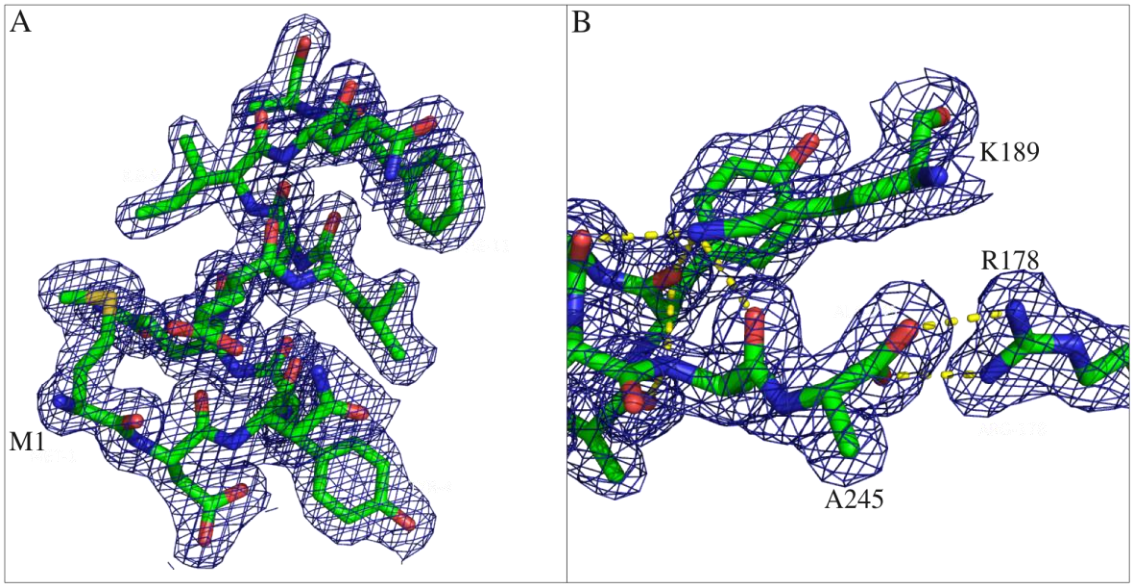

Figure 3.5. Electron density of RVFV N at the N and C-termini.
(A) $2F_o$-F_c map of the N-terminal helix contoured at 1σ. Residues 1-12 are shown in sticks. **(B)** 2Fo-Fc map of residues 241-245 at the C-termi- nus. Residues Arg178 and Lys189 are also depicted along with the salt bridge and hydrogen bonds they form with the C-terminus (Ala 245). *(Contributed by D. Raymond)*

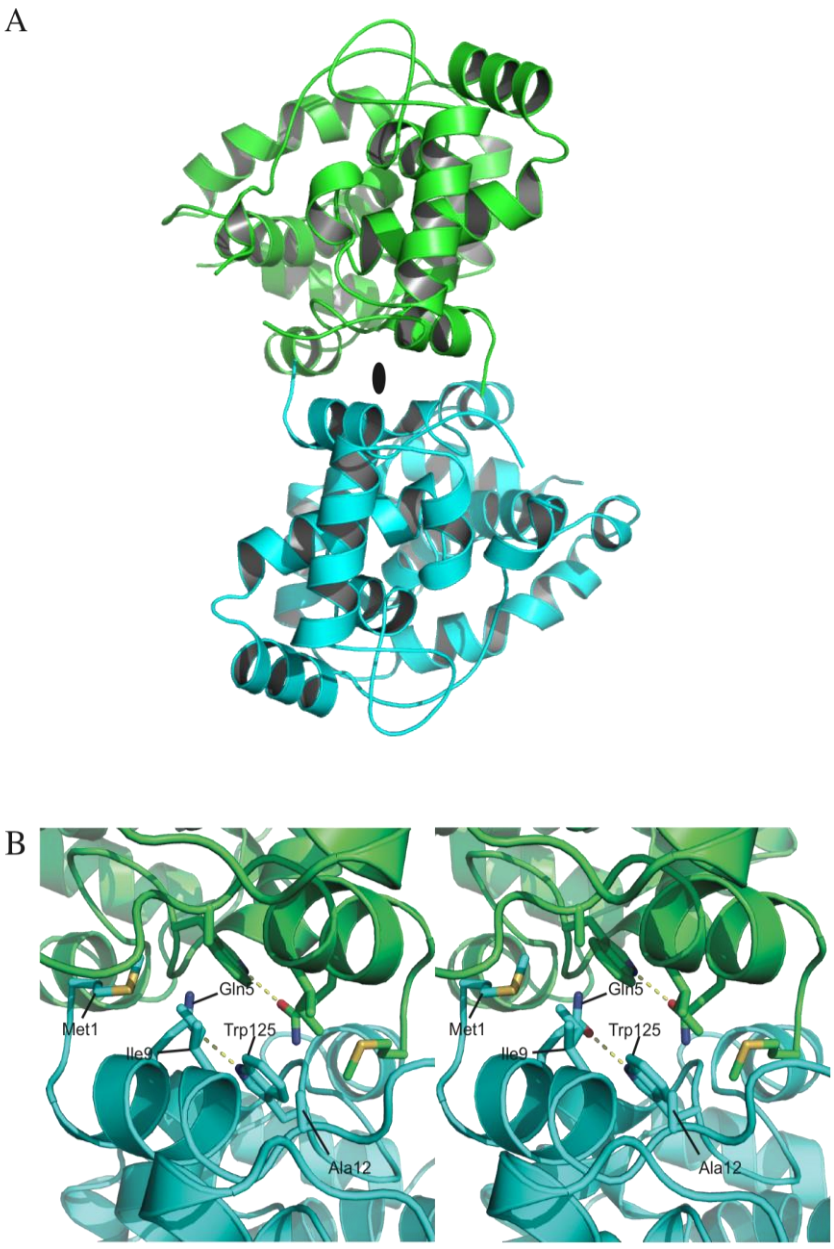

Figure 3.6. RVFV N dimer.
(A) Front view along the dimer axis. Monomers are in green and cyan and the molecular twofold is indicated by an ellipse. **(B)** Details of the dimer interface. The chains are colored as in (A), side chains with dimer contacts are shown in stick form in the stereo view. Hydrogen bonds are shown as dashed lines. *(Contributed by D. Raymond)*

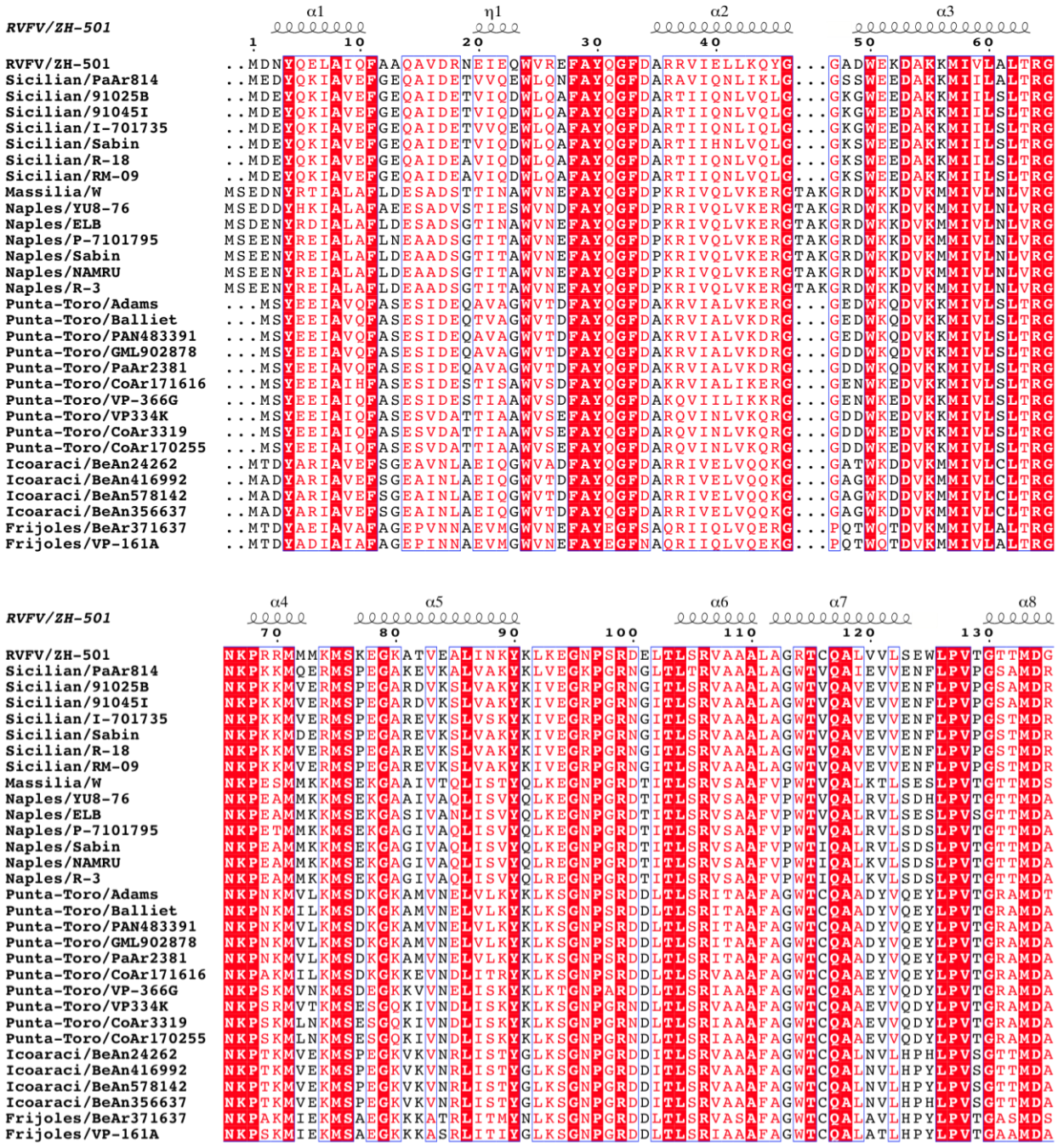
α1
η1
α2
α3
RVFV/ZH-501
1 10 20 30 40 50 60
RVFV/ZH-501 ..MDNYQELAIQFAAQAVDRNEIEQWVREFAYQGFDARRVIELLKQYG...GADWEKDAKKMIVLALTRG
Sicilian/PaAr814 ..MEDYQKIAVEFGEQAIDETVVQEWLQNFAYQGFDARAVIQNLIKLG...GSSWEEDAKKMIILALTRG
Sicilian/91025B ..MDEYQKIAVEFGEQAIDETVIQDWLQAFAYQGFDARTIIQNLVQLG...GKGWEEDAKKMIILSLTRG
Sicilian/91045I ..MDEYQKIAVEFGEQAIDETVIQDWLQAFAYQGFDARTIIQNLVQLG...GKGWEEDAKKMIILSLTRG
Sicilian/I-701735 ..MDEYQKIAVEFGEQAIDETVVQEWLQAFAYQGFDARTIIQNLIQLG...GKGWEEDAKKMIILSLTRG
Sicilian/Sabin ..MDEYQKIAVEFGEQAIDETVIQDWLQAFAYQGFDARTIIHNLVQLG...GKSWEEDAKKMIILSLTRG
Sicilian/R-18 ..MDEYQKIAVEFGEQAIDEAVIQDWLQAFAYQGFDARTIIQNLVQLG...GKSWEEDAKKMIILSLTRG
Sicilian/RM-09 ..MDEYQKIAVEFGEQAIDEAVIQDWLQAFAYQGFDARTIIQNLVQLG...GKSWEEDAKKMIILSLTRG
Massilia/W MSEDNYRTIALAFLDESADSTTINAWVNEFAYQGFDPKRIVQLVKERGTAKGRDWKKDVKMMIVLNLVRG
Naples/YU8-76 MSEDDYHKIALAFAEESADVSTIESWVNDFAYQGFDPRRIVQLVKERGTAKGRDWKKDVKMMIVLNLVRG
Naples/ELB MSDENYRDIALAFLDESADSGTINAWVNEFAYQGFDPKRIVQLVKERGTAKGRDWKKDVKMMIVLNLVRG
Naples/P-7101795 MSEENYREIALAFLNEAADSGTITAWVNEFAYQGFDPKRIVQLVKERGTAKGRDWKKDVKMMIVLNLVRG
Naples/Sabin MSEENYREIALAFLDEAADSGTITAWVNEFAYQGFDPKRIVQLVKERGTAKGRDWKKDVKMMIVLNLVRG
Naples/NAMRU MSEENYREIALAFLDEAADSGTITAWVNEFAYQGFDPKRIVQLVKERGTAKGRDWKKDVKMMIVLNLVRG
Naples/R-3 MSEENYREIALAFLDEAADSGTITAWVNEFAYQGFDPKRIVQLVKERGTAKGRDWKKDVKMMIVLNLVRG
Punta-Toro/Adams ...MSYEEIAVQFASESIDEQAVAGWVTDFAYQGFDAKRVIALVKERG...GEDWKQDVKKMIVLSLTRG
Punta-Toro/Balliet ...MSYEEIAVQFASESIDEQTVAGWVTDFAYQGFDAKRVIALVKDRG...GEDWKQDVKKMIVLSLTRG
Punta-Toro/PAN483391 ...MSYEEIAVQFASESIDEQAVAGWVTDFAYQGFDAKRVIALVKDRG...GEDWKQDVKKMIVLSLTRG
Punta-Toro/GML902878 ...MSYEEIAVQFASESIDEQAVAGWVTDFAYQGFDAKRVIALVKDRG...GDDWKQDVKKMIVLSLTRG
Punta-Toro/PaAr2381 ...MSYEEIAVQFASESIDEQAVAGWVTDFAYQGFDAKRVIALVKDRG...GDDWKQDVKKMIVLSLTRG
Punta-Toro/CoAr171616 ...MSYEEIAIHFASESIDESTISAWVSDFAYQGFDAKRVIALIKERG...GENWKEDVKKMIVLSLTRG
Punta-Toro/VP-366G ...MSYEEIAIQFASESIDESTIAAWVSDFAYQGFDAKQVIILIKKRG...GENWKEDVKKMIVLSLTRG
Punta-Toro/VP334K ...MSYEEIAIQFASESVDATTIAAWVSEFAYQGFDARQVINLVKQRG...GDDWKEDVKKMIVLSLTRG
Punta-Toro/CoAr3319 ...MSYEEIAIQFASESVDATTIAAWVSEFAYQGFDARQVINLVKQRG...GDDWKEDVKKMIVLSLTRG
Punta-Toro/CoAr170255 ...MSYEEIAIQFASESVDATTIAAWVSEFAYQGFDARQVINLVKQRG...GDDWKEDVKKMIVLSLTRG
Icoaraci/BeAn24262 ..MTDYARIAVEFSGEAVNLAEIQGWVADFAYQGFDARRIVELVQQKG...GATWKDDVKMMIVLCLTRG
Icoaraci/BeAn416992 ..MADYARIAVEFSGEAINLAEIQGWVTDFAYQGFDARRIVELVQQKG...GAGWKDDVKMMIVLCLTRG
Icoaraci/BeAn578142 ..MADYARIAVEFSGEAINLAEIQGWVTDFAYQGFDARRIVELVQQKG...GAGWKDDVKMMIVLCLTRG
Icoaraci/BeAn356637 ..MADYARIAVEFSGEAINLAEIQGWVTDFAYQGFDARRIVELVQQKG...GAGWKDDVKMMIVLCLTRG
Frijoles/BeAr371637 ..MTDYAEIAVAFAGEPVNNAEVMGWVNEFAYEGFSAQRIIQLVQERG...PQTWQTDVKMMIVLALTRG
Frijoles/VP-161A ..MTDYADIAIAFAGEPINNAEVMGWVNEFAYEGFNAQRIIQLVQEKG...PQTWQTDVKMMIVLALTRG
α4
α5
α6
α7
α8
RVFV/ZH-501
70 80 90 100 110 120 130
RVFV/ZH-501 NKPRRMMMKMSKEGKATVEALINKYKLKEGNPSRDELTLSRVAAALAGRTCQALVVLSEWLPVTGTTMDG
Sicilian/PaAr814 NKPKKMQERMSPEGAKEVKALVAKYKLVEGKPGRNGLTLTRVAAALAGWTVQAIEVVENFLPVPGSAMDR
Sicilian/91025B NKPKKMVERMSPECARDVKSLVAKYKIVEGRPGRNGITLSRVAAALAGWTVQAVEVVENFLPVPGSAMDR
Sicilian/91045I NKPKKMVERMSPEGARDVKSLVAKYKIVEGRPGRNGITLSRVAAALAGWTVQAVEVVENFLPVPGSAMDR
Sicilian/I-701735 NKPKKMVERMSPEGAREVKSLVSKYKIVEGRPGRNGITLSRVAAALAGWTVQAVEVVENFLPVPGSTMDR
Sicilian/Sabin NKPKKMDERMSPECAREVKSLVAKYKIVEGRPGRNGITLSRVAAALAGWTVQAVEVVENFLPVPGSTMDR
Sicilian/R-18 NKPKKMVERMSPEGAREVKSLVAKYKIVEGRPGRNGITLSRVAAALAGWTVQAVEVVENFLPVPGSTMDR
Sicilian/RM-09 NKPKKMVERMSPEGAREVKSLVAKYKIVEGRPGRNGITLSRVAAALAGWTVQAVEVVENFLPVPGSTMDR
Massilia/W NKPESMMKKMSEKCAAIVTQLISTYQLKEGNPGRDTITLSRVSAAFVPWTVQALKTLSESLPVTGTTMDS
Naples/YU8-76 NKPEAMMKKMSEKCAAIVAQLISVYQLKEGNPGRDTITLSRVSAAFVPWTVQALRVLSDHLPVTGTTMDA
Naples/ELB NKPEAMMKKMSEKCASIVANLISVYQLKEGNPGRDTITLSRVSAAFVPWTVQALRVLSESLPVSGTTMDA
Naples/P-7101795 NKPETMMKKMSEKCAGIVAQLISVYQLKEGNPGRDTITLSRVSAAFVPWTVQALRVLSDSLPVTGTTMDA
Naples/Sabin NKPEAMMKKMSEKCAGIVAQLISVYQLKEGNPGRDTITLSRVSAAFVPWTIQALRVLSDSLPVTGTTMDA
Naples/NAMRU NKPEAMMKKMSEKCAGIVAQLISVYQLREGNPGRDTITLSRVSAAFVPWTIQALKVLSDSLPVTGTTMDA
Naples/R-3 NKPEAMMKKMSEKCAGIVAQLISVYQLREGNPGRDTITLSRVSAAFVPWTIQALKVLSDSLPVTGTTMDA
Punta-Toro/Adams NKPNKMVLKMSDKCKAMVNELVLKYKLKSGNPSRDDLTLSRITAAFAGWTCQAADYVQEYLPVTGRAMDT
Punta-Toro/Balliet NKPNKMILKMSDKCKAMVNELVLKYKLKSGNPSRDDLTLSRITAAFAGWTCQAADYVQEYLPVTGRAMDA
Punta-Toro/PAN483391 NKPNKMVLKMSDKCKAMVNELVLKYKLKSGNPSRDDLTLSRITAAFAGWTCQAADYVQEYLPVTGRAMDA
Punta-Toro/GML902878 NKPNKMVLKMSDKCKAMVNELVLKYKLKSGNPSRDDLTLSRITAAFAGWTCQAADYVQEYLPVTGRAMDA
Punta-Toro/PaAr2381 NKPNKMVLKMSDKCKAMVNELVLKYKLKSGNPSRDDLTLSRITAAFAGWTCQAADYVQEYLPVTGRAMDA
Punta-Toro/CoAr171616 NKPAKMILKMSDKCKKEVNDLITRYKLKSGNPSRDDLTLSRVAAAFAGWTCQAAEYVQEYLPVTGRAMDA
Punta-Toro/VP-366G NKPSKMVNKMSDECKKVVNELISKYKLKTGNPARDDLTLSRIAAAFAGWTCQAAEYVQDYLPVTGRAMDA
Punta-Toro/VP334K NKPSRMVTKMSESCQKIVNDLISKYKLKSGNPGRNDLTLSRVAAAFAGWTCQAAEVVQDYLPVTGRAMDA
Punta-Toro/CoAr3319 NKPSKMLNKMSESCQKIVNDLISKYKLKSGNPGRNDLTLSRIAAAFAGWTCQAAEVVQDYLPVTGRAMDA
Punta-Toro/CoAr170255 NKPSKMLNKMSESCQKIVNDLISKYKLKSGNPGRNDLTLSRIAAAFAGWTCQAAEVVQDYLPVTGRAMDA
Icoaraci/BeAn24262 NKPTKMVEKMSPECKVKVNRLISTYGLKSGNPGRDDITLSRVAAAFAGWTCQALNVLHPHLPVSGTTMDA
Icoaraci/BeAn416992 NKPTKMVEKMSPECKVKVNRLISTYGLKSGNPGRDDITLSRVAAAFAGWTCQALNVLHPYLPVSGTTMDA
Icoaraci/BeAn578142 NKPTKMVEKMSPEGKVKVNRLISTYGLKSGNPGRDDITLSRVAAAFAGWTCQALNVLHPYLPVSGTTMDA
Icoaraci/BeAn356637 NKPTKMVEKMSPECKVKVNRLISTYGLKSGNPGRDDITLSRVAAAFAGWTCQALNVLHPHLPVSGTTMDA
Frijoles/BeAr371637 NKPAKMIEKMSAECKKKATRLITMYNLKSGNPGRDDLTLSRVASAFAGWTCQALAVLHPYLPVTGASMDS
Frijoles/VP-161A NKPSKMIEKMSAEGKKKASRLITIYGLKSGNPGRDDLTLSRIAAAFAGWTCQALATLHPYLPVTGAAMDA

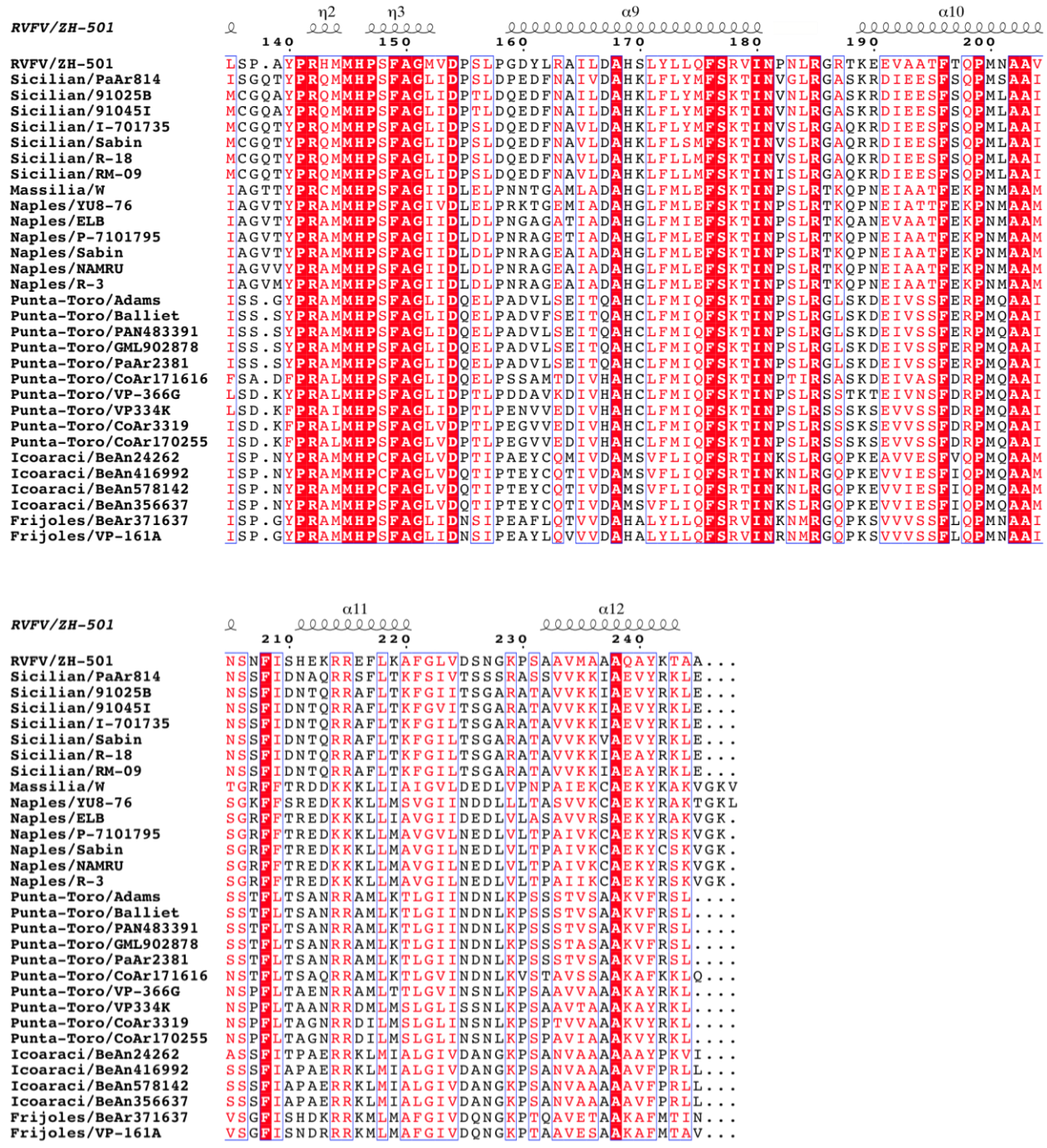

Figure 3.7. Sequence alignment of N from the phlebovirus genus.
Invariant residues are show in white with red background, consensus residues are shown in red with white background, and variable residues are show in black with white background. The observed α and η (3_{10}) helices are indicated above the alignment. Accession numbers are listed in Table S3. The sequence alignment was generated by clust- alW[2] and the secondary structure annotations were assigned using ESPript[3]. *(Contributed by D. Raymond)*

Serocomplex	Virus	Strain	Accession	AA Length
Rift Valley fever	*RVF*	ZH-501	ABD38729	245
Frijoles	*Joa*	BeAr371637	ABQ23528	245
Frijoles	*Frijoles*	VP-161A	ABQ23526	245
Icoaraci	*Icoaraci*	BeAn24262	ABQ23524	245
Icoaraci	*Belterra*	BeAn356637	ABQ23522	245
Icoaraci	*Salobo*	BeAn416992	ABQ23520	245
Icoaraci	*Salobo*	BeAn578142	ABQ23518	245
Massilia	*Massalia*	W	ABG56148	254
Naples	*Sandfly Fever Naples-like*	NAMRU	ABQ23544	253
Naples	*Sandfly Fever Naples-like*	P-7101795	ABQ23548	253
Naples	*Sandfly Fever Naples-like*	R-3	ABQ23552	253
Naples	*Sandfly Fever Naples*	Sabin	ABQ23546	253
Naples	*Toscana*	ELB	ABQ23554	253
Naples	*Sandfly Fever Naples-like*	YU 8-76	ABQ23550	254
Punta Toro	*Buenaventura*	Co Ar 3319	ABQ23566	243
Punta Toro	*Co Ar 170255*	Co Ar 170255	ABQ23568	243
Punta Toro	*Co Ar 171616*	Co Ar 171616	ABQ23560	244
Punta Toro	*GML 902878*	GML 902878	ABQ23562	243
Punta Toro	*Pa Ar 2381*	Pa Ar 2381	ABQ23570	243
Punta Toro	*PAN 483391*	PAN 483391	ABQ23576	243
Punta Toro	*Punta Toro*	Balliet	P03515	243
Punta Toro	*Punta Toro*	Adams	ABQ23558	243
Punta Toro	*VP 334K*	VP 334K	ABQ23572	243
Punta Toro	*VP-366G*	VP-366G	ABQ23564	243
Sicilian	*Corfou*	Pa Ar 814	ABQ23530	246
Sicilian	*Sandfly Fever Sicilian-like*	91025B	ABQ23534	246
Sicilian	*Sandfly Fever Sicilian-like*	91045I	ABQ23536	246
Sicilian	*Sandfly Fever Sicilian-like*	I-701735	ABQ23542	246
Sicilian	*Sandfly Fever Sicilian-like*	R-18	ABQ23540	246
Sicilian	*Sandfly Fever Sicilian-like*	RM-09	ABQ23538	246
Sicilian	*Sandfly Fever Sicilian*	Sabin	CAH18876	246

Table 3.2. Phlebovirus N catagorized by serocomplex.
Phlebovirus N catagorized by serocomplex. The virus names, strains, accession numbers, and lengths of N (amino acids) are listed. (Adapted from Xu F et al. J Gen Virol (2007)).

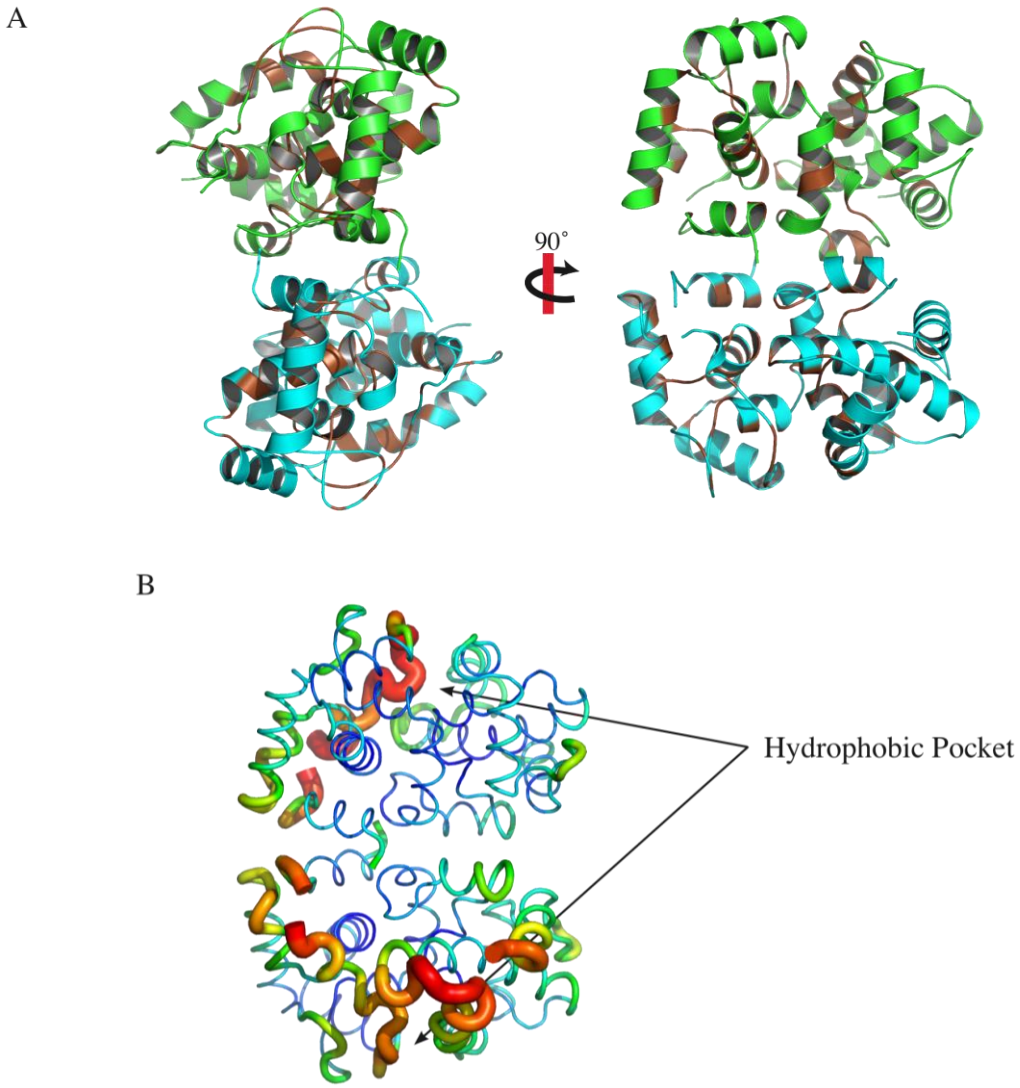

Figure 3.8. Conservation and atomic mobility in the RVFV N dimer.
(A) Sequence conservation. Front and side views of the N dimer with chain A and B colored green and cyan, respectively. The residues that are invariant among phleboviruses N (brown) are located primarily in the core of the protein. **(B)** Atomic mobility. Side view of the N dimer is colored as a rainbow according to average atomic B factors from low B (blue, narrow tube) to high B (red, wide tube). *(Contributed by D. Raymond)*

Allele	RLU (Std. dev.)	% Activity
WT	773 (169)	100
W125A	26.1 (2.8)	3.4
R178E	51.4 (9.4)	6.7
R178Q	193 (27)	25
No N	1.0 (0.1)	0.1

Table 3.3. Formation of dimer and C-terminal salt bridge are required for N function.
Wild type (WT), W125A, R178Q, and R178E N alleles were analyzed for function by the transcription assay described in the Material and Methods. Renilla luciferase (RLU) activity was measured at 48 h post-infection and is expressed relative to the no-N control and as a percent of WT activity. Data are the average of six experiments, with standard deviations in parentheses. *(Contributed by M. Piper)*

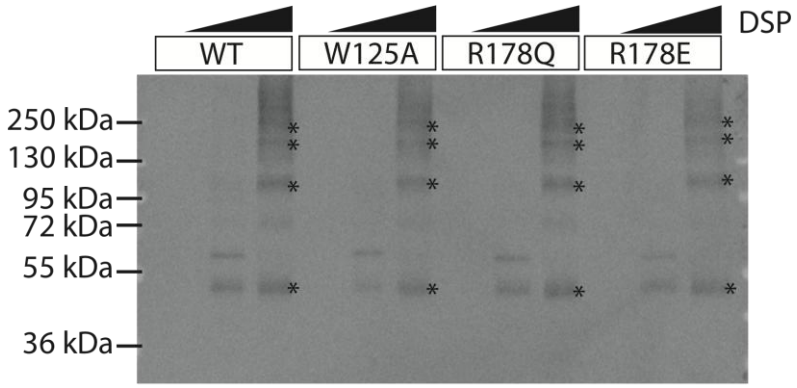

Figure 3.9. Protein levels and multimer formation for N mutant and wild type alleles.
The same cells used for the RdRp transcription assay (Table 3.2) were also analyzed for protein expression and N complex formation. Extracts were cross-linked using 0.0, 5.0 or 20.0 μM DSP. Protein complexes were then separated by SDS-PAGE and visualized by immunoblot. The dominant cross-linked species are indicated by asterisks (*). *(Contributed by M. Piper)*

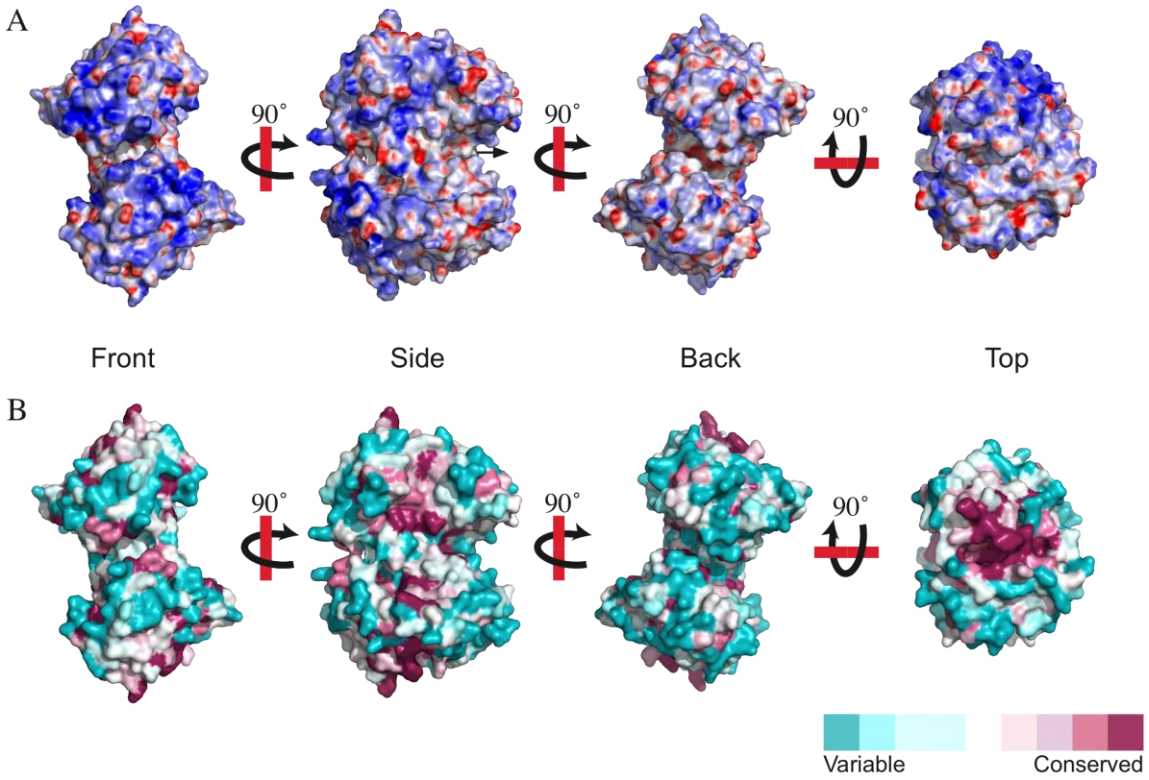

Figure 3.10. Properties of the RVFV N surface.
(A) Electrostatic surface potential. The surface potential from –20 kT in red to +20 kT in blue is shown for the front, side, back, and top of the RVFV N dimer. The front view is along the dimer axis as in (3A). **(B)** Sequence conservation. The surface of the RVFV N dimer is colored by conservation among phleboviruses N with burgundy most conserved and cyan most variable. *(Contributed by D. Raymond)*

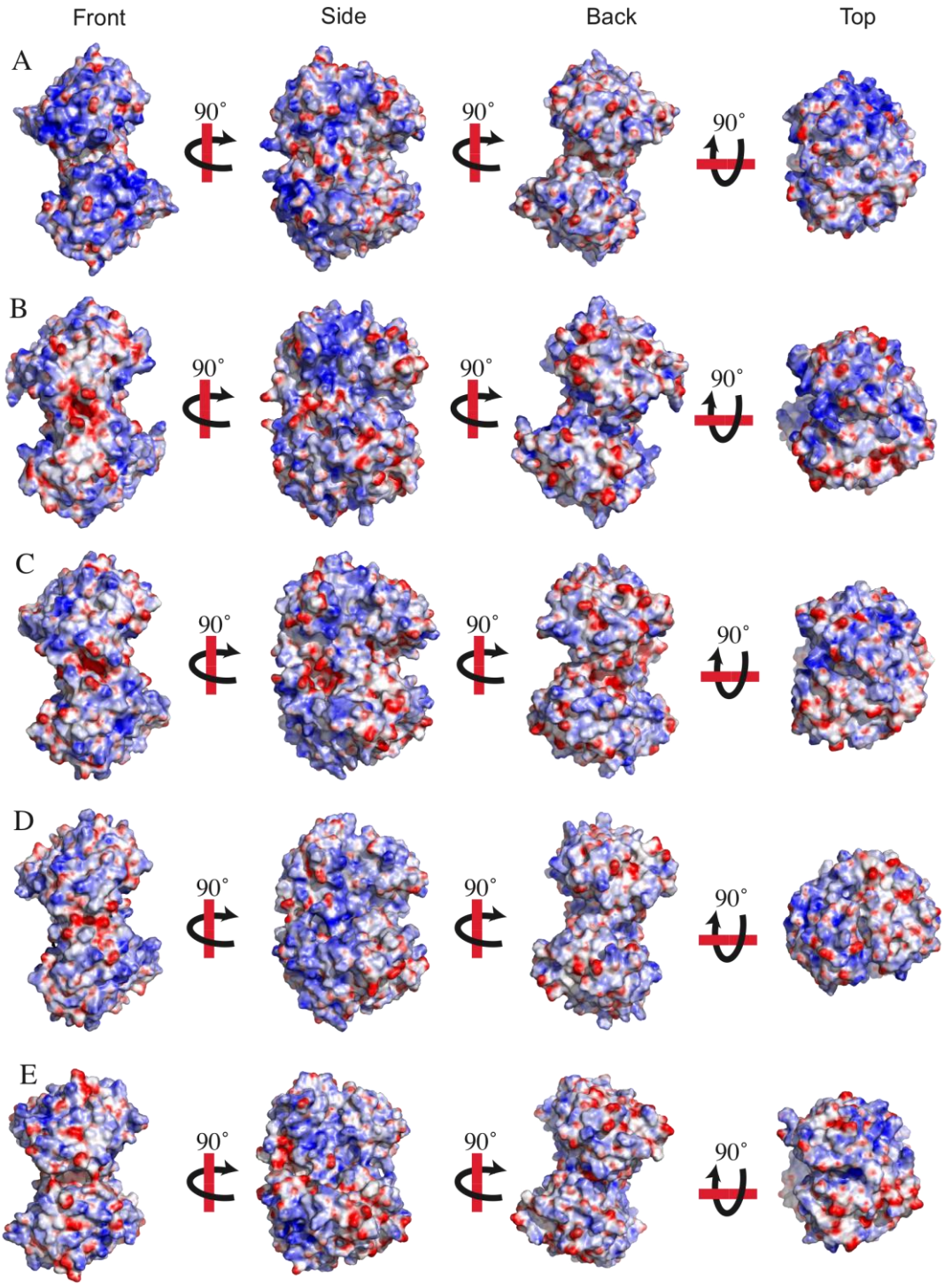

Figure 3.11. Homology models of N dimers from representative phleboviruses.
Electrostatic potential surface is shown for of the front (left), side, back and top (right) of phlebovirus N dimers from **(A)** RVFV (ZH-501) crystal structure, **(B)** Naples (ELB), **(C)** Punta Toro (Adames), **(D)** Icoaraci (BeAn356637), and **(E)** Uukuniemi (Uukuniemi). Surface potential is shown by color from -20 kT in red to +20 kT in blue. *(Contributed by D. Raymond)*

Chapter 4

Encapsidated Genome Triggers Cellular Release of the Rift Valley Fever Virus

Introduction

Rift Valley fever virus (RVFV) is an aerosol- and mosquito-borne virus endemic to sub-Saharan Africa (40). RVFV causes periodic, explosive epizootics, affecting livestock and humans (40). Sheep and cattle are particularly susceptible to the virus, with abortion rates approaching 100% and high mortality rates among young animals (30). By contrast, most humans infected with RVFV have a flu-like illness (40). However, a small percentage of cases are more severe and include manifestations such as, hemorrhagic disease and encephalitis (29, 32, 120). Despite the severity of the disease to the economy and human health, there are no USDA or FDA-approved therapeutic or prophylactic treatments. A better understanding of the RVFV replication cycle may lead to the identification of novel therapeutic targets. In this study, we have identified roles for each of the viral structural components in the assembly and release of the RVFV and have identified a potential conserved target for therapeutic development.

RVFV is a segmented, negative-sense RNA virus belonging to the family *Bunyaviridae*, genus *Phlebovirus*. The 12 kilobase genome is comprised of three segments termed L, M and S, which encode for the RNA-dependent RNA polymerase (RdRp), envelope glycoproteins (Gn/Gc) and nucleocapsid protein (N), respectively (40). The S and M segments also encode nonstructural proteins known as NSs and NSm, however these proteins are dispensable for RVFV replication in cell culture (40, 47, 48, 54, 121). Upon entry into host cells, the encapsidated genome and RdRp are released into the cytoplasm where transcription and replication of the viral genome occurs (122). The RdRp acts as both transcriptase and replicase (85), but requires N for both activities (57). RdRp and N do not contain signal peptides, and presumably translation of the

RdRp and N occurs in the cytoplasm. The glycoproteins enter the secretory pathway as a precursor polyprotein, which is cleaved by signal peptidase into the mature Gn and Gc proteins (49). Gn and Gc form a complex and localize to the Golgi apparatus, the site of virus assembly, due to a localization signal on Gn (49, 58, 123). It is not known how the encapsidated genome and RdRp are recruited to the Golgi apparatus for virus assembly or which viral components are involved in the cellular release of virus.

Utilizing a Rift Valley fever virus-like particle (RVF-VLP) system, we have determined that the encapsidated genome acts as the primary stimulus for RVFV release from the cell, illustrating a novel, elegant mechanism for the efficient release of infectious particles. We demonstrate that Gn is necessary and sufficient for packaging of the RdRp and encapsidated genome. Furthermore, we show that distinct and non-overlapping regions of the Gn cytosolic tail are responsible for binding to RdRp and encapsidated genome.

Results

RVFV and RVF-VLPs have similar morphology and protein content.

A T7 RNA polymerase-dependent system was used for the efficient generation of RVF-VLPs (Chapter 2). Briefly, RVF-VLPs were produced by expression of an S segment-based minigenome (pSTrRVFV-SΔNΔNSs::hRLuc), N, RdRp, Gn, and Gc in BSR-T7/5 cells. The minigenome contains a humanized renilla luciferase (RLuc) gene in place of the NSs ORF, and an internal deletion in the N gene that prevents expression of N. RVFV and RVF-VLPs were harvested by ultracentrifugation and analyzed for particle morphology by transmission electron microscopy (Fig. 4.1A) or for protein composition by immunoblot (Fig. 4.1B). RVFV and the RVF-VLPs exhibited similar morphology by transmission electron microscopy, although the RVF-VLPs were slightly larger than RVFV. The difference in size may reflect the fact that RVF-VLPs package only the S segment-based minigenome, while RVFV packages all viral genomic segments. RVFV has been shown to package multiple copies of a single genomic segment, and it is possible that the RVF-VLPs may package more S segments than the total number of segments packaged by RVFV.

All of the viral proteins were detected in the cell lysates (C) and within the harvested particles (P) in similar relative levels for RVFV and the RVF-VLPs (Fig. 4.1B). In addition to similarities in particle morphology and protein composition, RVFV and the RVF-VLPs are antigenically indistinguishable and respond similarly to inhibitor compounds (Chapter 2). All of our data suggest the RVF-VLPs function similar to virus and will be useful in dissecting steps of the RVFV replication cycle.

Gn is sufficient for recruitment of the RdRp to the Golgi apparatus for assembly.

Replication and transcription of the viral genome by the RdRp occurs in the cytoplasm, while the assembly of virus particles takes place at the Golgi apparatus (40). We investigated the localization of the RdRp in the absence of other viral proteins. While it is believed that the RdRp of bunyaviruses are translated on free ribosomes in the cytoplasm (122), the localization of wild-type RVFV RdRp has not been investigated previously. When expressed in the absence of other viral proteins, the RVFV RdRp was found distributed diffusely throughout the cytoplasm (Fig. 4.2A). The RdRp did not co-localize with the resident Golgi protein, GS-28 (Fig. 4.2A). By contrast, the envelope glycoprotein, Gn, co-localized with β-COP, another resident Golgi protein in agreement with previously published reports (Fig. 4.2A) (123) . The C-terminal cytoplasmic tails of the envelope glycoproteins are presumably available for interaction with the RdRp. To determine whether the glycoproteins are capable of targeting the RdRp to the Golgi apparatus, the RdRp was expressed together with Gn and Gc. RVFV Gn and Gc are both integral membrane proteins that are expressed as a polyprotein that enters the secretory system (124). The polyprotein is cleaved by signal peptidase, generating the mature Gn and Gc proteins (49), and it is believed that the mature Gn glycoprotein retains the signal peptide of Gc (49, 125). Expression of the glycoproteins along with the RdRp resulted in localization of RdRp to a focus of intense staining co-localizing with the Gn and Gc complex at the Golgi apparatus (Fig. 4.2B), indicating that one or both of the glycoproteins are necessary for recruitment of RdRp to the Golgi for virus assembly. When Gc was expressed alone with the RdRp, the cytoplasmic localization of the RdRp was not altered (Fig. 4.2B). By contrast, co-expression of Gn with the RdRp was sufficient to target the RdRp to the site of assembly (Fig. 4.2B). Therefore, Gn is necessary and sufficient for the recruitment of RdRp to the Golgi apparatus.

To identify the domain of Gn that interacts with RdRp, a mutant Gn allele that lacks the last 40 amino acids of the cytoplasmic tail and the Gc signal peptide (GnK48) was investigated for its ability to interact with the RdRp. Although the GnK48 mutant localizes properly to the Golgi apparatus (123) and is capable of forming a complex with Gc (data not shown), it was unable to recruit the RdRp to the Golgi apparatus (Fig. 4.2B). Therefore, the last 40 amino acids of the Gn cytoplasmic tail and/or the Gc signal peptide is necessary for the recruitment of the RdRp to the Golgi apparatus.

Generation of infectious RVF-VLPs requires packaging of a catalytically active RdRp.

To investigate whether assembly of the RdRp at the Golgi apparatus corresponded to packaging of the RdRp into particles, we investigated the protein profiles of the RVF-VLPs containing all viral components (WT), lacking the RdRp (-RdRp), or containing the GnK48 allele (GnK48). BSR-T7/5 cells were transfected with minigenome, pN, pRdRp, pGn, and pGc or one or more of the components were replaced with an equivalent amount of empty vector or pGnK48. RVF-VLPs were visualized by transmission electron microscopy and protein composition was determined by immunoblot. Particles were generated for all conditions and there were no gross differences in size or morphology (Fig. 4.3A), indicating the RdRp is not required for generation of particles. As expected, no RdRp signal was observed with RVF-VLPs that lacked RdRp (-RdRp) or contained GnK48, but RdRp was present when all components were expressed (WT) (Fig. 4.3B). Next, we determined whether a catalytically active RdRp is required for interaction with Gn. We investigated two RdRp catalytic domain mutants, RdRp^{cat1} and RdRp^{cat2} (126), for recruitment by Gn to the Golgi apparatus. Using immunofluorescence microscopy, we found that Gn co-localized with both RdRp^{cat1} and RdRp^{cat2}, indicating that RdRp catalytic activity is not required for interaction with Gn (Fig. 4.3C). These results are supported by our immunoblot results showing that RdRp^{cat1} is packaged into RVF-VLPs (Fig. 4.3B). Finally, we investigated whether catalytically active RdRp co-expressed with N in target cells *(trans* expression*)* could rescue infectivity of RdRp-deficient or RdRp^{cat1} RVF-VLPs. Wild-type RVF-VLPs were capable of infecting untransfected target cells and expressing the RLuc reporter at levels 700-fold above background (Table 4.1). Transcription of the RLuc reporter in target cells could be enhanced through expression of a catalytically active RdRp with N in *trans*, increasing RLuc signal to

4,000-fold background levels (Table 4.1). Expression of a catalytically inactive RdRp mutant with N in target cells did not enhance RLuc signal as compared to untransfected target cells (Table 4.1). These results indicate the catalytically active RdRp expressed in *trans* could access the encapsidated genome delivered by the wild-type RVF-VLPs for enhancement of RLuc expression (Table 4.1). However, RVF-VLPs packaging $RdRp^{cat1}$ or RVF-VLPs lacking the RdRp (-RdRp) could not be complemented in *trans* with an active RdRp (Table 4.1). Wild-type RVF-VLPs were the only RVF-VLPs to generate a significant RLuc signal as compared to background (-Gn/-Gc) (Table 4.1). Therefore, virion-derived, catalytically active RdRp must be present in order for replication to begin in a target cell.

Encapsidated genome is packaged into virions by Gn.

After transcription and replication of the viral genome in the cytoplasm, we hypothesized that encapsidated genome and RdRp were recruited as a complex to the Golgi apparatus for assembly through interaction between the RdRp and Gn. However, we discovered that the encapsidated genome could be packaged into RVF-VLPs lacking the RdRp (Fig. 4.3B, -RdRp and GnK48). Therefore, the encapsidated genome and the RdRp can be packaged independently. Phlebovirus N localizes to the cytoplasm when expressed alone (data not shown), similar to N of tomato spotted wilt virus (*Tospovirus* genus) (127) and La Crosse virus (*Orthobunyavirus* genus) (128), but in contrast to Hantaan and Black Creek Canal viruses N (*Hantavirus* genus) (129, 130). Therefore, N from phleboviruses presumably interact with one or both of the envelope glycoproteins in order to be assembled into virions. The GnK48 allele was able to package RVFV N (Fig. 4.3B), which indicates that the last 40 amino acids of the 70 amino acid Gn cytoplasmic tail and the Gc signal peptide are not required for packaging of N. Accordingly, Gc and/or the first 30 amino acids of the Gn cytoplasmic tail appear necessary for its packaging. To determine whether Gn or Gc is involved in N packaging, we transfected cells with all viral components or equivalent amounts of plasmid encoding the GcW1 allele or empty vector. GcW1 has a premature stop codon at Trp1189, which deletes the predicted Gc cytoplasmic domain in its entirety. Particles lacking Gn or Gc, or containing GcW1, were analyzed for morphology and protein content (Fig. 4.4A and B). All conditions produced RVF-VLPs as determined by transmission electron microscopy (Fig.

4.4A), except no particles could be found when either both glycoproteins or N were omitted. RVF-VLPs lacking either Gn or Gc were smaller than wild-type RVF-VLPs (Fig. 4.4A), possibly due to differences in the packing of glycoproteins in the envelope. The level of glycoproteins expressed in the transfected cells varied by experimental condition (Fig. 4.4B). Co-expression of full-length Gn and Gc was required for high-level expression of each glycoprotein. Previous studies with the Bunyamwera virus (*Bunyaviridae* family) identified a chaperone-like role of Gn in the folding of Gc, and the requirement of the Gc ectodomain, which extends into the ER/ Golgi lumen, for efficient Golgi trafficking of Gn (131, 132). Therefore, these results were not surprising. The average glycoprotein signal within RVF-VLPs generated with Gn or Gc alone was near background levels (Fig 4.4B). Interestingly, N was still packaged into RVF-VLPs that lack Gc (Fig. 4.4B). By contrast, no N was found in RVF-VLPs that lacked Gn (Fig. 4.4B), demonstrating that Gn is necessary and sufficient for packaging of N, presumably in the form of encapsidated genome. When Gn was expressed with GcW1, both N and the RdRp were packaged into RVF-VLPs, supporting the view that Gn alone recruits both encapsidated genome and RdRp (Fig 4.4B). Consistent with the immunoblot results (Fig. 4.4B), the GcW1 RVF-VLPs were infectious and yielded RLuc signals significantly above background levels in target cells complemented in *trans* with active RdRp and N (Table 4.2). Based on these data we can conclude that Gn is capable of packaging the encapsidated genome in the absence of Gc. However, generation of infectious particles requires co-expression of the ecto- and transmembrane domains of Gc.

Encapsidated genome triggers cellular release of virus.

Gn can package both the RdRp and encapsidated genome independently into RVF-VLPs. Therefore, we investigated the individual roles of each of these viral components in the release of RVF-VLPs from cells. To determine the minimal viral components necessary for the efficient cellular release of RVF-VLPs, cells were transfected with minigenome, pN, pRdRp, pGn, and pGc, or one or more of the constructs were replaced by an equivalent amount of empty vector. The RVF-VLPs were visualized by transmission electron microscopy, analyzed for protein content by immunoblot, and examined for infectivity by RLuc expression in target cells. RVF-VLPs were visualized by transmission electron microscopy for all conditions; however, no

particles could be found when both envelope glycoproteins or N were absent (data not shown). The RVF-VLPs did not differ morphologically from RVFV (Fig. 4.1). When wild-type viral proteins and genome were expressed, RVF-VLPs were released from the cell and all viral proteins could be visualized (Fig. 4.1). No particles were visualized by electron microscopy when the genome, N, and RdRp, which form the viral ribonucleoprotein complex, were expressed without the envelope glycoproteins (-Gn/-Gc) (data not shown) and there was no expression of the RLuc reporter above background levels in target cells (Table 4.3). Our results corroborate the results of previous findings that ribonucleoprotein complexes are not released from the cell in the absence of glycoproteins (133). Additionally, RVF-VLPs lacking N produced no RLuc signal above background, demonstrating that naked genome is not packaged and/or is not infectious (Table 4.3).

To determine which viral components are necessary for efficient RVF-VLP release, we quantified RVF-VLP release efficiency for all experimental conditions. For the purpose of this analysis we equated RVF-VLP release with Gn/Gc levels. Gn/Gc expression levels from the immunoblots of the RVF-VLPs were measured and normalized to expression levels in transfected cells. The experimental condition that included all structural proteins and genome (WT) was designated as 100% release efficiency, and the condition in which both envelope glycoproteins were omitted from the transfection (-Gn/Gc) was considered background (Fig. 4.5B, Table 4.4). The samples lacking N or the genome exhibited average release efficiencies of only 15.6 and 18.1%, respectively, compared to wild-type (Table 4.4). These efficiencies were similar to when the entire ribonucleoprotein complex was absent (Table 4.4, -RNPC). Our results demonstrate an absolute requirement for both N and the genome, presumably in the form of encapsidated genome, for efficient virus release. Conversely, the absence of RdRp did not significantly affect the efficiency of release of the glycoproteins (Fig. 4.5B and Table 4.4), indicating that RdRp does not play a critical role in viral budding or release. In all individual experiments, we detected increased release efficiency for RdRp-deficient RVF-VLPs, with average release efficiency corresponding to 169.5% of wild-type RVF-VLPs, although the increase was not statistically significant (Table 4.4). While particles can be generated at low levels lacking either Gn or Gc (Fig. 4.4A), the amount of Gn or

Gc in RVF-VLPs was at or below the limit of detection by immunoblot; therefore, release efficiencies could not be calculated. The RVF-VLPs lacking the cytoplasmic portions of Gn or Gc exhibited decreased release efficiencies in all individual experiments, but only for Gn was this significant (Table 4.4). The encapsidated genome is packaged in both conditions (Fig. 4.3B and 4.4B); therefore, the glycoprotein cytoplasmic tails likely perform additional functions in the release process. These results indicate that genome and N, presumably in the form of encapsidated genome, are required but RdRp is dispensable for efficient RVF-VLP release.

Discussion

The encapsidated genome of RVFV acts as a trigger for the cellular release of virus. Viral genomes have not been implicated in stimulating the budding and/or release of any negative or positive-sense RNA virus prior to this report. Our results suggest a model for RVFV assembly and release that is diagrammed in Figure 4.6. The envelope glycoproteins enter the secretory system as a polyprotein and are then cleaved by signal peptidase to yield mature Gn and Gc (49). Gn and Gc form a heteromeric complex in the endoplasmic reticulum and localize in steady-state to the Golgi apparatus by virtue of a signal found on Gn (Fig. 4.6, #1) (123). The cytoplasmic RdRp and encapsidated genome are recruited to the site of assembly through independent interactions with Gn (Fig. 4.6, #2). Multiple interactions between the encapsidated genomic segments and Gn proteins induce membrane curvature and trigger the budding of viral particles into the lumen of the Golgi apparatus (Fig. 4.6, #3), followed by release of virus from the cell (Fig. 4.6, #4).

With the encapsidated genome acting as the stimulus for budding, nearly all RVFV particles should contain genome. Thus, it is a reasonable expectation that most particles should be infectious. While most enveloped, RNA viruses typically yield particle-to-plaque-forming unit (pfu) ratios in the tens or hundreds (134-137), studies with Bunyamwera virus (*Orthobunyavirus* genus) determined that the particle-to-pfu ratio approaches one (138). We propose that efficient generation of infectious particles is achieved through the encapsidated genome promoting the cellular release of virus. The L, M, and S segments are proposed to be packaged at a molar ratio of approximately 1:4:4 in RVFV particles (1 L segment, 4 M segments, 4 S segments) (41). Therefore, we

hypothesize that there is a minimum amount of encapsidated genome (~28 kilobases) necessary to induce sufficient membrane curvature at the Golgi apparatus; however, we have no data to support or contradict this hypothesis. We propose the interactions between the encapsidated genomic segments and multiple Gn proteins results in accumulation of the glycoproteins and ribonucleoprotein complexes at specific areas of the Golgi apparatus, causing a change in membrane curvature and virus particle budding into the Golgi lumen. The virus buds when the critical quantity of genome is bound.

Our results support studies performed by Liu et. al. using a baculovirus expression system for generation of RVF-VLPs in insect cells. Liu et. al. found that particles could be generated through expression of Gn and/or Gc with N. Similarly, we could not identify any particles by electron microscopy unless N and Gn or Gc were expressed. Based on their ability to visualize particles, Liu et. al. concluded that only N and the envelope glycoproteins were required for efficient generation of particles (73). Liu et. al. did not calculate release efficiency of RVF-VLPs, so the viral components required for efficient release could not be determined. Similar to Liu et. al., we observed particles that lacked genome using EM (Fig. 4.5); however, our quantitative analysis indicates that genome, in addition to N, is absolutely required for the efficient cellular release of virus (Table 4.4).

Most RNA viruses require a matrix protein for the packaging of the ribonucleoprotein complexes and release of viral particles (40, 139-152), however viruses of the *Bunyaviridae* family do not encode a matrix protein. Based on our results, the Gn cytoplasmic tail appears to function in place of matrix and interacts directly with the ribonucleoprotein complexes and RdRp. We identified Gn as being necessary and sufficient for the assembly and packaging of the RdRp and the encapsidated genome into particles. RdRp could be recruited to the Golgi apparatus and packaged into virions by full-length Gn. However, the RdRp could not be packaged by a Gn allele (GnK48) that lacked the last 40 amino acids of the cytoplasmic tail and the Gc signal peptide, although particles were formed. These results suggest that the interaction domain of Gn with the RdRp contains the C-terminal half of the Gn cytoplasmic tail, since the Gc signal peptide likely remains in the membrane and thus could not interact with cytoplasmic RdRp. By contrast, N, presumably bound to genome, could be packaged into virions by the

truncated Gn allele (GnK48). This result indicates that the interaction domain of Gn with the encapsidated genome is located within the first 30 amino acids of the cytoplasmic tail. Thus, different regions of the Gn cytoplasmic tail are required for independent interactions with RdRp and the encapsidated genome. The Gn interaction domain for the encapsidated genome corresponds to a region that is highly hydrophobic in RVFV Gn. The hydrophobic character of this domain is conserved amongst phleboviruses (123) and could function in protein-protein interactions with N. In concert with our study, Raymond et. al. (Chapter 3) have crystallized the RVFV N and discovered a hydrophobic pocket that is highly conserved amongst phlebovirus N. This hydrophobic pocket is dynamic and likely to be involved in protein-protein interactions (Chapter 3). We hypothesize that the hydrophobic pocket of N interacts with the hydrophobic residues of the Gn cytoplasmic tail for the packaging of the encapsidated genome and for triggering virus release. Studies performed with the Uukuniemi virus (*Phlebovirus* genus) similarly found that the Gn cytoplasmic tail to be required for the packaging of N, but identified a different region to be important for this interaction (86). However, the envelope glycoproteins and N of Uukuniemi virus are divergent from the rest of the phlebovirus genus, which may explain why our results contrast. Gn interaction with N is unlikely to be conserved across the five genera within family *Bunyaviridae*, as the envelope glycoproteins and N are not similar. The N (and RdRp) of the hantaviruses independently localize to perinuclear membrane structures when expressed alone, suggesting a distinct mode of assembly (129, 153). For tospoviruses, independent interactions between Gn and Gc with N were discovered, indicating a possible requirement for both glycoproteins during recruitment (127).

We found no role for Gc in recruitment of encapsidated genome or RdRp, however, Gc is necessary for optimal Gn expression, as well as minigenome expression in RVF-VLP-infected target cells. These results suggest that Gc plays a role in entry, perhaps through recognition of cell surface receptors and/or fusion. Studies performed by Bellesar and Blackburn (154) suggest a requirement for Gc in virus entry, as they were able to neutralize virus using antibodies recognizing either Gn or Gc, either pre- or post-virus absorption. These results indicate that both glycoproteins play a role in entry into target cells. Computational studies have predicted RVFV Gc to be a class II viral fusion

protein (155), and previous experiments with other viruses of the *Bunyaviridae* family support Gc being the main determinant of cell fusion (156-158). Fusion assays utilizing Gn and Gc of Bunyamwera virus (*Orthobunyavirus* genus, *Bunyaviridae* family) found that deletions in Gc prevented syncitia formation (158). Additional experiments with La Crosse and Tahyna viruses (*Orthobunyavirus* genus) identified Gc as fusion protein using chimeras, site-directed mutagenesis, and cell-cell-fusion assays (156, 157).

Although it has been widely acknowledged that the RdRp is fundamental to replication and transcription of the RNA virus genome, other roles for the RVFV RdRp have not been previously explored. We have discovered that while the RdRp was not required for the efficient cellular release of virus or packaging of the encapsidated genome, a catalytically active RdRp must be packaged for RdRp expressed in *trans* to transcribe the genome. Complementing in *trans* with viral components required for transcription/replication is not unprecedented. Studies with the Ebola virus (*Ebolavirus* genus, *Filoviridae* family), which is a non-segmented negative-sense RNA virus, investigated the viral components necessary for the generation of infectious particles. The Ebola virus VP30 protein, which is required for replication/transcription by the RdRp, could be complemented in *trans* for restoration of activity in Ebola-VLP-infected target cells (159). For RVFV, it is necessary that the genome, N, and the RdRp be packaged, and the RdRp appears to be essential for an early step in the RVFV replication cycle. While the RdRp may play a role in entrance into target cells, it is more likely that the encapsidated genome is initially not accessible to the RdRp expressed in *trans.* We hypothesize that catalytically active RdRp must be bound to the genome for the initial round of replication and/or transcription.

Previous studies with the positive-sense RNA viruses, poliovirus (*Picornaviridae* family) and Flock house virus (*Nodaviridae* family) found that only actively replicating genomes were recruited for virus assembly (160-162). For poliovirus, it is hypothesized that translation is coupled to replication of the genome and assembly of the virus, so that only genomes that encode functional proteins are replicated and packaged (160). For the Flock house virus, it is hypothesized that the replicating and non-replicating RNA genomes segregate to distinct sub-cellular locations, allowing for packaging of only the replicating RNA (162). In contrast to poliovirus and Flock house virus, RVFV can

package replicating or non-replicating ribonucleoprotein complexes (as measured by packaging of N and RdRp). However, only catalytically active complexes can be significantly enhanced through the expression of RdRp and N in *trans*. Perhaps the concentration of genome is too low in cells that are replication-defective to be enhanced by expression of RdRp and N in *trans*. Alternatively, catalytically active RdRp may need to be bound to the encapsidated genome for an early event in the replicative cycle.

We have illuminated roles for each of the viral components in the assembly, cellular release, and infectivity of RVFV. The interaction between the encapsidated genome and the Gn cytoplasmic tail triggers release of virus, likely through stimulating budding of the virus into the Golgi, illustrating a novel mechanism for the efficient generation of infectious virus particles. The design and screening of therapeutics targeting the Gn cytoplasmic tail may offer a novel target for inhibition of both virus release and packaging of the RdRp and encapsidated genome.

Materials and Methods

Plasmid Constructs

All plasmids were generated using standard molecular cloning techniques and were confirmed by sequencing. The constructs pTrRVFV-SΔNSs::GFP, pN-Amp, pRdRp-Amp, pGn/Gc-Amp, and pGnK48Stop-Amp have been described previously (54, 123). The minigenome, pSTrRVFV-SΔNΔNSs::hRLuc, was derived from pTrRVFV-SΔNSs::GFP by replacing the GFP gene with a humanized renilla luciferase gene (RLuc), then deleting a 237 nucleotide Sma I fragment of the N gene. The expression constructs for N and RdRp were generated through cloning the open reading frames into pVAX1 (Invitrogen) using the HindIII/EcoRI and BamHI/NotI sites, respectively. The open reading frames from pGn/Gc-Amp and pGnK48Stop-Amp were cloned into pVAX1 using BamHI and EcoRI sites, generating pGn/Gc, pGc, pGn, and pGnK48. The expression plasmid, pGcW1, was generated by site-directed mutagenesis of Trp1189 to a stop codon in pGc, thus deleting the entire predicted cytoplasmic tail. Site-directed mutagenesis of pRdRp generated the catalytic domain RdRp mutant alleles pRdRp^{cat1} and pRdRp^{cat2}, which were mutated to Ala at residues Asp1134 and Ser1132, respectively.

Cells and virus

BSR-T7/5 cells were a generous gift of Dr. K. Conzelmann (Max-von Pettenkofer-Institut, Munchen, Germany). The BSR-T7/5 clonal cell line was generated through limiting dilution of the BSR-T7 cells. The cells were grown in Dulbecco's Modified Eagle Medium (Invitrogen) supplemented with 10% fetal calf serum, and 1 mg/mL Geneticin. RVFV ZH548 MP12 vaccine strain was a generous gift of Dr. R. Tesh (World Reference Center of Emerging Viruses and Arboviruses).

Antibodies

Hybridomas that secrete neutralizing monoclonal antibodies recognizing Gn and Gc (R1-4D4-1-1 and R5-3G2-1A) were a generous gift of Dr. G. Ludwig (USAMRIID). Polyclonal antibodies that were generated against RVFV in mice were a generous gift of Dr. P. Rollin (CDC). The N-terminal 150 amino acids of the RdRp and full-length N were expressed with N-terminal histidine tags and purified under denaturing conditions on Ni-NTA agarose columns (Qiagen Inc.). RdRp and N polyclonal antibodies were generated in rabbits using these purified proteins as antigens (Harlan Laboratories). Monoclonal antibodies recognizing GS-28 and β-COP were purchased from Transduction Labs and ABR, respectively. Horseradish peroxidase-conjugated secondary antibodies, goat anti-rabbit and goat anti-mouse, were acquired from Amersham and MP Biomedical, respectively. AlexaFluor 488-labelled goat anti-rabbit and AlexaFluor 594-labelled goat anti-mouse were purchased from Invitrogen.

Virus-like particle production

BSR-T7/5 cells were plated at a density of 1.2 x10^6 cells/plate. After 24 h, cells were transfected using 2 μL TransIT LT1 (Mirus Corporation) /μg DNA and plasmids in the ratio 6.0 μg minigenome: 6.0 μg pN: 6.0 μg pRdRp: 3.0 μg pGn: 3.0 μg pGc/10 cm plate. The amount of plasmid transfected was scaled to the number of cells. The media was changed 24 h post-transfection. After 48 h post-transfection, the RVF-VLPs were harvested, then clarified by low-speed centrifugation (300 rcf for 10 min at 4˚C) to remove cellular debris. The transfected cells were analyzed by RLuc assay (Promega) as a means to determine transfection efficiency. Only experiments exhibiting high transfection efficiencies were further analyzed for RVF-VLP production. The RVF-

VLPs were purified by high-speed ultracentrifugation for visualization by electron microscopy, immunoprecipitated for analysis by immuno-blot, or diluted for infection of target cells. RVF-VLP-infected target cells were harvested 24 h post-infection and were analyzed for RLuc activity. The raw luciferase units (RLU)/mL of RVF-VLPs added to target cells was calculated for three or more separate experiments. The log of the average RLU/mL was calculated for analysis by Independent T-Test (SPSS Statistical Package 14.0), and compared to the negative control (-Gn/-Gc). The p-values were calculated for an α-value of 0.05.

Immunoprecipitation of RVF-VLPs

Mouse monoclonal antibodies recognizing either Gn (R1-4D4-1-1) or Gc (R5-3G2-1A) were conjugated to Dynal magnetic beads (Invitrogen) by incubating overnight at 4˚C. The antibody-coated beads were incubated overnight at 4˚C with RVFV or RVF-VLPs, then washed with Wash buffer (10mM Tris, 5mM $MgCl_2$, and 100mM NaCl, pH 7.8), and resuspended in 1X sample buffer for analysis by immuno-blot. To prevent variation between conditions, generation of RVF-VLPs, immunoprecipitation, and immunoblotting were performed for all conditions at the same time. The representative immunoblots in the figures are from a single immunoblot split into the different figures. Therefore, each figure displays the same positive (WT) and negative (-Gn/-Gc) controls for comparison. The extensive experiments were performed multiple times, but only an immunoblot from a single experiment is shown.

Transmission electron microscopy

RVFV and RVF-VLPs were pelleted by high-speed ultracentrifugation (82,705 rcf for 4 h at 4˚C), resuspended in 0.1M Sorenson's buffer, and distributed onto a carbon-coated grid. The particles were fixed with 2.5 % glutaraldehyde in Sorensen's buffer and negative stained with aqueous 1% uranyl acetate, which was performed by the Microscopy Imaging Laboratory (University of Michigan). The particles were viewed on a Philips CM100 transmission electron microscope at 60 KV. Images were recorded digitally using a Hamamatsu ORCA-HR digital camera system, which was operated using AMT software (Advanced Microscopy Techniques Corp., Danvers, MA). The sizes of RVFV and RVF-VLPs were measured for three or more particles.

Efficiency of RVF-VLP Cellular Release

Efficiency of cellular release was determined through quantitation of Gn/Gc levels in the cell lysates and within the RVF-VLPs. Immunoblots were analyzed using ImageQuant 5.2 (Molecular Dynamics) to determine the signal intensity (volume). The Gn/Gc expression levels were normalized to Gn/Gc expression in transfected cells, and calculated as a percentage of the WT condition, which was designated as 100% release efficiency. Statistics were performed for the comparison of Gn/Gc expression levels from experiments performed in triplicate using one-sample t-tests (SPSS Statistical Package 14.0). The p-values were calculated for an α-value of 0.05.

Immunofluorescence

BSR-T7/5 cells were plated on glass coverslips at 5.0×10^4 cells/well of a 24-well plate. After 24 h, the cells were transfected using 2 μl TransIT/μg DNA. The cells were fixed 24 h post-transfection with 4% paraformaldehyde in phosphate-buffered saline (PBS), then permeablilized using 0.2% Triton X-100 in PBS with 1% bovine serum albumin. Mouse monoclonal antibodies recognizing Gn and Gc and rabbit polyclonal antibodies recognizing the RdRp and N were used as primary antibodies, while AlexaFluor488-labelled goat anti-rabbit and AlexaFluor 594-labelled goat anti-mouse were used as secondary antibodies (Invitrogen). Fluorescence visualization and imaging were performed using an Olympus 51-X fluorescent light microscope at the Microscopy Imaging Laboratory (University of Michigan). Cells with clear signals for both red (λ594) and green channels (λ488) were counted, then, analyzed for co-localization. Positive co-localization was defined as the RdRp exhibiting a focus of intense staining corresponding to the Golgi/glycoprotein signal. Diffuse cytoplasmic staining and small puncta in the cytoplasm were not counted for positive co-localization.

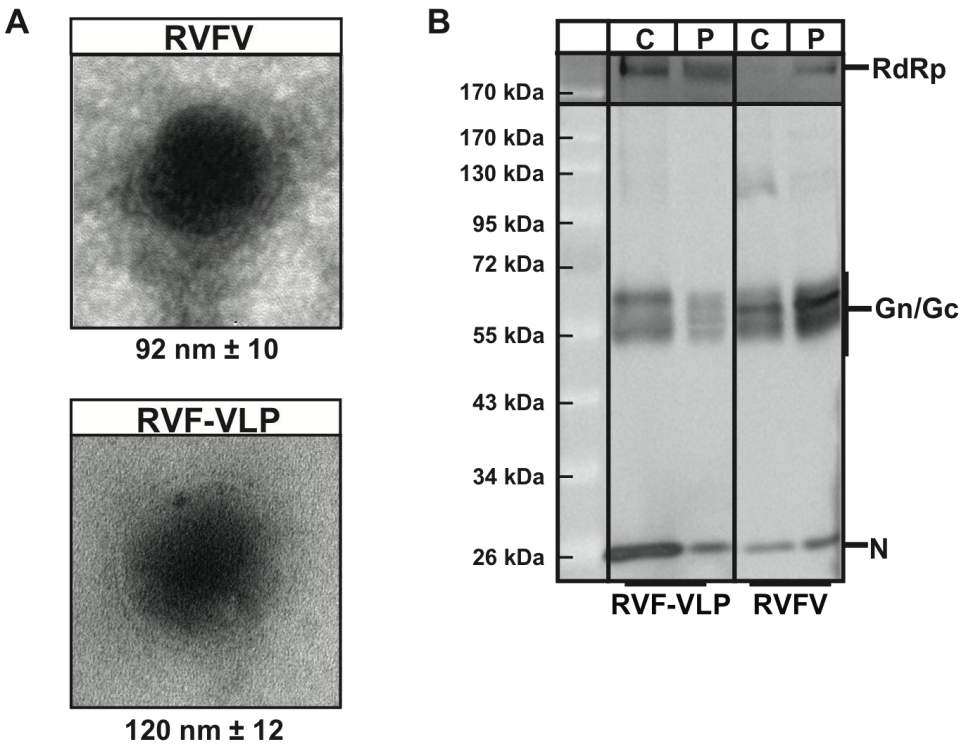

Figure 4.1. RVFV and RVF-VLPs have similar morphology and protein composition.
(A) RVFV and RVF-VLPs were harvested by ultracentrifugation and analyzed by transmission electron microscopy with negative staining. The particle sizes were measured, and the values listed are the mean sizes of particles with standard deviation. (**B)** BSR-T7/5 cells were transfected with pSTrRVFV-SΔNΔNSs::hRLuc, pN, pRdRp, pGn, and pGc or were infected with RVFV ZH-548 MP12 vaccine strain at an MOI of 1. The media, containing either RVF-VLPs or RVFV, was harvested, clarified, and the particles pelleted by ultracentrifugation. Lysates from transfected or RVFV-infected cells (C), and pelleted particles (P) were analyzed by immunoblot.

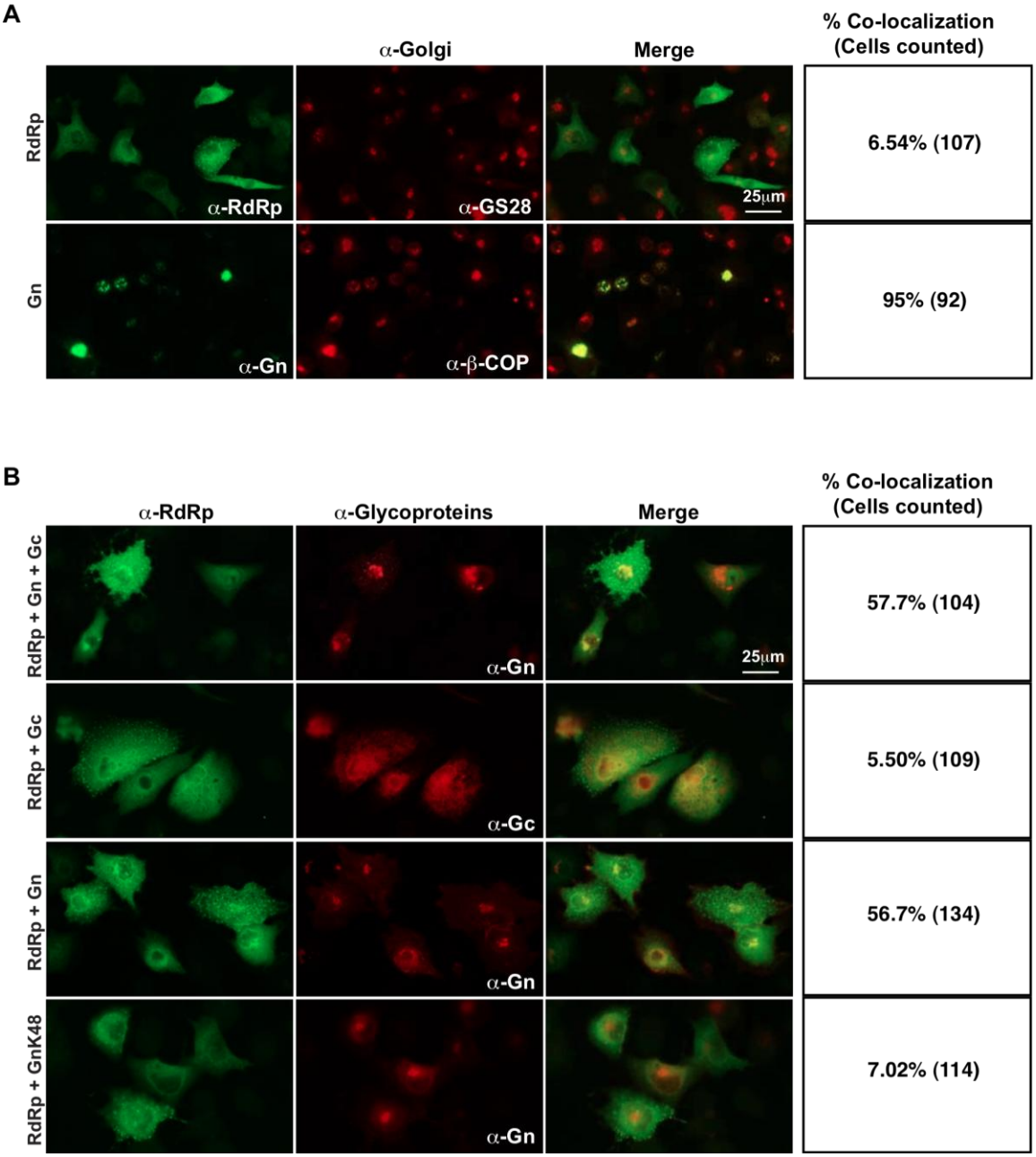

Figure 4.2. Gn recruits RdRp to the Golgi apparatus.
(A) BSR-T7/5 cells were transfected with pRdRp or pGn, and the proteins were visualized with anti-RdRp and anti-Gn, respectively (green channel). Cellular resident Golgi apparatus proteins, GS-28 or β-COP were also labeled (red channel). Percentage of cells displaying co-localization of viral proteins with Golgi apparatus is indicated with the number of cells counted in parentheses. (**B)** BSR-T7/5 cells were transfected with pRdRp and either pGn/pGc, pGc, pGn, or pGnK48. Cells were incubated with anti-RdRp (green channel) and anti-Gn or anti-Gc (red channel), then analyzed by immunofluorescence microscopy. Percentage of cells displaying co-localization of RdRp with Gn or Gc is indicated with the number of cells counted in parentheses.

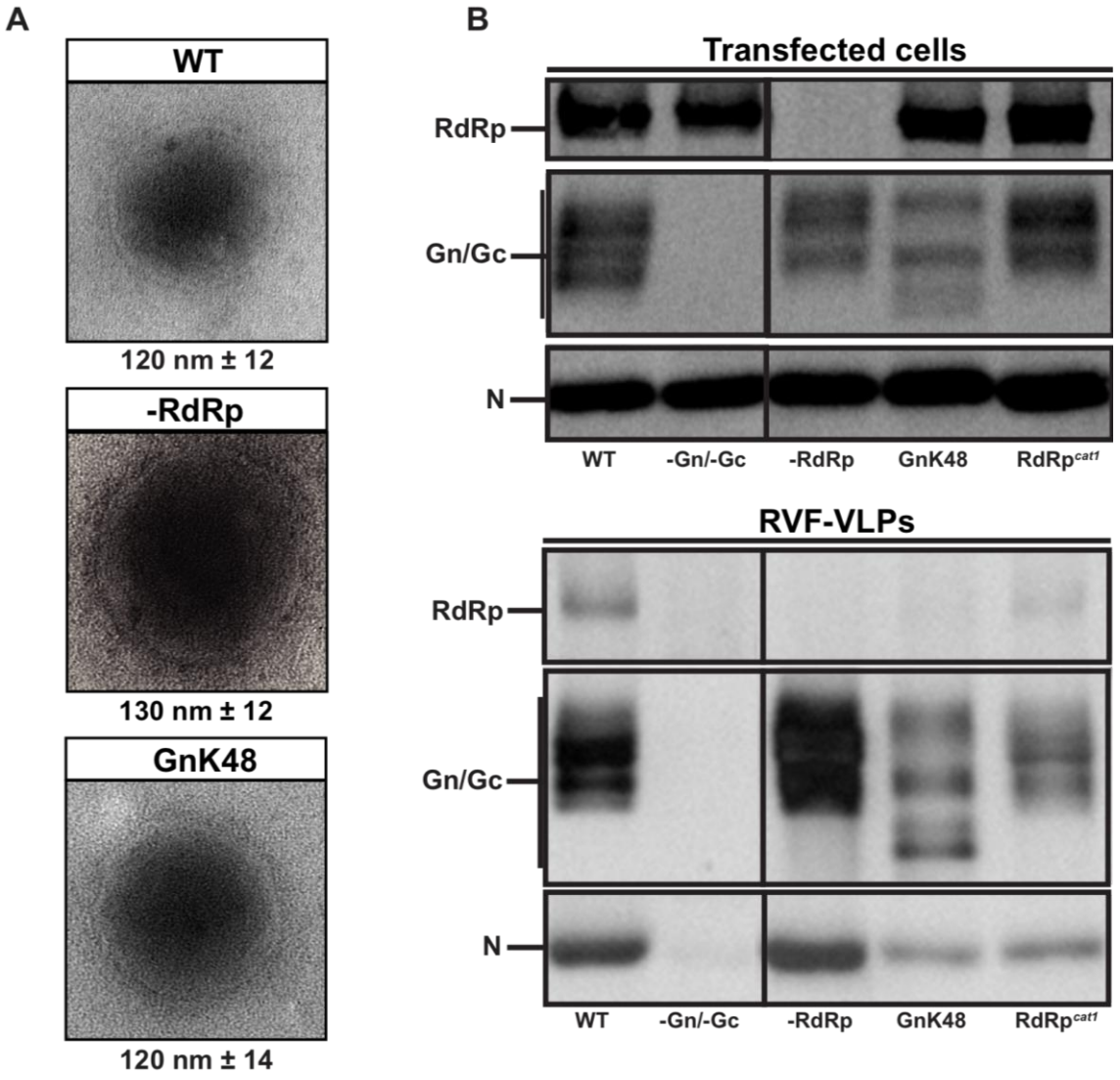
A
WT
120 nm ± 12
-RdRp
130 nm ± 12
GnK48
120 nm ± 14
B
Transfected cells
RdRp
Gn/Gc
N
WT
-Gn/-Gc
-RdRp
GnK48
RdRpcat1
RVF-VLPs
RdRp
Gn/Gc
N
WT
-Gn/-Gc
-RdRp
GnK48
RdRpcat1

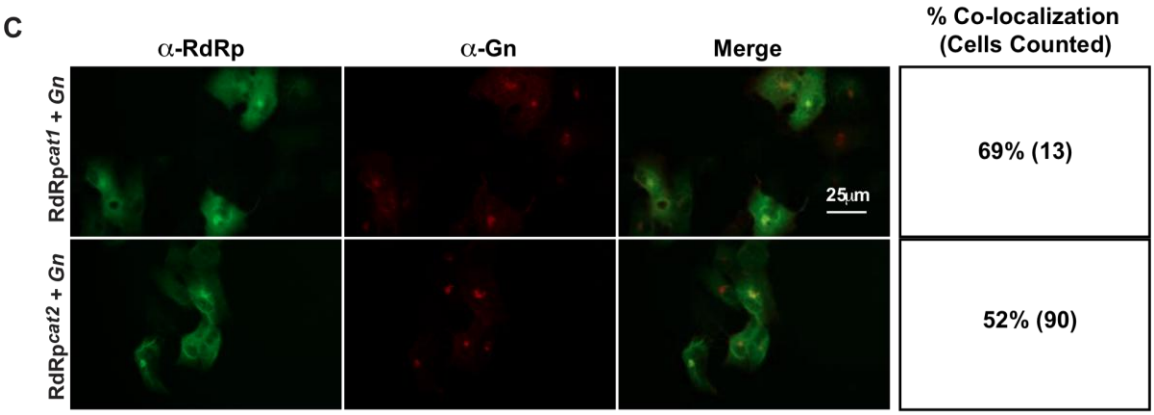

Figure 4.3. Packaged, catalytically active RdRp is necessary for an early event in the RVFV replication cycle.

(A) RVF-VLPs were harvested by ultracentrifugation and visualized by transmission electron microscopy with negative staining. The particle sizes were measured, and the values listed are the mean sizes with standard deviation. (**B)** BSR-T7/5 cells were transfected with plasmids expressing an artificial S segment and all of the structural proteins (pSTrRVFV-SΔNΔNSs::hRLuc, pN, pRdRp, pGn, and pGc), this condition is referred to as WT. Or, one or more of the components was replaced with an equivalent amount of empty vector (-Gn/Gc and –RdRp) or with plasmids expressing mutant alleles of Gn or RdRp (GnK48 or pRdRp^{cat1}). Transfected cells were analyzed for protein expression by immunoblot. RVF-VLPs were immunoprecipitated from the clarified media from transfected cells and analyzed by immunoblot. (**C)** BSR-T7/5 cells were transfected with pGn and either pRdRp or RdRp catalytic domain mutants, pRdRp^{cat1} or pRdRp^{cat2}. Cells were incubated with anti-Gn (red channel) and anti-RdRp (green channel) then analyzed by immunofluorescence microscopy. Percentage of cells displaying co-localization of RdRp alleles with Gn is indicated with the number of cells counted in parentheses.

Sample	Untransfected		$RdRp^{cat1}$/N		RdRp/N	
	Average Log (RLU/mL)	Std. Dev.	Average Log (RLU/mL)	Std. Dev.	Average Log (RLU/mL)	Std. Dev.
WT	6.61*	0.782	6.51*	1.10	8.15*	0.471
-Gn/-Gc	3.76	0.296	3.42	0.325	4.47	0.515
-RdRp	-	-	3.53	0.319	4.60	1.00
GnK48	-	-	3.56	0.317	4.78	0.484
$RdRp^{cat1}$	-	-	3.60	0.231	4.22	0.815

* Values are significantly different from -Gn/-Gc at α=0.05 and $p < 0.005$.

Table 4.1. RdRp and N in trans fail to rescue RdRp-deficient RVF-VLPs.

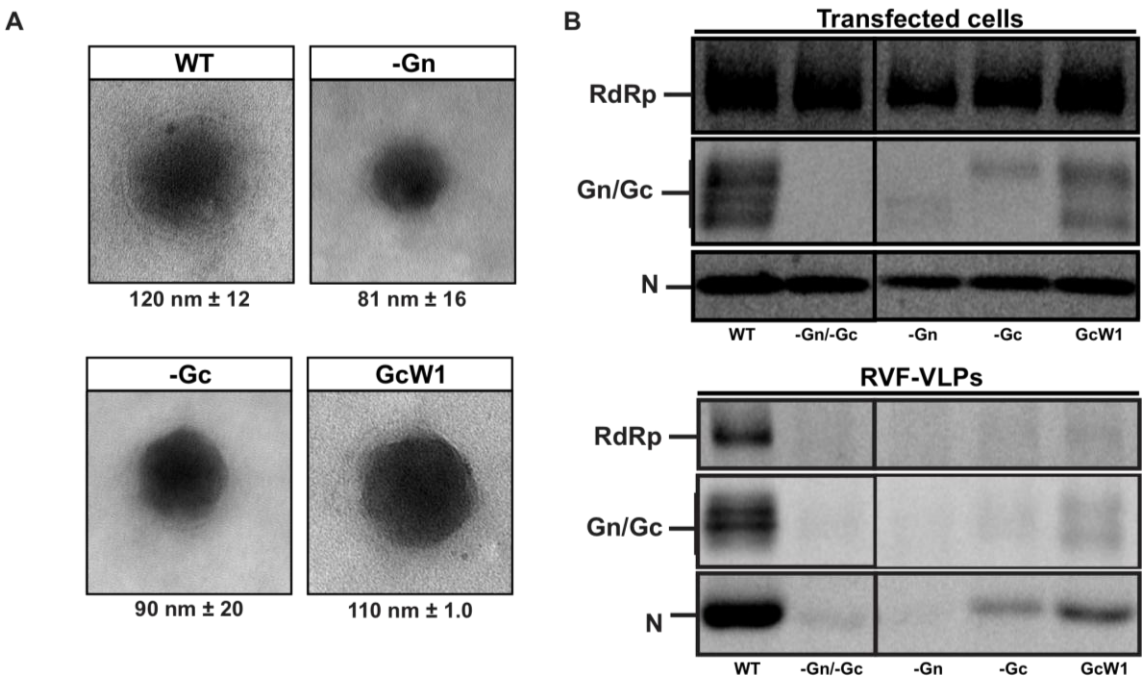

Figure 4.4. Gn packages encapsidated genome.
(A) RVF-VLPs were harvested by ultracentrifugation and analyzed by transmission electron microscopy with negative staining. The particle sizes were measured, and the values listed are the mean sizes of particles with standard deviation. (**B)** BSR-T7/5 cells were transfected with plasmids expressing an artificial S segment and all of the structural proteins (pSTrRVFV-SΔNΔNSs::hRLuc, pN, pRdRp, pGn, and pGc), this condition is referred to as WT. Or, one or more of the components was replaced with an equivalent amount of empty vector (-Gn/-Gc, -Gn, or -Gc) or a plasmid expressing an allele of Gc that lacks the entire cytoplasmic tail (GcW1). Transfected cells were analyzed for protein expression by immunoblot. RVF-VLPs were immunoprecipitated from the clarified media from transfected cells and analyzed by immunoblot.

Table 4.2. Gc cytosolic tail is dispensable for infectivity.

Sample	Average Log (RLU/mL)	Std. Dev. Log (RLU/mL)
WT	8.15*	0.471
-Gn/-Gc	4.47	0.515
-Gn	4.52	0.672
-Gc	4.82	1.10
GcW1	5.86*	0.748

* Values are significantly different from -Gn/-Gc at α=0.05 and $p < 0.01$.

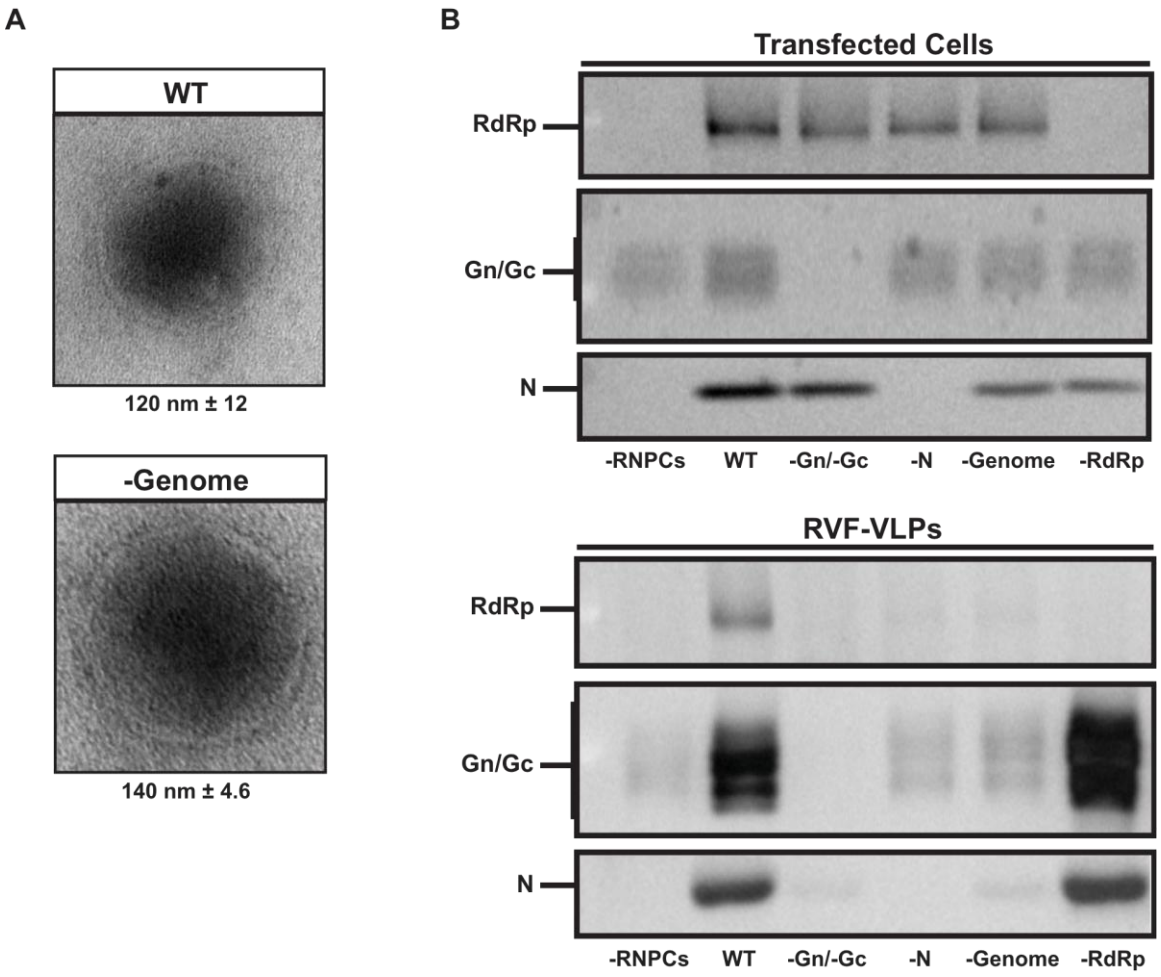

Figure 4.5. Viral components required for efficient RVF-VLP release.
(A) RVF-VLPs were harvested by ultracentrifugation and visualized by transmission electron microscopy with negative staining. The particle sizes were measured, and the values listed are the mean with standard deviation. **(B)** BSR-T7/5 cells were transfected with plasmids expressing an artificial S segment and all of the structural proteins (pSTrRVFV-SΔNΔNSs::hRLuc, pN, pRdRp, pGn, and pGc), this condition is referred to as WT. Or, one or more of the components was replaced with an equivalent amount of empty vector (-RNPCs, -Gn/Gc, -N, -genome, -RdRp). RNPCs refer to ribonucleoprotein complexes and are defined as genome, N, and RdRp. Transfected cells were analyzed for protein expression by immunoblot. RVF-VLPs were immunoprecipitated from the clarified media from transfected cells and analyzed by immunoblot.

Table 4.3. Encapsidated genome required for infectivity.

Sample	Average Log (RLU/mL)	Std. Dev. Log (RLU/mL)
WT	8.15*	0.471
-Gn/-Gc	4.47	0.515
-NP	4.22	0.696
-Genome	3.78	0.741

* Values are significantly different from -Gn/-Gc at α=0.05 and $p < 0.001$.

Table 4.4. Encapsidated genome required for efficient cellular release

Sample	% Efficiency	% Std. Dev.
-RNPs	14.2	‡
-N	15.6*	8.8
-Genome	18.1*	3.7
-RdRp	169.5	71.8
GnK48	49.9†	13.3
RdRp^{cat1}	37.1‡	16.5
-Gn	Δ	
-Gc	Δ	
GcW1	56.9	20.4

* Values significantly different from "Wild-type" RVF-VLP release efficiency at $\alpha = 0.05$, $p<0.005$.

† Values significantly different from "Wild-type" RVF-VLPs release efficiency at $\alpha = 0.05$, $p<0.05$.

Δ Yields were below the limit of detection.

‡ Insufficient number of replicates for std. dev. and/or p-value calculations.

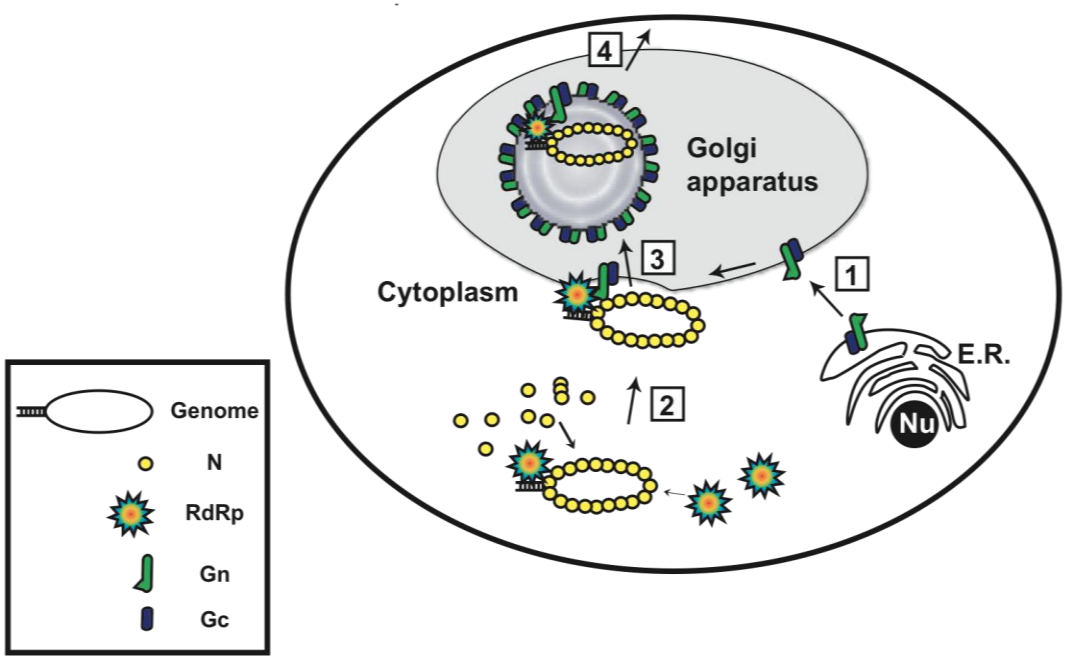

Figure 4.6. Model for the assembly and budding of RVFV.
Upon entry of RVFV into the cell, replication and transcription of the viral proteins occur in the cytoplasm. The RdRp and N are translated in the cytoplasm, while the envelope glycoproteins are translated as a polyprotein on the endoplasmic reticulum. 1) The polyprotein is cleaved into the individual Gn (green cylinders) and Gc (blue cylinders) proteins, which form a complex and localize to the Golgi apparatus by a localization signal on Gn. 2) The RdRp (starbursts) and N (yellow circles) form the ribonucleoprotein complex with the genome, and localize to the Golgi apparatus through independent interactions with the Gn cytoplasmic tail. 3) Interaction between the encapsidated genome and the glycoproteins induces negative membrane curvature and budding of virus particles into the lumen of the Golgi apparatus. 4) The disintegration of the Golgi apparatus leads to egress of the virus from the cell.

Chapter 5

Limitations to Phlebovirus Reassortment

Introduction

Segmented, RNA viruses rapidly evolve to new geographical niches or hosts utilizing mechanisms of antigenic drift and antigenic shift. Genetic drift involves the gradual accumulation of point mutations in the viral genome through replication by an error-prone RNA-dependent RNA polymerase (RdRp) (20). Genetic shift leads to virus evolution through exchanging viral genomic segments with closely related viruses co-infecting the same cell (20). Genetic shift is referred to as reassortment and generates novel viruses that contain segments from each of the parental viruses. The progeny virus may exhibit pathological features similar to either virus, or alternatively, may display a unique form of pathogenesis (20).

In 2001, a reassorted virus from the *Bunyaviridae* family (*Orthobunyavirus* genus) emerged in East Africa. The virus contained genomic segments from the Bunyamwera (BUNV) and Batai (BATV) viruses (11, 17, 19). While BUNV typically produces febrile disease in humans and BATV has not been implicated in human disease, the reassorted virus caused hemorrhagic fever disease in the human population, exhibiting a similar, yet more extreme pathological phenotype to BUNV (11). The discovery of this virus, termed the Ngari virus, established the capacity of different viruses within the *Bunyaviridae* family to reassort in nature.

The Rift Valley fever virus (RVFV) belongs to the *Phlebovirus* genus of the *Bunyaviridae* family. RVFV is the causative agent of explosive epizootics throughout the African continent and the Arabian Peninsula, primarily targeting humans and livestock (163). The mosquito vectors for RVFV can be found throughout the world (21-24, 26-28, 51), and the capacity of RVFV to spread to previously unaffected regions has been demonstrated in Egypt in 1977 and in the Arabian Peninsula in 2000 (30). There

are no FDA- or USDA-approved therapeutics or prophylactics available, and spread of the virus is detrimental to the regional economy and public health. Upon introduction to a new region of the world, RVFV may be capable of reassorting with other viruses in the *Phlebovirus* genus (*Bunyaviridae* family), which are present throughout Eurasia and the Americas (40). Understanding whether phleboviruses can reassort and the limitations governing reassortment, if any, will allow us to address or evade public health threats in the future.

Similar to all phleboviruses, RVFV is a spherical, enveloped virus encoding four structural proteins on the S (small), M (medium), and L (large) genomic segments (40). The S segment encodes the nucleocapsid protein (N), while the M and L segments encode the envelope glycoproteins (Gn and Gc) and the RdRp, respectively (40). The RdRp acts as replicase and transcriptase (85), but requires N bound to the genome (57), as the encapsidated genome, for these processes to proceed. Prior to release, the virus assembles at the Golgi apparatus (40). Gn can recruit both the RdRp and encapsidated genome individually for assembly and packaging (Chapter 4). Efficient cellular release of RVFV is dependent upon interactions between the encapsidated genome and the envelope glycoproteins (Chapter 4).

We have developed and characterized a virus-like particle (VLP) system for RVFV (Chapter 2). This RVF-VLP system allows us to investigate the protein-protein and protein-genome interactions necessary for generating infectious virus. In our highly sensitive RVF-VLP system, we can substitute viral proteins from other viruses within the *Phlebovirus* genus to determine whether there is a block in virus replication/transcription, assembly, release, or entry processes. Using representative viruses from several of the phlebovirus serocomplexes, we have identified barriers to reassortment between the RdRp and N, as well as the RdRp and Gn. The interactions between the N and genome and N and Gn are conserved, but due to the RdRp limitations, viruses within the *Phlebovirus* genus have significant barriers to overcome in order to reassort. Our results describe the molecular mechanisms underlying the barriers to phlebovirus reassortment.

While we have identified protein-protein interactions with the RdRp as limiting phlebovirus reassortment, we have yet to clone functional heterologous RdRps to demonstrate the functionality of the heterologous N and Gn/Gc in replication,

transcription and the infection of target cells. Therefore, we cannot make any firm conclusions until we provide the positive control for heterologous protein function.

Results

Representative N from the different serocomplexes of the Phlebovirus genus are highly conserved.

The N proteins from the RVFV (ZH501 strain, RVFV serocomplex), Toscana virus (TOSV) (Naples serocomplex, ELB strain), Punta Toro virus (PTV) (Punta Toro serocomplex, Adames strain), and Belterra virus (BEV) (Icoaraci serocomplex, BeAn356637 strain) exhibit high sequence identity at the amino acid level (Fig. 5.1). The high sequence identities suggest that all of the N proteins have similar structures and bind RNA similarly (Chapter 3). Sequence alignments and pair-wise comparisons determined the amino acid identities of these selected viruses to vary between 49-57%, with the Toscana virus as the most divergent among these compared (Chapter 3).

Heterologous N cannot function in place of RVFV N for transcription of the RVFV genome.

BSR-T7 cells were transfected with minigenome, pN, pRdRp, and empty vector (pVAX1). The RdRp requires N for replication and transcription of the genome (57); therefore, the raw luciferase units (RLU) generated when the minigenome and RdRp were expressed in the absence of N (Fig. 5.2) represents background levels. Increasing concentrations of N increases the expression of RdRp, as well as transcriptional activity (Fig. 5.2). In contrast, increased expression of RdRp does not produce a corresponding increase in transcriptional activity (Fig. 5.2).

To determine whether the heterologous N could function in place of RVFV N in transcription of the RVFV minigenome with the RVFV RdRp, BSR-T7 cells were transfected with minigenome, pRdRp, and pN, pTOSVN, pPTVN, or pBEVN, and analyzed by replicon assay and immunoblot (Fig. 5.3). Expression of RVFV N resulted in luciferase activity of greater than 1000-fold background levels (-N) (Fig. 5.3). In contrast, the expression of TOSV N, PTV N, or BEV N did not increase luciferase activity above background levels (Fig. 5.3). These results demonstrate that none of the heterologous N can function in transcription of the RVFV minigenome, indicating the

heterologous N cannot functionally interact with either the RVFV RdRp and/or minigenome.

Heterologous N do not exhibit dominant-negative inhibition.

BSR-T7 cells were transfected with minigenome, pRdRp, and equivalent amounts of pN and empty vector (pVAX1), pN, pTOSVN, pPTVN, or pBEVN, then analyzed by replicon assay and immunoblot. The luciferase expression was similar regardless of whether RVFV N was co-expressed with empty vector, TOSV N, PTV N, or BEV N (Fig. 5.3), indicating that the heterologous N do not function as dominant-negative inhibitors. Additionally, the heterologous N cannot complement the RVFN for RLuc transcription, suggesting that the RVFN and heterologous N do not interact.

The interactions between the N and RdRp are conserved between Phlebovirus serocomplexes.

BSR-T7 cells were transfected with combinations of minigenome, pN or pTOSVN, and pRdRp, then cross-linked with DSP, lysed, immunoprecipitated and analyzed by SDS-PAGE electrophoresis and immunoblot (Fig. 5.4). The RVFV RdRp was immunoprecipitated only when co-expressed with RVFV N or TOSV N. The expression of the RVFV minigenome was not required for RdRp immunoprecipitation, indicating that the heterologous N can interact with the RdRp independent of genome. We could not examine TOSV N expression levels due to weak detection levels of the antibody.

Heterologous N cannot generate replication/transcription complexes.

When expressed alone, the RVFV RdRp exhibits diffuse cytoplasmic staining (Chapter 4). However, in the presence of N, the RVF RdRp forms large perinuclear puncta, which are believed to be the replication and/or transcription complexes (Fig. 5.5A). RdRp mutants incapable of producing puncta in the presence of N are also defective for transcribing the genome (Fig. 5.6 and 5.7). We investigated RdRp mutants in conserved residues throughout three of the conserved RdRp domains (Fig. 5.6 and 5.7). RdRp mutants Y928A, K1003A, and SS1093/4AA were found unable to form puncta, as well as transcriptionally defective (Fig. 5.6 and 5.7). K1003A and SS1093/4AA may be misfolded due to their inability to form puncta, demonstrate

transcriptional activity, or interact with Gn, while RdRp mutant Y928A is likely properly folded due to its ability to be recruited by Gn. (Fig. 5.6, 5.7, and 5.8). Therefore the inability of Y928A to form puncta may be due to an inability to form replication/ transcription complexes.

To investigate whether the heterologous N form replication/transcription complexes, we transfected cells with pN, pTOSVN, pPTVN, or pBEVN alone or co-expressed with pRdRp. The heterologous N failed to change the localization of the RdRp to the large perinuclear puncta, suggesting that although the proteins may interact with the RdRp (Fig. 5.4), they may not form replication/ transcription complexes (Fig. 5.5B). The results were similar regardless of whether minigenome was co-expressed with RdRp and the heterologous N (Fig. 5.5B).

Gn interactions necessary for N recruitment and particle release are conserved in the heterologous N.

BSR-T7 cells were transfected with minigenome, pRdRp, pGn, pGc, and pN, pTOSVN, pPTVN, or pBEVN. The VLPs released into the media were harvested, clarified, and pelleted by high-speed ultracentrifugation. The pelleted VLPs were analyzed by transmission electron microscopy (Fig. 5.5A) or by SDS-PAGE electrophoresis and immunoblot (Fig. 5.5B). In previous studies, it has been suggested that RVF-VLPs cannot form without the N and envelope glycoproteins; therefore, VLPs expressing RVFV N or TOSV N were imaged using transmission electron microscopy. The VLPs were similar in size and morphology, incidating that TOSVN can function to form particles (Fig. 5.9A). Previously, the genome and N have been found to be necessary for efficient cellular release of RVFV through interaction with the Gn envelope glycoprotein (Chapter 3). The ability of the heterologous N to allow for efficient cellular release of VLPs was investigated. Release efficiencies, as determined by release of the RVFV Gn/Gc, appeared similar for VLPs packaging RVFV N or the heterologous N (Fig. 5.9B), suggesting that the N interactions with the genome and Gn are conserved among the different phlebovirus serocomplexes.

Heterologous envelope glycoproteins cannot form infectious particles with RVFV RNP complexes.

Since the Gn and encapsidated genome interaction is conserved for efficient release of virus, we hypothesized the TOSV Gn/Gc would be capable of packaging RVF ribonucleoprotein complexes (genome, N, and RdRp). BSR-T7 cells were transfected with minigenome, pN or pTOSVN, pRdRp, pGn or pTOSV-Gn, and pGc or pTOSV-Gc. The VLPs were harvested and used to infect untransfected target cells. Luciferase activity in transfected cells and VLP-infected target cells was analyzed. Infectious VLPs were only produced by cells expressing all RVFV components (Fig. 5.10). TOSV Gn and Gc were incapable of generating infectious VLPs containing RVFV minigenome, N, and RdRp, indicating the interactions with the RVF RNPs are not conserved between phlebovirus serocomplexes. Since the encapsidated genome can interact with Gn, it is likely that the TOSV Gn cannot recruit the RVFV RdRp for virus assembly and packaging.

Discussion

The elucidation of the molecular barriers preventing phlebovirus reassortment is crucial to predicting the emergence of novel phleboviruses. Gaining an understanding of the limitations to RVFV reassortment is particularly pertinent due to its severe pathogenesis and its capacity to spread to previously unaffected regions of the world. Although the phlebovirus genus is comprised of highly-related viruses, our results suggest that there are substantial barriers preventing their reassortment.

The limitations governing phlebovirus reassortment appear to be dependent on the RdRp. The heterologous N fail to allow transciption of the RVFV minigenome in the replicon assay, which contrasts previous studies showing that the RVFV RdRp and TOSV N can transcribe the RVFV minigenome (164). Interestingly, Accardi et. al. did not detect any transcription by RVFV RdRp of the TOSV N-encapsidated minigenome, although they did detect transcription of the TOSV minigenome with the RVFV RdRp and RVFV N (164). Our replicon assay is very sensitive and quantitative, with levels reaching over 1000-fold background levels, so if there were signal generated, we should have been able to detect it. However, we have not yet shown TOSV N to be functional for replication/transcription. We are currently working to clone the TOSV RdRp to

verify all of the TOSV proteins are functional for replication/transcription and generation of infectious particles.

We also demonstrated that the RdRp fails to functionally interact with the heterologous N to generate replication/transcription complexes and, likely, the TOSV Gn for assembly and packaging into virus particles. To verify the RdRp cannot interact with the TOSV Gn, immunoprecipitation and immunofluorescence experiments determining the ability of TOSV Gn to interact with the RdRp for recruitment to the Golgi are currently being explored.

Since the N and Gn are encoded by the S and M segments, respectively, the RdRp-encoding RVFV L segment must sort together with the RVFV S and M segments. Despite the stringency of the RVFV L segment, the RVFV S and M segments could sort with a more promiscuous L segment of a different virus. Once we understand the protein-protein interactions between the RdRp and N and better define the interaction domain of the RdRp with Gn, we may be able to predict whether other viral RdRps could function with RVFV S and M segments. Since there are separate blocks for RdRp interaction with N and Gn, it is less likely that a more promiscuous RdRp could circumvent both barriers. Therefore, if RVFV reassortants were generated, then we would anticipate that either the RVFV S or M segment would be switched rather than both segments.

The restrictions for phlebovirus reassortment appear slightly different from those of other genera in the *Bunyaviridae* family. The reassorted Ngari virus contained the S and L segments from BUNV and the M segment from BATV (11, 17), and experiments using cell culture systems with viruses within the *Orthobunyavirus* and *Hantavirus* genera of the *Bunyaviridae* family support a requirement for the S and L segments to sort together (5, 10-16, 18). In studies with viruses within the *Hantavirus* genus, cells were co-infected either with two different strains of the same virus or with two different viruses. The progeny viruses were analyzed for generation of reassortants. The investigators found strains of the same virus could reassort all of the segments, however, different viruses could only form viral reassortants that contained S and L segments from one virus and the M segment from the other virus (5). It is likely that the S and L segments must sort together to prevent a barrier in replication and/or transcription of the genome. These viruses may also have unique requirements for formation of

replication/transcription complexes. However, these viruses do not require the M segment to sort together with the L (5, 11), indicating that the other genera do not exhibit the same block in RdRp packaging. Therefore, the *Phlebovirus* genus differs in the limitations governing reassortment from the other genera of the *Bunyaviridae* family.

Through investigating the ability of the highly conserved heterologous proteins to function in various steps in the replicative cycle, we can narrow the regions of interaction between the proteins. While the N proteins from viruses within the *Phlebovirus* genus are ~50% identical at the amino acid level, the majority of the conserved residues map to the core of the structure (Chapter 3). The surface-exposed regions available for protein-protein interactions diverge significantly, which suggests why some of the protein-protein interactions with N may not be conserved between the phleboviruses. Additionally, the RVFV N structure identified a RVFV N dimer as the basic unit of N multimerization, and the interactions necessary for dimer formation were discovered to be crucial for replication/transcription of the genome by the RdRp. In support of our results showing no effect of the heterologous N on replication/transcription by RVFV N, the residues important for the N-N dimer interaction (RVFV N: Ala12, Trp 125) are not conserved between phleboviruses, suggesting that the heterologous N should not interact with RVFV N.

Surprisingly, the heterologous N could interact with the RVFV RdRp, but could not form replication/transcription complexes. The interaction with RVFV RdRp may be unstable or nonfunctional for the translocation of the RdRp to the replication/ transcription complexes. Alternatively, RVFV N could change the localization of a host protein necessary for interaction with RdRp and its cytoplasmic aggregation. The domain of N necessary for formation of these complexes appears not to be conserved within the *Phlebovirus* genus. The generation of RVFV N constructs containing mutations within the divergent, surface-exposed regions could be examined for their ability to generate replication/transcription complexes. These studies could identify the N-RdRp interaction domain necessary for complex formation and a target for RVFV antiviral development.

The packaging of the encapsidated genome and efficient cellular release of RVFV requires interactions between the genome, N, and Gn. The heterologous Gn and N

proteins were able to efficiently generate particles, and therefore, the interactions between the genome, N, and Gn appear conserved. The interaction domain of Gn with N has been previously identified as the first 30 amino acids of the cytoplasmic tail following the transmembrane domain (Chapter 4). Based on our results, the region of interaction should be conserved between the phlebovirus Gn. The Gn interaction domain contains several highly conserved bulky hydrophobic residues that we predict to be involved in N binding. We solved the structure of RVFV N and modeled the structures of TOSV N, PTV N, BEV N, and Uukuniemi virus N (Chapter 3). The structures share a conserved hydrophobic pocket predicted to be involved in protein-protein interactions. We propose that the highly conserved bulky hydrophobic amino acids within the Gn interaction domain insert into the conserved N hydrophobic pocket for the packaging of the encapsidated genome. The only other evidence of phlebovirus assembly and budding is from the Uukuniemi virus, the most divergent of all phleboviruses. Overby et. al. identified a region of Gn involved in N binding, which is non-existent in RVFV (86). Based on our data, the conserved Gn-N interaction domains could be targeted for the design of antivirals targeting the entire phlebovirus genus (except the divergent Uukuniemi virus), as well as any phlebovirus reassortant viruses generated in the future.

Materials and Methods

Cells

BSR-T7 cells were a generous gift of Dr. K. Conzelmann (Max-von Pettenkofer-Institut, Munchen, Germany). Clonal BSR-T7 cell lines expressing the T7-RNA polymerase at high levels were obtained through limiting dilution. The C3 clonal line was used for all experiments and was grown in Dulbecco's Modified Eagle Medium (Invitrogen) supplemented with 10% fetal calf serum, and 1 mg/mL Geneticin.

Viruses

RVFV (ZH548 MP-12 vaccine strain), Toscana virus (ELB), Punta Toro virus (Adames strain), and Belterra virus (BeAn356637) were generous gifts of Dr. R. Tesh (World Reference Center of Emerging Viruses and Arboviruses).

Plasmid Constructs

All plasmid constructs were generated by standard molecular cloning techniques and confirmed by sequencing. The transcription and expression constructs for the RVFV plasmids, including pSTrRVFV-SΔNΔNSs::hRLuc, pRdRp, pN, pGc, and pGn, have been previously described (165). The TOSVN was cloned from Toscana virus (ELB)-infected cells through purifying the RNA using Trizol reagent, and using SuperScript3 reverse transcriptase for generation of cDNA. Similar methods were used to generate cDNA for PTVN (Adames), BEVN (BeAn356637), TOSV-Gc (ELB), and TOSV-Gn (ELB), except M-MLV reverse transcriptase generated the TOSV-Gn cDNA. The TOSVN and PTVN genes were amplified using Phusion polymerase and primers 5'-GGATCCATGTCAGACGAGAATTATCG-3'/ 5'-CTCGAGTCACTTGCCAACCTTGGCGC and 5'-GGATCCATGTCATACGAAGAGATTGC-3'/ 5'-GTCGACCTAGAGGGATCTGAAGAC-3', respectively, and ligated into pCR-Blunt. TOSVN was liberated by digesting with BamHI and XhoI, then, ligated into pVAX1. PTVN was digested with SalI and XhoI and ligated into pVAX1. BEVN, TOSV-Gn and TOSV-Gc were amplified from the cDNA using Phusion polymerase and primers 5'-GCCAGATCCATGGCTGATTACGCTAGGATTG-3'/ 5'-ACGACTCGAGTCAGAGCAGACGTGGGAAAACAG-3', 5'-ACTAGGATCCATGAGAAACCAGTGCGTAGAC-3'/ 5'-CTGCCTCGAGCTAGCTATGCACATTACCTAATAGG-3' and 5'-ACTAGGATCCATGTATTCATTTTATGGAGTGATG-3'/ 5'-CTGCCTCGAGTTACTTGTTTTTCTTTTTTAGGGC-3', respectively. The gene products were gel purified, digested with BamHI and XhoI, and ligated into pVAX1.

Antibodies

Polyclonal antibodies that were generated against RVFV, TOSV, BEV, and PTV in mice were generous gifts of Dr. P. Rollin (CDC). Polyclonal antibodies recognizing RVFVN and RVFV RdRp were described previously (Chapters 2 and 4). Hybridomas secreting neutralizing monoclonal antibodies recognizing RVFVN or RVF Gc were generous gifts of Dr. G. Ludwig (USAMRIID).

Replicon Assay

BSR-T7 cells were plated at 1.2 x 10^6 cells/10 cm plate. The cells were transfected in the ratio 3.0ug pSTrRVFV-SΔNΔNSs::hRLuc, 6.0ug pN, and 9.0ug pRdRp/10 cm plate. The amount of plasmid was scaled to the number of cells transfected. The media was changed 24 h post-transfection, and the cells were harvested 48 h post-transfection using Reporter Lysis Buffer (Promega) or Renilla Luciferase Lysis Buffer (Promega). The cells were frozen at -80^{o}C, then, thawed for the analysis of luciferase activity.

VLP Assay

BSR-T7 cells were plated at 1.2 x 10^6 cells/10 cm plate. The cells were transfected in the ratio 6.0ug pSTrRVFV-SΔNΔNSs::hRLuc, 6.0ug pN, 6.0ug pRdRp, 3.0ug pGn, and 3.0ug pGc or the equivalent amount of heterologous expression plasmids/10 cm plate. The amount of plasmid was scaled to the number of cells transfected. The media was changed 24 h post-transfection and Benzonase (4ul/mL) was added. VLP-containing media was harvested at 48 h post-transfection and clarified by low-speed centrifugation for 10 minutes at 1200rpm. The clarified media was treated with Benzonase (4ul/mL) for 2h at 37^{o}C shaking, then, added to target cells. After 24 h post-infection, the cells were harvested and analyzed for luciferase activity.

Immunoblotting

VLP-containing media from transfected cells was clarified by low-speed centrifugation, then, pelleted by high-speed ultra-centrifugation at 82,705 rcf for 4h at 4oC. The pelleted particles were analyzed by SDS-PAGE electrophoresis and immunoblot.

Immunofluorescence confocal microscopy

BSR-T7 cells were plated at 1.0 x 10^5 cells/well of a 24-well plate. The cells were transfected in the ratio of 0.25 ug minigenome, 0.5 ug pN, and 0.75 ug pRdRp, or a similar amounts of heterologous N constructs or empty vector were transfected. After 24h, the cells were fixed using 4% paraformaldehyde, perforated with PBS/BSA/1%Triton-X100, then stained with the appropriate antibodies. The primary antibodies recognizing RVFVN, TOSVN, PTVN, and BEVN were monoclonal mouse

anti-RVFVN, polyclonal mouse anti-TOSV, polyclonal mouse anti-PTV, and polyclonal mouse anti-BEV, respectively. RVFV RdRp was recognized with polyclonal rabbit anti-RdRp. Secondary antibodies goat anti-rabbit-488 and goat anti-mouse-Cy5 were used. The Olympus confocal microscope with Fluorview software at the University of Michigan Microscopy Imaging Laboratory was used for imaging of the replication complexes.

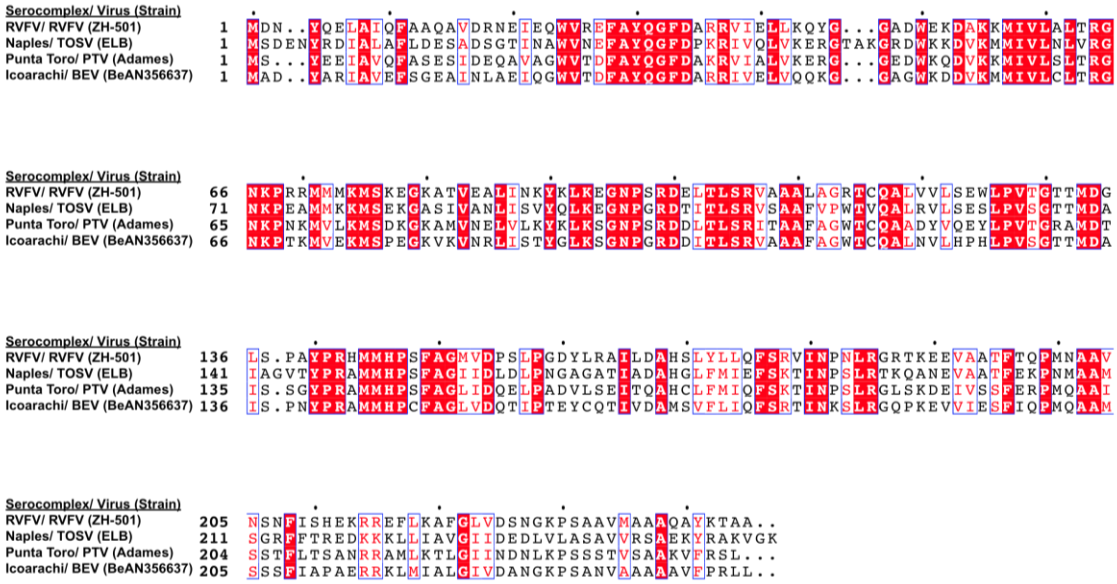

Figure 5.1. Phlebovirus genus N alignment.

The N proteins from representative viruses from different serocomplexes of the *Phlebovirus* genus were cloned into mammalian expression vectors. The invariant residues are listed in white with red background. Consensus residues are shown in red with white background and are boxed. Variable residues are black with white background.

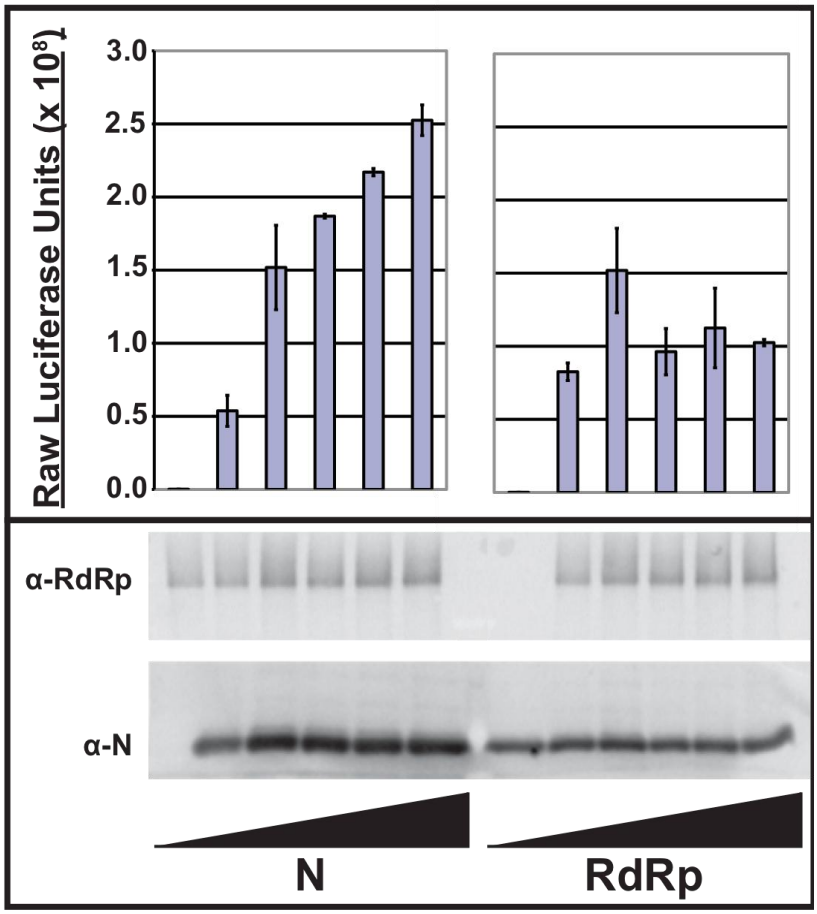

Figure 5.2. Increasing concentrations of N increase RdRp expression and transcriptional activity. BSR-T7 cells were transfected with RVFV minigenome, RVFV N, and RVFV RdRp, with increasing concentrations of RVFV N or RVFV RdRp. After 24h post-transfection, the cells were harvested and analyzed by RLuc assay and immunoblot.

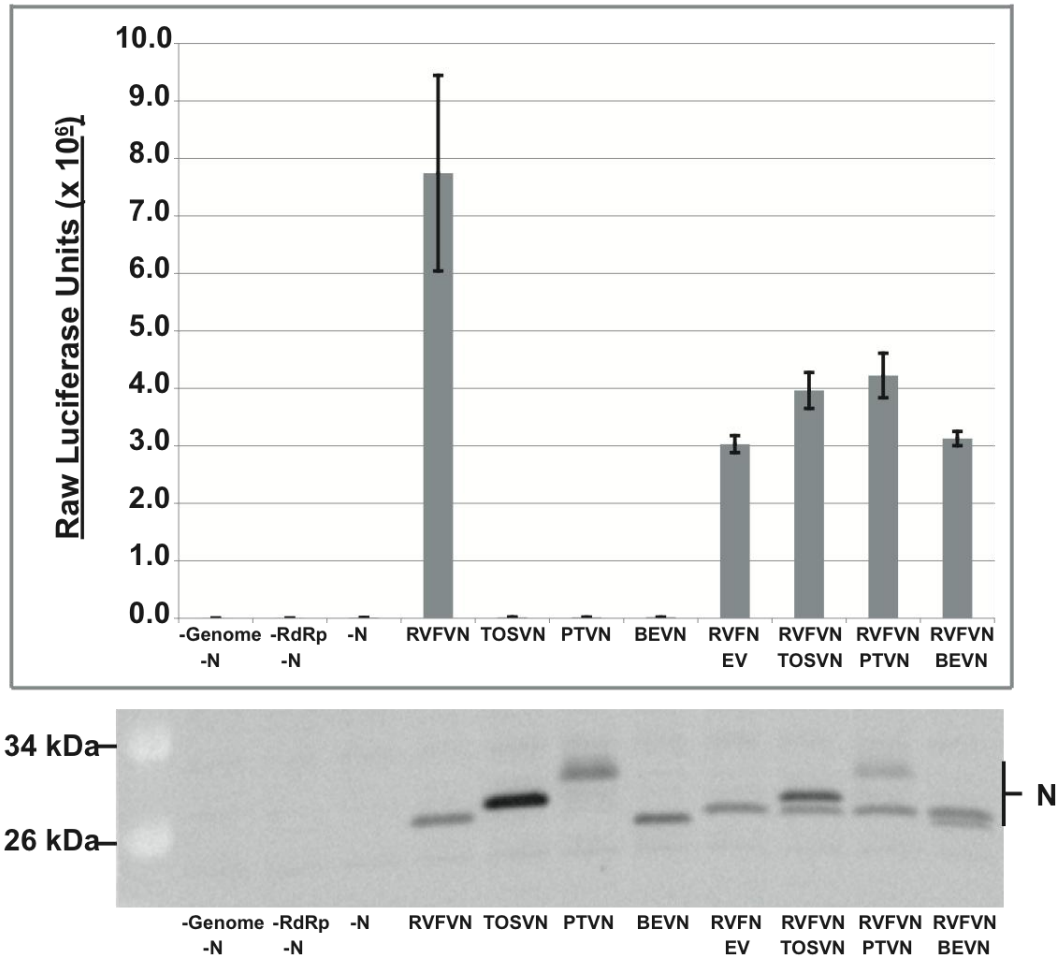

Figure 5.3. RVF replicon with heterologous N.
BSR-T7 cells were transfected with RVFV minigenome, RVFV RdRp, and combinations of empty vector (pVAX), RVFV N, TOSV N, PTV N, and BEV N. The raw luciferase units are shown with standard deviation along with an immunoblot of the heterologous N proteins expressed.

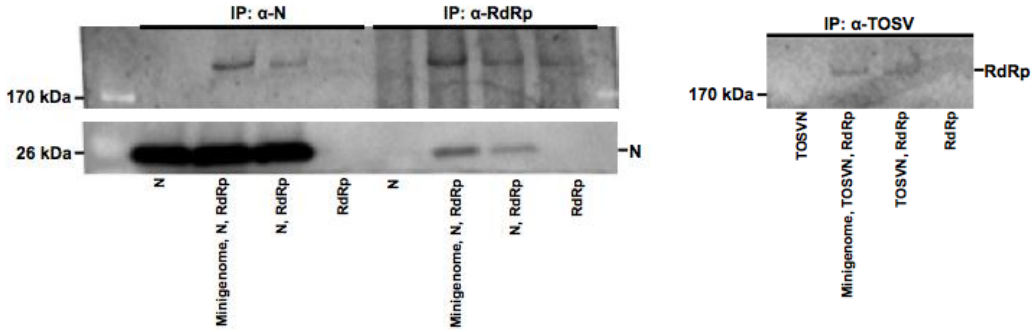

Figure 5.4. Heterologous N interact with RdRp.
BSR-T7 cells were transfected with combinations of RVFV minigenome, RVFV RdRp and RVFV N or TOSV N. The cells were lysed, cross-linked with DSP, and immunoprecipitated as indicated.

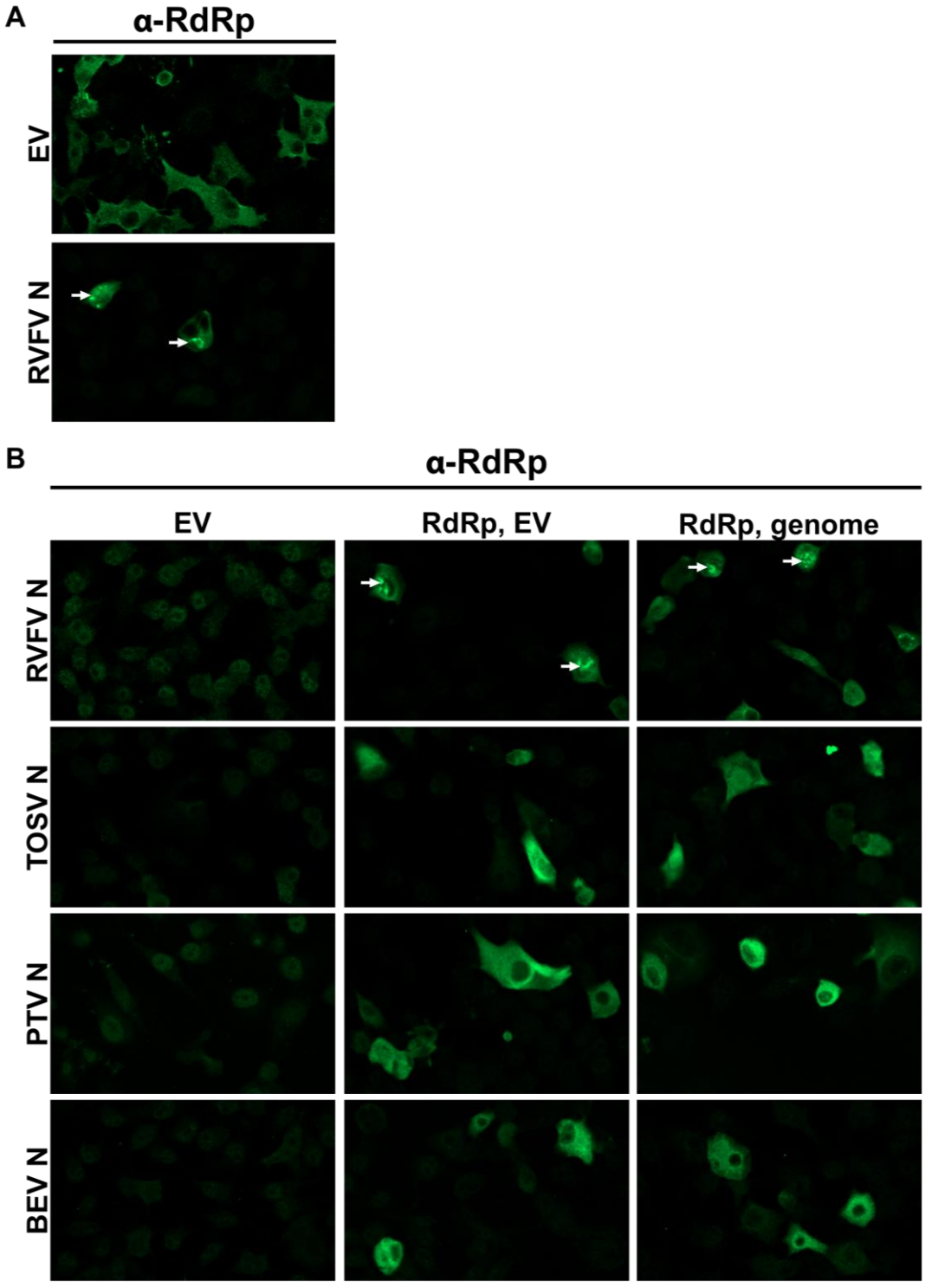

Figure 5.5. Heterologous N do not generate RdRp replication/transcription complexes.
(A) BSR-T7 cells were transfected with RVFV RdRp and empty vector(EV) or RVFV RdRp was co-expressed with RVFV N (RVFV N). **(B)** Heterologous N proteins were co-expressed with empty vector (EV), the RVFV RdRp (RdRp, EV) or RVFV RdRp and RVFV minigenome (RdRp, genome). RdRp localization is shown with white arrows depicting the RdRp puncta.

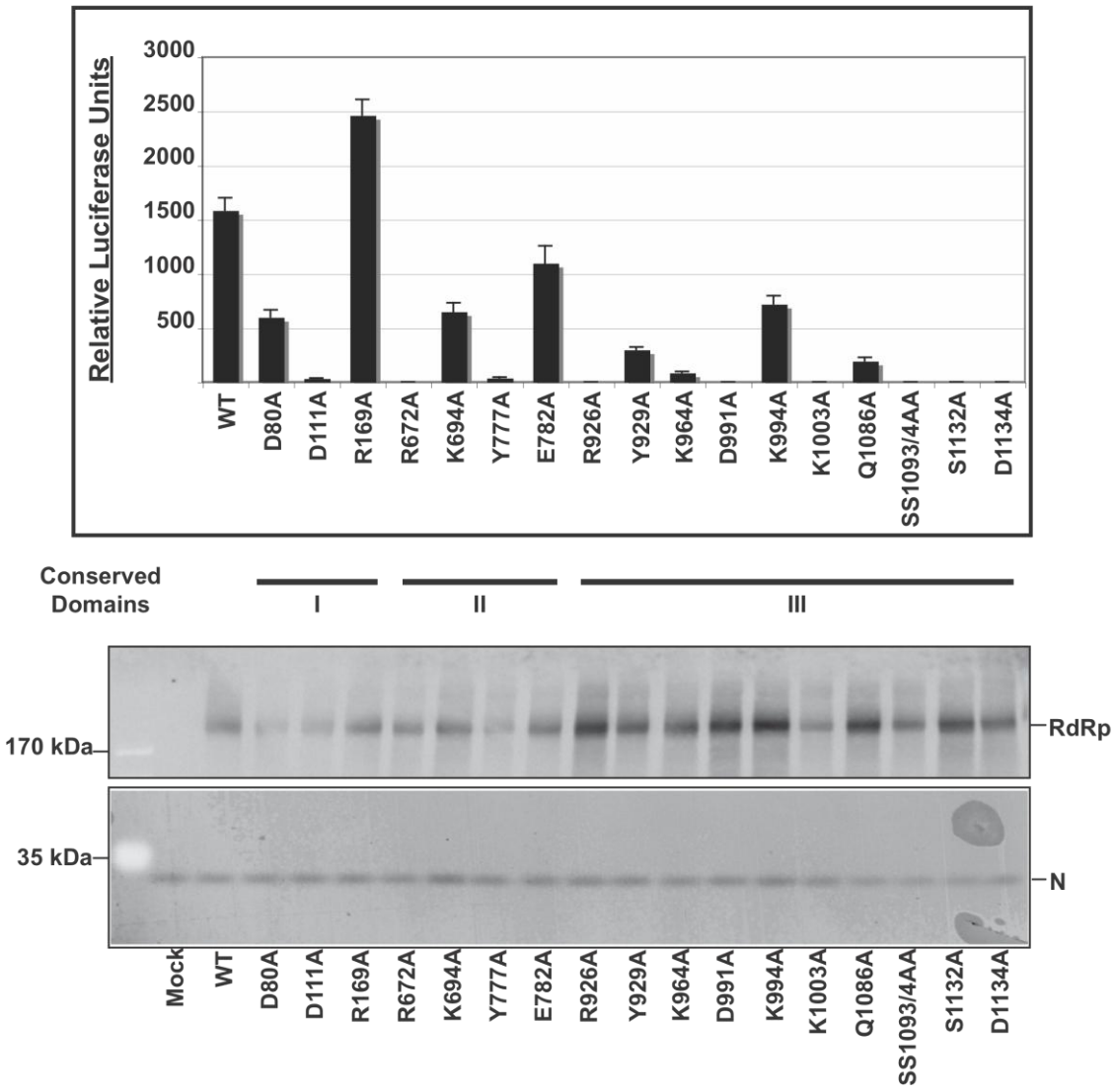

Figure 5.6. Expression and transcriptional activity of wild-type RdRp and RdRp mutants.
Wildtype (WT) or mutant RdRp was co-expressed with RVFV N and RVFV minigenome. Transcription of the RLuc reporter was determined by replicon assay with the values reported being relative to the Mock condition (lacking RdRp). The cell lysates were analyzed for RdRp and N expression by immunoblot.

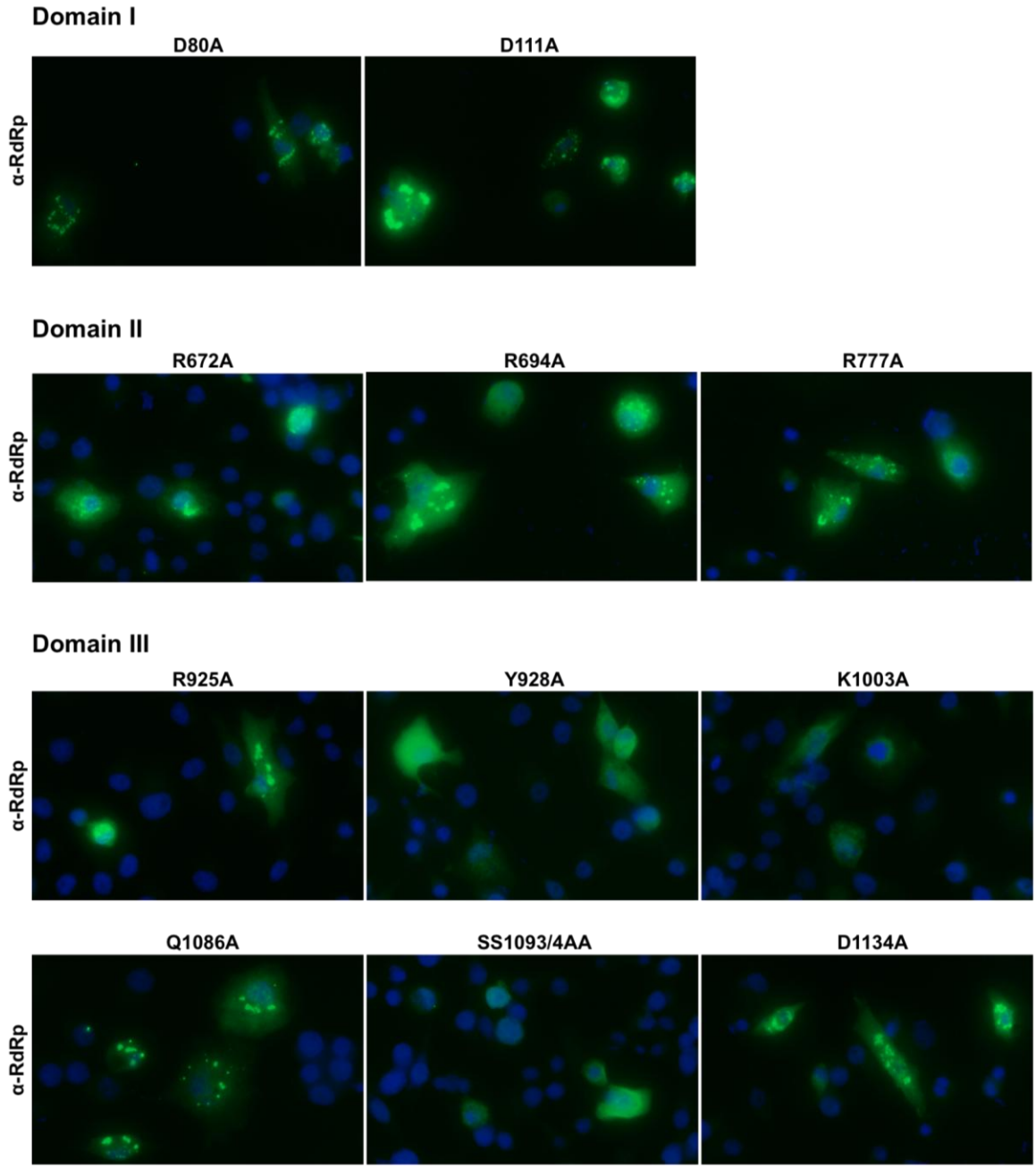

Figure 5.7. RdRp mutant localization in presence of N.
RdRp mutants (green channel) were analyzed by immunofluoresence microscopy when co-expressed with RVFV N and RVFV minigenome.

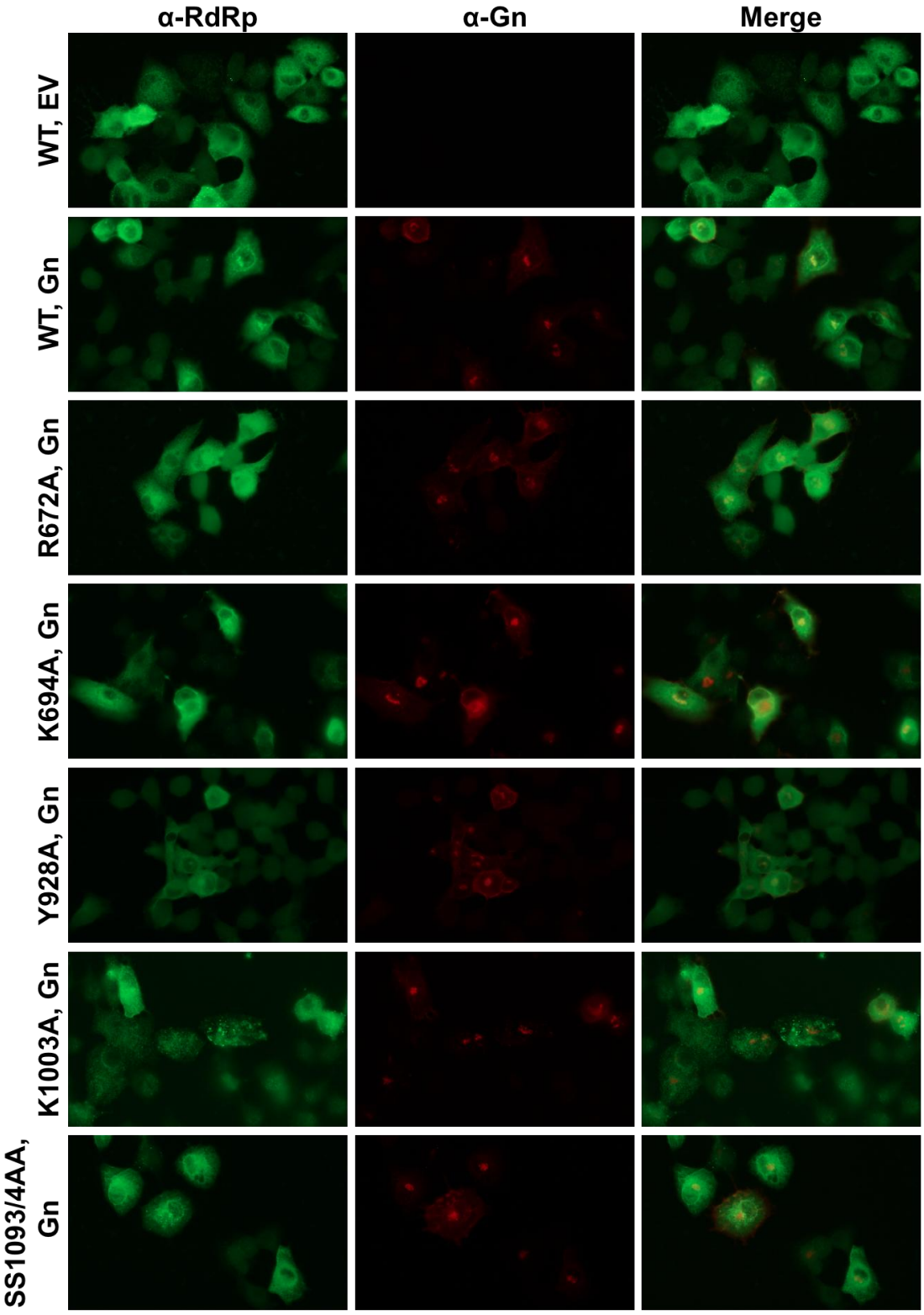

Figure 5.8. Gn recruitment of RdRp mutants.
Gn (red channel) was co-expressed with wildtype RdRp (WT) or mutants (green channel) and co-localization was analyzed using immunofluorescence microscopy.

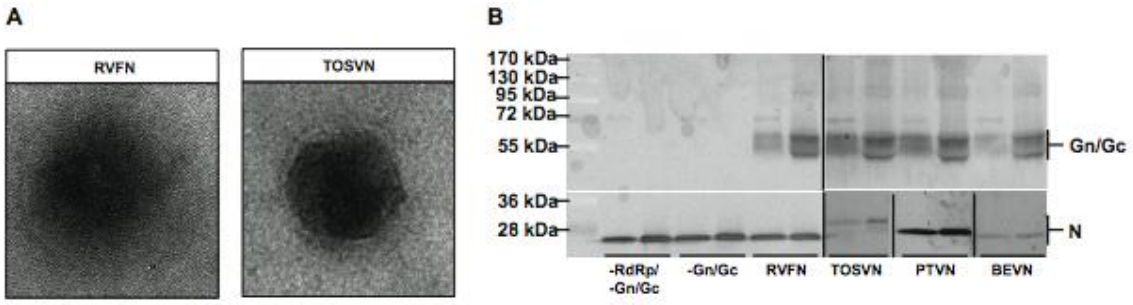

Figure 5.9. Heterologous N allow for efficient cellular release of VLPs.
BSR-T7 cells were transfected with combinations of RVFV minigenome, RVFV RdRp, RVFV Gn/Gc and RVFV N, TOSV N, PTV N, or BEV N. The VLPs were harvested and analyzed either by electron microscopy **(A)** or by immunoblot **(B)**.

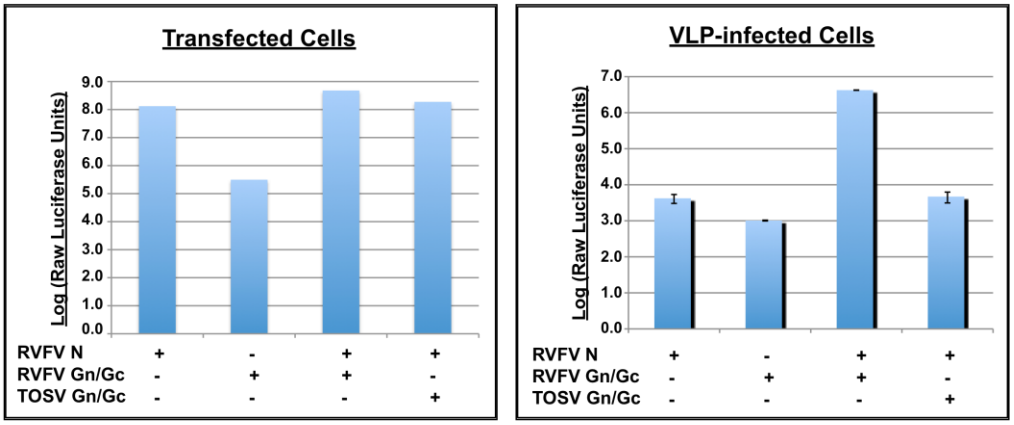

Figure 5.10. Heterologous Gn/Gc cannot interact with RVF RNPs for generation of infectious particles. BSR-T7 cells were transfected with combinations of RVFV minigenome, RVFV N or empty vector, RVFV RdRp, and RVFV Gn/Gc, TOSV Gn/Gc, or empty vector for VLP assay. Luciferase activities in transfected and VLP-infected cells are listed as average raw luciferase units with standard deviation.

Chapter 6

Conclusion

Negative-sense RNA viruses

Negative-sense RNA viruses share common steps in their viral replicative cycles, including transcription and replication of the viral genome, assembly at cellular membranes, and release of virus from the cell for the infection of naïve cells. Viruses have evolved intricate mechanisms to achieve these fundamental processes, utilizing both host and viral components. Although the replicative cycles differ vastly in the possible methods of hijacking the host cell, all of the negative-sense RNA viruses express N, RdRp, and envelope glycoprotein(s). While these proteins often perform multiple virus-specific functions, they must also perform the general functions required for the propagation of all negative-sense RNA viruses. Through the study of these general steps in the viral replicative cycle of RVFV, mechanisms unique to RVFV have been identified, as well as features common to other viruses in the *Bunyaviridae* family. We have discovered Gn to be sufficient for the independent recruitment and packaging of the encapsidated genome and the RdRp. Through the interaction with Gn, the encapsidated genome functions as a trigger for virus release from the host cell, representing a novel and elegant mechanism for the cellular release of RNA viruses.

Replication and transcription

The interactions between the RdRp, N, and genome necessary for replication and transcription have been well-characterized for several negative-sense RNA viruses containing segmented or non-segmented genomes, but not for any of the viruses in the *Bunyaviridae* family. To gain greater insight into the replication and transcription mechanisms utilized by RVFV, the replication and transcription strategies of other negative-sense RNA viruses are compared and contrasted with RVFV.

Replication and transcription strategies for viruses of the order Mononegavirales

The *Mononegavirales* (MNV) order is comprised of non-segmented negative-sense RNA viruses, including the measles virus (*Paramyxoviridae* family), rabies virus (*Rhabdoviridae* family), Ebola virus (*Filoviridae* family), and borna disease virus (*Bornaviridae* family), which exhibit similar genome organization and replication and transcription strategies. Replication and transcription are dependent upon the expression of the viral genome, N, RdRp, and an RdRp cofactor known as the phosphoprotein (P) (166). P functions to stabilize the RdRp and is required for the interaction of the RdRp with N, bridging the two molecules and allowing RdRp access to the viral genome for transcription and replication (166). The increasing synthesis of P enhances these viral processes (166). Viral transcription continues until the accumulation of free N surpasses a threshold, promoting a switch from transcription to replication (167).

The crystal structures and electron microscopy images for N and P from several viruses within the MNV order suggest the utilization of similar replication and transcription strategies. The N from respiratory syncytial virus (RSV) (*Paramyxoviridae*), rabies virus (*Rhabdoviridae*), and vesicular stomatitis virus (*Rhabdoviridae*) have been crystallized as multimeric ring-like structures bound to RNA (88-90). The borna disease virus (*Bornaviridae*) N has also been crystallized, in the absence of RNA (91). All of the MNV N structures exhibit similar folds for the N- and C-terminal lobes, which are separated by a positively charged RNA-binding groove (89). The non-conserved regions among the MNV N form a variable region and the N- and C-terminal arms (89). The N- and/or C- arms interact laterally for N-N contacts, adding stability to the RNP structures (89). The C-arms are also suggested to interact with P for replication and transcription (168, 169).

The RSV and vesicular stomatitis virus N structures have been modeled onto 3D reconstructed EM images of helical viral RNPs (89, 170). The crystal structure of vesicular stomatitis virus was superimposed on that of RSV, and the N were found to bind RNA similarly, forming specific contacts with the RNA backbone, as well as non-specific interactions with the RNA bases (89). The binding of P to N is proposed to generate a hinge movement of the N- and C-terminal lobes relative to each other. The hinge movement would expose the buried RNA bases and RNA synthesis by the RdRp

(89). The N-RNA complex appears to be highly conserved within the MNV order (88-91, 168, 170), and, based on the biological, biochemical, and structural studies, the viruses belonging to the MNV order likely replicate and transcribe the genome using similar strategies.

The replication and transcription processes for the negative-sense non-segmented viruses differ significantly from the segmented viruses. Nevertheless, RVFV shares some similarities with the non-segmented negative-sense RNA viruses. While there is no P protein that is required for interaction between RVFV N and RdRp for replication and transcription, the RVFV N may functionally replace the MNV P in some respects. For example, P stabilizes the expression of the RdRp for viruses within the MNV order, and our data suggest a similar phenomenon occurring with RVFV N (Chapter 5). Upon expression of greater amounts of RVFV N, we detect greater levels of RdRp and increased transcriptional activity, suggesting that N is a limiting factor and can stabilize RdRp expression. Additionally, RVFV N is similar in character to the MNV N. Upon expression of recombinant RVFV N in *E. coli*, a multimeric complex was formed tightly bound to the *E. coli* RNA. The encapsidated RNA was resistant to extremes of salt and pH, as well as extensive treatment with RNase (Chapter 3). Therefore, the RVFV N-RNA complex was highly stable, and the RNA backbone was protected from RNase digestion. The resistance to RNase digestion suggested that RVFV N binds to the RNA phosphate backbone, similar to MNV N. Therefore, the negatively-charged RNA backbone would be predicted to bind a highly basic (positively charged) region on RVFV N. However, upon crystallization of the RVFV N dimer, we detected no such groove. Although the RVFV N structure contained N- and C-terminal lobes, similar to MNV N, they were not separated by a positively charged RNA-binding groove (Chapter 3). Additionally, in contrast to MNV N, there were no N- or C-terminal arms extending from the core structure for lateral interactions with other N. Instead, the N-terminus was involved in N-N interactions for formation of the dimer interface (Chapter 3). Using a replicon assay, we found that mutation of a critical residue (Trp125) in the dimer interface resulted in loss of transcriptional activity of RdRp, suggesting that the dimer is a functional unit required for RVFV replication and transcription (Chapter 3). However, a defect in dimerization could not be identified using protein cross-linking. The mutation

likely destabilizes the dimer interface, allowing the dimers and multimers to form transiently. To further demonstrate the defect, the N mutants should be investigated using size-exclusion chromatography and RNA binding studies.

Since the RVFV N structure did not exhibit any obvious RNA binding groove, we sought to identify possible RNA-binding sites. The phlebovirus genus contains N that are at least 41% identical at the amino acid level, with the exception of the Uukuniemi virus, which is much more divergent. Therefore, the N should fold and bind to RNA similarly. As a result, the RNA-binding region should be conserved amongst phleboviruses, as well as be highly basic and surface exposed. Most of the phlebovirus N conservation mapped to the core of N, and the majority of surface-exposed residues were highly divergent or hydrophobic (Chapter 3). A single potential RNA-binding site was identified (Chapter 3). To determine whether these residues are, indeed, involved in interaction with the genomic RNA, mutagenesis studies should be completed using the potential RNA binding region that we have identified. Additionally, efforts should be continued for crystallizing N bound to RNA.

Replication and transcription of segmented RNA viruses

Most of the transcription and replication studies of the segmented negative-sense RNA viruses are performed with influenza A virus (FLUVA) from the *Orthomyxoviridae* family, and very little is known about these processes for the *Bunyaviridae* or *Arenaviridae* families. Since the transcription and replication strategies for FLUVA have been well-studied, they may provide better insight into these processes for RVFV. In contrast to RVFV, FLUVA contains eight genomic segments and requires N in addition to three polymerase subunit proteins (PA, PB1, and PB2) for replication and transcription of the genomic RNA (171). Additionally, these processes for FLUVA occur in the nucleus instead of the cytoplasm. For FLUVA transcription, PB2 binds to m7G methyl caps of host mRNAs, while PB1, possibly in concert with PA, cleaves the m7G methyl caps plus 10-15 nucleotides of RNA and uses them to prime transcription of the viral genes (171, 172). Similar to FLUVA, RVFV utilizes the m7G methyl caps to prime transcription of the viral genes (40), however the caps are acquired in the cytoplasm for RVFV opposed to the nucleus for FLUVA (40, 171). FLUVA PB1 appears to function as the transcriptase and replicase, as it contains the four conserved sequence motifs of

viral RdRps (171, 173). Additionally, PB1 interacts with N and functions in RNA elongation (92).

Structure of the N proteins

Although RVFV performs replication and transcription within the cytoplasm and FLUVA carries out these processes in the nucleus, the strategies involved may be similar. The FLUVA N was crystallized in the absence of RNA, and a highly basic RNA-binding groove was suggested. The RNA binding groove corresponded to the interface of the N- and C-terminal lobes (87), similar to the RNA-binding grooves identified for the viruses of the MNV order. Recently, the predicted RNA-binding groove of FLUVA was verified through the generation of biologically active FLUVA RNP complexes, which were visualized using cryo-EM, and the bound RNA was resistant to RNase treatment (92). The crystal structures of FLUVA N and fragments of the RdRp were mapped onto the EM structures for the determination of the N-N interaction domains. FLUVA N-N interaction was found to involve an extension of the N-terminus laterally to other N subunits (92), similar to the MNV N.

Overall, the RVFV N structure is unique from FLUVA N and MNV N. Through the crystallization of RVFV N we have identified a novel type of RNA binding protein. RVFV N represents a new classification of viral N, which binds RNA differently than the other viral N with known structures. Despite the differences in N structure, the N crystallized from the *Paramyxoviridae*, *Rhabdoviridae*, *Orthomyxoviridae*, and *Bunyaviridae* families bind RNA non-specifically, are comprised of N- and C-terminal lobes, are predominantly α-helical in composition, and protect the RNA backbone (88-90, 92, 174, 175). In contrast to all known N structures, RVFV N does not appear to bind RNA in a binding groove separating the N- and C-terminal lobes; therefore, it will be exciting to investigate how RVFV N interacts with the RNA genome. Future work will focus on crystallizing the multimeric RVFV N bound to RNA, as well as examining RVFV N mutants in the predicted RNA binding region for changes in multimerization, RNA binding affinity, and transcription by the RdRp.

RdRp-N interactions

While the RVFV and FLUVA N structures are unique, both N proteins interact with the RdRp. The RVFV RdRp was found to interact with N in the absence of genome, and co-expression of N altered the localization of RdRp to perinuclear aggregates of unknown identity (Chapter 5). Presumably, these RdRp aggregates are transcription and/or replication complexes, as we have identified RdRp mutants that no longer localize to these perinuclear punta in the presence of N and have reduced transcriptional activity (Chapter 5). One of the RdRp mutants was still capable of interacting with Gn; therefore, inability to form puncta was not due to misfolding of the RdRp (Chapter 5).

The conservation of the RdRp and N interaction amongst viruses belonging to other serocomplexes of the *Phlebovirus* genus was also investigated. While the heterologous N could interact with the RVFV RdRp as determined through immunoprecipitation studies in the presence of cross-linker, the N could not recruit the RdRp to the perinuclear structures (Chapter 5). Additionally, the heterologous N could not support transcription by the RdRp in replicon assays, supporting the role of the perinuclear aggregates as replication/ transcription factories (Chapter 5). Interestingly, the N from the *Hantavirus* genus (*Bunyaviridae* family) localize to cytoplasmic puncta, which have been previously identified as processing bodies (p-bodies) (176). The function of p-bodies is to store and degrade cellular RNAs, resulting in degradation of m7G methyl caps (177, 178). Hantavirus N have been found to aid in the acquisition of m7G methyl caps from host mRNAs for priming of hantavirus transcription (179). RVFV N may also interact with the p-bodies and recruit the RdRp. The localization of RdRp to p-bodies is an intriguing theory since the RdRp could acquire m7G methyl caps from host mRNA to initiate viral transcription.

Future studies investigating the interactions between the RdRp and N necessary for the generation of the predicted replication/ transcription complexes should include the construction of N chimeras. The crystal structure of N, as well as the homology models for the heterologous N would aid in the construction of the chimeric constructs. The region required for generation of the replication/ transcription factories should not be conserved, since the heterologus N cannot recruit the RVFV RdRp to these structures. Therefore, the divergent surface exposed regions of N would be predicted to interact with

the RdRp. A possible region of interest would be the C-terminus of N, which is a region of N that is more divergent (Chapter 3 and 5). Moreover, the C-terminal salt bridge was identified as being critical for replication/ transcription by the RdRp (Chapter 3); this could be due to its inability to form replication/ transcription complexes. In addition to investigating this mutant by immunofluorescence with co-expression of the RdRp, to narrow the region of interaction, chimeras expressing the N-terminus of RVFV N and the C-terminus of the heterologous N could be constructed. A more detailed investigation of the N structure with regard to interaction with the RdRp may also yield other lucrative regions of N to investigate.

Identification of the interaction domain between N and RdRp would aid in our understanding of how the RVFV replication/ transcription complexes are formed, but the discovery of the identity of the perinuclear structures would allow for increased investigation of the host interactions necessary for RVFV propagation and potential therapeutic targets. The identity of the replication/ transcription complexes could be investigated using immunofluorescence microscopy. The p-bodies could be stained along with the RdRp, and visualized by confocal microscopy in the presence and absence of N. The localization of the RdRp to p-bodies would be anticipated only when co-expressed with N. Additionally, live cell imaging could be pursued with tagged RdRp constructs. The RdRp still exhibits catalytic activity with a tag fused to the C-terminus (data not shown) (180). Therefore, for identification of the replication/ transcription factories, live cell imaging studies could be performed with tagged RdRp co-expressed with tagged actin, tubulin, or p-body components.

Shared mechanisms for replication and transcription

Regardless of the differences between RVFV N and FLUVA N structures, parallels can be drawn between FLUVA and RVFV for replication and transcription. A recent study has provided detailed insight into the processes of replication and transcription for FLUVA. Jorba et. al. purified FLUVA RNP complexes containing transcription or replication deficient RdRp, then, investigated whether the defective RdRp-containing RNPs could be complemented in *trans* with wild-type RdRp (181). The transcription-deficient RNPs could not be complemented with wild-type RdRp,

leading the authors to conclude that FLUVA transcription of the RNA genome requires cis-acting RdRp (181). In contrast, replication-deficient RNPs could be complemented in *trans* with wild-type RdRp, suggesting that genome replication in FLUVA is achieved by newly synthesized RdRp molecules in *trans* (181). Jorba et. al. developed a model for FLUVA replication and transcription based on their results with the transcription and replication defective RdRps. The initiation of genome replication was proposed to require an interaction between parental and newly synthesized RdRp that allows the newly synthesized RdRp access to the 3' end of the genome (181). The FLUVA RdRp oligomerizes *in vivo*, and it was suggested that replication of the genome may require oligomers of RdRp, perhaps forming a fixed scaffold for the generation of multiple newly synthesized RNPs (181). A soluble RdRp distinct from the replicating RdRp is proposed to bind the newly synthesized RNP on the 5' terminus and becomes the *cis*-acting RdRp on the new template (181).

The processes of primary transcription and replication have been greatly elucidated for FLUVA using trans-complementation experiments. Similar to the FLUVA we have investigated the ability of RdRp to complement replication and transcription in *trans* for RVFV (Chapter 4). However, we did not have the capacity to differentiate between replication and transcription, nor did we use purified RNPs. Infectious VLPs were used to deliver the RVF-RNPs to target cells, and RdRp and N were expressed in *trans*. We found that expression of RdRp and N in *trans* could enhance replication and transcription by RNPs that were non-defective for replication and transcription (Chapter 4). However, if the particles were replication and transcription defective, then we could not complement in *trans*, similar to FLUVA. Because we were using VLPs to deliver RNPs to the target cells, these results could be due to any of the following: the VLPs lacking competent RNPs are non-infectious, the VLPs are infectious, but the RNPs cannot access the RdRp/N expressed in *trans* due to subcellular localization, or, similar to FLUVA, the VLPs are infectious, but transcription of the viral genome cannot occur in *trans*. Without a cis-acting transcriptionally active RdRp, the soluble RdRp may fail to gain access to the 3' end. Therefore, although the structure of RVFV N and FLUVA N are very distinct, RVFV and FLUVA may share mechanisms for replication and transcription.

Viral assembly

Following transcription and replication, negative-sense RNA viruses assemble the viral components at cellular membranes prior to budding and release. While negative-sense RNA viruses generally require matrix or matrix-like proteins for the recruitment and packaging of the viral RNP complexes (182), the *Bunyaviridae* family of viruses does not encode these proteins. Few studies with bunyaviruses have addressed the process of RNP recruitment and packaging. However, with RVFV N and RVFV RdRp expressed in the cytoplasm and the envelope glycoproteins localizing to the Golgi apparatus (35), we hypothesized that the cytoplasmic portions of the envelope glycoproteins would recruit the RNP complexes for assembly at the Golgi.

To investigate the processes of RVFV assembly and cellular release, we developed an RVF-VLP system. Our RVF-VLP system generated particles antigenically indistinguishable from virulent RVFV. The RVF-VLPs also responded to inhibitor compounds similar to RVFV (Chapter 2). The minigenome design utilized the ambi-sense nature of the S-segment, replacing the NSs gene with a GFP or RLuc reporter gene. Additionally, the minigenome had an internal deletion in the N gene, preventing its expression, thereby, allowing us to investigate the roles of N separately from the genome. The transcription of the minigenome reporter required the expression of RdRp and N and generated RLuc reporter signals over 1,500-fold background in transfected cells. When the envelope glycoproteins were expressed as well, RVF-VLPs were produced, and RLuc reporter signals consistently exceeded 3,000-fold background levels in VLP-infected target cells (Chapter 2).

Initially we utilized this highly-sensitive RVF-VLP system to investigate the recruitment of the RdRp and the encapsidated genome to the Golgi apparatus for packaging into virus particles. We hypothesized that the cytoplasmic tail of Gn and/or Gc were necessary for the recruitment and packaging of the viral RNP complexes. Therefore, the packaging of the RdRp and encapsidated genome was investigated in the absence of Gn or Gc. Particles were not efficiently produced lacking either glycoprotein; however, particles were detected in both conditions, and N was packaged in the absence of Gc (Chapter 4). To verify Gc was not required for the packaging of N, a truncated Gc mutant lacking the entire predicted cytoplasmic tail (GcW1) was expressed with Gn. In

the absence of the Gc cytoplasmic tail, Gn packaged the RdRp and encapsidated genome, generating infectious RVF-VLPs (Chapter 4). Therefore, Gn was sufficient for recruitment and packaging of the RdRp and encapsidated genome. To investigate the regions of the Gn cytoplasmic tail required for these interactions, a Gn mutant lacking the C-terminal 40 amino acids of the 70 amino acid cytoplasmic tail was investigated (GnK48). The GnK48 mutant RVF-VLPs packaged N, but not the RdRp, indicating that the Gn may utilize different regions of the cytoplasmic tail for interaction with the encapsidated genome and the RdRp (Chapter 4).

The RVF-VLP results for packaging of RdRp were supported by studies using immunofluorescence microscopy. Gn was shown to be necessary and sufficient for the recruitment of the RdRp to the Golgi apparatus. Specifically, the terminal 40 amino acids of the Gn cytoplasmic tail were required for interaction between the RdRp and Gn (Chapter 4). The immunofluorescence microscopy also demonstrated that Gn could recruit the RdRp in the absence of encapsidated genome (Chapter 4). These results, in combination with the GnK48 mutant RVF-VLPs packaging of N, but not the RdRp, suggest that the encapsidated genome is not recruited as an RNP complex with the RdRp bound. Very few studies involving negative-sense RNA viruses have investigated the requirements for the packaging of the RdRp. Usually, the packaging of N is interpreted as packaging of the entire RNP complex. However, our data suggest that the encapsidated genome and the RdRp can be packaged separately, and assumptions should not be made regarding the packaging of all of the RNP components.

Since the other families of negative-sense RNA viruses use matrix or matrix-like proteins for recruitment of the RNP complexes, parallels with RVFV assembly are difficult to establish outside of the *Bunyaviridae* family. However, the mechanism utilized by RVFV may be similar to other bunyaviruses. We investigated whether the Gn interactions with the encapsidated genome and the RdRp were conserved within the *Phlebovirus* genus (Chapter 5). Using the VLP system, we discovered that heterologous N were packaged by RVFV Gn/Gc; therefore, the interaction between Gn and encapsidated genome was conserved among various serocomplexes of the *Phlebovirus* genus (Chapter 5). In contrast, the interaction between the RdRp and Gn did not appear conserved. Expression of the Gn and Gc from the Toscana virus (*Phlebovirus* genus)

with RVF-RNP complexes generated VLPs, but the particles did not generate reporter expression in target cells, suggesting the RdRp was not packaged (Chapter 5). Therefore, we anticipate the interaction domain of Gn with N is conserved, and the interaction domain with the RdRp is not conserved amongst phleboviruses. An amino acid sequence alignment of the Gn cytoplasmic tail from phleboviruses identified high sequence identity in the predicted N interaction domain, but low sequence identity for phleboviruses in the predicted RdRp interaction region (Fig. 6.1), supporting our results. The N interaction domain contains several highly conserved bulky hydrophobic residues (Fig. 6.1), which would be likely candidates for interaction with the conserved hydrophobic pocket of N that we previously identified in the crystal structure of RVFV N (Chapter 3).

The other viruses in the *Bunyaviridae* family that have been investigated for RNP assembly and packaging are the Tomato spotted wilt virus (TSWV) (*Tospovirus* genus) and the Uukuniemi virus (UUK) (*Phlebovirus* genus) (86, 127). The interactions between the envelope glycoproteins and N from the TSWV were investigated previously using fluorescence resonance energy transfer (FRET) and fluorescence lifetime imaging microscopy (FLIM) techniques (127). Interactions between both Gn and Gc with N were discovered, and the independent interactions with N stabilized the expression of both glycoproteins. Competition experiments suggested that the interaction between N and Gn was much stronger than the interaction between N and Gc (127). While interactions between RVFV Gc and N may function in the RVFV replicative cycle, RVFV Gc-N interactions are not required for the recruitment or packaging of the encapsidated genome. Similar to RVFV, TSWV N interacted with the Gn cytoplasmic tail, and did not require the C-terminal region of the tail (20 amino acids) for interaction (127). The Gn and N from TSWV diverge greatly from RVFV, so it is unlikely that the interaction domain between Gn and N would be conserved; however, the same region of the Gn cytoplasmic tail appears to be important.

The only other study characterizing the assembly and packaging of viruses in the *Bunyaviridae* family was performed with the Uukuneimi virus (UUK) (*Phlebovirus* genus). A UUK-VLP system was utilized to investigate packaging of RNPs (86). Mutants were generated for the entire UUK Gn cytoplasmic tail, and the residues important for RNP recruitment were determined by the absence of packaged N and lack

of infectious particles. The investigators discovered that the Gn cytoplasmic tail was required for packaging of UUK N, similar to TSWV and our observations with RVFV (86). However, the region identified corresponded to the last two amino acids of the Gn cytoplasmic tail (86). In contrast, the RVFV N interaction domain did not require the last 40 amino acids of the C-terminal region of the tail (Chapter 4). These results suggest that UUK utilizes a different region of interaction for packaging N than RVFV and the other serocomplexes of the *Phlebovirus* genus. The use of a unique method for RNP packaging by UUK would not be surprising as UUK exhibits low sequence identity to the other phlebovirus serocomplexes. Therefore, the Gn-N interaction domain appears conserved for phleboviruses, with the exception of the UUK virus.

We are currently pursuing the design of peptides corresponding to the region of Gn predicted to interact with N. The peptides will be investigated for binding to N in the presence and absence of genome. We predict that the hydrophobic pocket will be the site of Gn interaction for N, as it is hydrophobic and conserved amongst phleboviruses. If peptides bind N, then crystallization of the N bound to the Gn peptide could be initiated. The peptides, themselves, may function as inhibitors to RVFV propagation and should be investigated for antiviral effects in an RVFV infection. Additionally, the crystallization of Gn peptides to N could allow for the design of small molecule inhibitors. The Gn-N interaction could represent a possible therapeutic target for viruses of the *Phlebovirus* genus, including any emergent reassorted viruses.

In contrast to the Gn-N interaction domain, the Gn region of interaction with the RdRp is not highly conserved for phleboviruses (Fig. 6.1). The RVFV Gn-RdRp interaction may be further refined through the generation of Gn cytoplasmic tail chimeras. The TOSV Gn appears to package the RVFV encapsidated genome, but not the RVFV RdRp (Chapter 5). Based on our results demonstrating the RVFV Gn tail residues 31-70 (Fig. 6.1) contain a region required for recruitment and packaging of the RVFV RdRp (Chapter 4), a chimera containing TOSV Gn residues 1-25 and RVFV Gn residues 26-70 (Fig. 6.1) should be capable of RdRp recruitment. Therefore, the expression of chimeric Gn with TOSV Gc, and RVFV RNP complexes should generate infectious VLPs. The region of Gn-RdRp interaction could be narrowed further through generation of a chimera containing TOSV Gn residues 1-47 and RVFV Gn residues 48-

70 (Fig. 6.1). Successful Gn-RdRp interaction could be determined by generation of reporter signal in VLP-infected cells.

Based on our studies of RVFV assembly, the encapsidated genome and RdRp can be independently recruited by Gn. However, we did not decipher whether the genome and N could interact with Gn independently. The interaction of Gn with N in the presence and absence of genome can be investigated using immunoprecipitation experiments. Whether there is an interaction between Gn and the genome could also be investigated using filter binding assays. If Gn binds the genome, then affinities could be calculated for the binding of Gn to specific RNAs. Through this method, it is possible that the RVFV genome packaging signal could be identified.

Cellular release of virus

The budding and release of virus from the host cell is the final stage of the viral replicative cycle. Using the RVF-VLP system, we investigated the RVFV components necessary for efficient cellular release of particles. We transfected cells with all the viral structural components or mixtures lacking one or more of the components, then harvested the particles to determine whether the RVF-VLPs were efficiently released from the cell. The RVF-VLPs were analyzed by EM or by immunoblot, and the efficiency of RVF-VLP cellular release was calculated. Using our RVF-VLP system, we discovered that the encapsidated genome was necessary for efficient RVF-VLP release, demonstrating a novel mechanism for virus release utilizing the viral genome as a trigger.

RVF-VLPs were efficiently produced only when the encapsidated genome was expressed in combination with the envelope glycoproteins. While no particles could be visualized for conditions lacking N or the envelope glycoproteins, particles were visualized by EM for conditions lacking genome; however, they were not efficiently released. When the RdRp was not expressed, RVF-VLPs were generated at levels similar to wild-type RVF-VLPs, indicating that the RdRp was not required for the cellular release of virus. Therefore, only the encapsidated genome and glycoproteins were required. The requirement for encapsidated genome for efficient release of RVFV illustrates an elegant mechanism. Through requiring genome for efficient release of particles, most RVFV particles should contain genome and be infectious. The efficient release of infectious particles by bunyaviruses is supported by experiments performed

using the Bunyamwera virus (*Orthobunyavirus* genus). Lowen *et. al.* (2005) determined the particle:plaque-forming unit ratio for the Bunyamwera virus to approach one, suggesting most of the particles generated were infectious, hence, contained genome (183).

Generally, negative-sense RNA viruses not only require matrix proteins for the assembly of virus particles at cellular membranes, but also for the budding of virus from the cell (139-147, 149-152, 184). Although the matrix protein might not be the only viral protein required for efficient release, it is usually necessary. After linking the viral RNPs with the envelope glycoprotein(s), the matrix protein can trigger particle budding and cellular release. To compensate for the lack of a matrix protein, bunyaviruses have developed an elegant mechanism for virus release. The Gn can independently recruit the encapsidated genome, RdRp, and Gc for formation of particles, and the cellular release of virus is dependent upon the interaction between the encapsidated genome and Gn. We propose the interaction between the encapsidated genome and Gn triggers virus release through stimulating the budding of virus particles into the lumen of the Golgi apparatus. The low particle-to-pfu ratio for the Bunyamwera virus demonstrates that all three genomic segments are packaged. Previous studies have suggested the RVFV L, M, and S segments to be packaged at the molar ratio of 1:4:4, respectively (41); therefore, we propose that a critical amount of genome must interact with Gn before sufficient curvature in the membrane is generated to allow budding. The critical amount of genome would encourage the packaging of all three segments similar to the molar ratio of 1L:4M:4S (~28 kb). The virus would bud upon Gn binding this critical quantity of encapsidated genome.

While we have identified the encapsidated genome as required for efficient cellular release of RVFV, similar studies with the UUK virus have demonstrated the use of different mechanisms for virus release. Using a VLP system developed for the UUK virus, Overby et. al. found the envelope glycoproteins to be released at high levels regardless of the presence of RNPs (185). The UUK Gn/Gc could bud into the lumen of the Golgi apparatus and release from the cell without the expression of any other viral component (185). The UUK Gn/Gc are very divergent in amino acid sequence from RVF Gn/Gc, and it is not surprising that there may be differences in the virus release

mechanisms. However, it has not been investigated whether the expression of the encapsidated genome may increase the efficiency of release for UUK.

In contrast to the UUK serocomplex, the viruses belonging to other phlebovirus serocomplexes contain a conserved region for Gn-N interaction, and the N from representative viruses of several serocomplexes functioned in the efficient cellular release of RVFV Gn/Gc. Since the encapsidated genome is required for efficient release, then the heterologous N must also functionally interact with the RVFV minigenome. Therefore, the regions of Gn and N necessary for efficient release of virus appear conserved amongst the phleboviruses, with the exception of the UUK virus.

Screening of small molecule inhibitors

The development of the RVF-VLP system was paramount in investigating the steps in the RVFV replicative cycle, but it also could be an invaluable tool for screening RVFV small molecule inhibitors. Using the RVF-VLP system, we could identify potent inhibitors of RVFV using a luciferase read-out that is scaleable for high-throughput screening. Our VLP system is extremely sensitive, and routinely generates luciferase expression of over 3000-fold background levels in VLP-infected cells. This extreme sensitivity allows for the differentiation between strong RVFV inhibitors from weak or moderate inhibitors targeting viral replication, transcription or cell entry. After inhibitors have been identified, all of the tools that we have developed for investigation of the RVFV replicative cycle could be utilized as secondary screening tools for determining the step in the replicative cycle that the inhibitor is acting upon. For example, we can perform RVF-VLP infection time-courses adding inhibitor at different times post-infection, replicon assays to determine whether inhibitors act on replication and/or transcription, as well as immunoprecipitations and immunofluorscence microscopy to determine whether inhibitors block the RdRp-N interaction or formation of replication and transcription complexes. Finally, we can investigate whether the inhibitors can reduce authentic RVFV titer using plaque assays.

Summary

The elucidation of the steps in the RVFV replicative cycle will aid in our understanding of RVFV and the identification of possible therapeutic targets. Using our

results in combination with studies from other negative-sense RNA viruses, we propose a model for the RVFV replicative cycle.

Upon entry of RVFV into host cells, the RNP complexes are released into the cytoplasm. Transcription of the viral genome is primed by m7G methyl caps cleaved from host mRNAs, and the cis-acting RdRp transcribes the genome, generating viral mRNAs to be translated by the host machinery. The newly synthesized RdRps interact with the cis-acting RdRps, and then replicate the genome. Newly synthesized N encapsidates the genomic RNA, and the encapsidated genome and RdRp are recruited to the Golgi apparatus through independent interactions with the Gn cytoplasmic tail. Multiple interactions between Gn proteins and the encapsidated genomic segments trigger budding of particles into the Golgi apparatus after sufficient quantity of encapsidated genomic segments bind to Gn proteins. The Golgi apparatus fragments, and the Golgi-derived vesicles containing RVFV fuse with the plasma membrane for RVFV release.

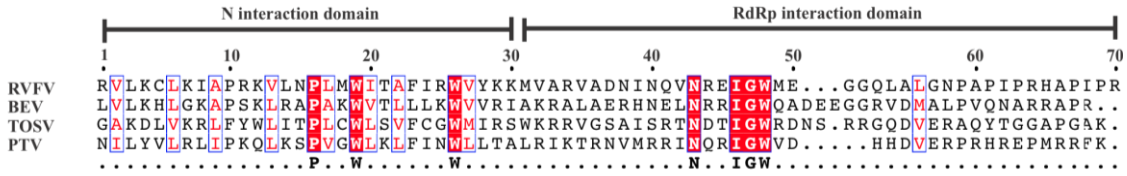

Figure 6.1. Alignment of the Phlebovirus Gn cytoplasmic tail.
The predicted N and RdRp interaction domains of the Gn cytoplasmic tail are defined. Invariant residues are show in white with red background, consensus residues are shown in red with white background, and variable residues are show in black with white background.

Bibliography

1. Garten RJ, *et al.* (2009) Antigenic and genetic characteristics of swine-origin 2009 A(H1N1) influenza viruses circulating in humans. (Translated from eng) *Science (New York, N.Y* 325(5937):197-201 (in eng).
2. Smith GJ, *et al.* (2009) Origins and evolutionary genomics of the 2009 swine-origin H1N1 influenza A epidemic. (Translated from eng) *Nature* 459(7250):1122-1125 (in eng).
3. Sall AA, *et al.* (1999) Genetic reassortment of Rift Valley fever virus in nature. (Translated from eng) *J Virol* 73(10):8196-8200 (in eng).
4. Bird BH, Khristova ML, Rollin PE, Ksiazek TG, & Nichol ST (2007) Complete genome analysis of 33 ecologically and biologically diverse Rift Valley fever virus strains reveals widespread virus movement and low genetic diversity due to recent common ancestry. (Translated from eng) *J Virol* 81(6):2805-2816 (in eng).
5. Rodriguez LL, Owens JH, Peters CJ, & Nichol ST (1998) Genetic reassortment among viruses causing hantavirus pulmonary syndrome. (Translated from eng) *Virology* 242(1):99-106 (in eng).
6. Bird BH, *et al.* (2008) Multiple virus lineages sharing recent common ancestry were associated with a Large Rift Valley fever outbreak among livestock in Kenya during 2006-2007. (Translated from eng) *J Virol* 82(22):11152-11166 (in eng).
7. Hewson R, *et al.* (2004) Evidence of segment reassortment in Crimean-Congo haemorrhagic fever virus. (Translated from eng) *J Gen Virol* 85(Pt 10):3059-3070 (in eng).
8. Reese SM, *et al.* (2008) Potential for La Crosse virus segment reassortment in nature. (Translated from eng) *Virol J* 5:164 (in eng).
9. Razzauti M, Plyusnina A, Sironen T, Henttonen H, & Plyusnin A (2009) Analysis of Puumala hantavirus in a bank vole population in northern Finland: evidence for co-circulation of two genetic lineages and frequent reassortment between strains. (Translated from eng) *J Gen Virol* 90(Pt 8):1923-1931 (in eng).
10. Bowen MD, *et al.* (2001) A reassortant bunyavirus isolated from acute hemorrhagic fever cases in Kenya and Somalia. (Translated from eng) *Virology* 291(2):185-190 (in eng).
11. Briese T, Bird B, Kapoor V, Nichol ST, & Lipkin WI (2006) Batai and Ngari viruses: M segment reassortment and association with severe febrile disease outbreaks in East Africa. (Translated from eng) *J Virol* 80(11):5627-5630 (in eng).
12. Briese T, Kapoor V, & Lipkin WI (2007) Natural M-segment reassortment in Potosi and Main Drain viruses: implications for the evolution of orthobunyaviruses. (Translated from eng) *Arch Virol* 152(12):2237-2247 (in eng).

13. Borucki MK, Chandler LJ, Parker BM, Blair CD, & Beaty BJ (1999) Bunyavirus superinfection and segment reassortment in transovarially infected mosquitoes. (Translated from eng) *J Gen Virol* 80:3173-3179 (in eng).
14. Beaty BJ, Sundin DR, Chandler LJ, & Bishop DH (1985) Evolution of bunyaviruses by genome reassortment in dually infected mosquitoes (Aedes triseriatus). (Translated from eng) *Science (New York, N.Y* 230(4725):548-550 (in eng).
15. Chandler LJ, *et al.* (1991) Reassortment of La Crosse and Tahyna bunyaviruses in Aedes triseriatus mosquitoes. (Translated from eng) *Virus research* 20(2):181-191 (in eng).
16. Rizvanov AA, Khaiboullina SF, & St Jeor S (2004) Development of reassortant viruses between pathogenic hantavirus strains. (Translated from eng) *Virology* 327(2):225-232 (in eng).
17. Yanase T, *et al.* (2006) Genetic characterization of Batai virus indicates a genomic reassortment between orthobunyaviruses in nature. (Translated from eng) *Arch Virol* 151(11):2253-2260 (in eng).
18. Rozhon EJ, Gensemer P, Shope RE, & Bishop DH (1981) Attenuation of virulence of a bunyavirus involving an L RNA defect and isolation of LAC/SSH/LAC and LAC/SSH/SSH reassortants. (Translated from eng) *Virology* 111(1):125-138 (in eng).
19. Gerrard SR, Li L, Barrett AD, & Nichol ST (2004) Ngari virus is a Bunyamwera virus reassortant that can be associated with large outbreaks of hemorrhagic fever in Africa. (Translated from eng) *J Virol* 78(16):8922-8926 (in eng).
20. Weber F & Elliott RM (2002) Antigenic drift, antigenic shift and interferon antagonists: how bunyaviruses counteract the immune system. *Virus research* 88(1-2):129-136.
21. Gad AM, Hassan AN, & Merdan AI (1989) Transmission of Rift Valley fever virus by different geographic strains of Culex pipiens in Egypt. (Translated from eng) *J Egypt Public Health Assoc* 64(5-6):363-379 (in eng).
22. Turell MJ, *et al.* (1996) Vector competence of Egyptian mosquitoes for Rift Valley fever virus. (Translated from eng) *The American journal of tropical medicine and hygiene* 54(2):136-139 (in eng).
23. Rodhain F (1995) Aedes albopictus: a potential problem in France. (Translated from eng) *Parassitologia* 37(2-3):115-119 (in eng).
24. Gargan TP, 2nd, Clark GG, Dohm DJ, Turell MJ, & Bailey CL (1988) Vector potential of selected North American mosquito species for Rift Valley fever virus. (Translated from eng) *The American journal of tropical medicine and hygiene* 38(2):440-446 (in eng).
25. Jup PG, *et al.* (2002) The 2000 epidemic of Rift Valley fever in Saudi Arabia: mosquito vector studies. (Translated from eng) *Med Vet Entomol* 16(3):245-252 (in eng).
26. Jupp PG & Cornel AJ (1988) Vector competence tests with Rift Valley fever virus and five South African species of mosquito. (Translated from eng) *J Am Mosq Control Assoc* 4(1):4-8 (in eng).
27. Meegan JM, Khalil GM, Hoogstraal H, & Adham FK (1980) Experimental transmission and field isolation studies implicating Culex pipiens as a vector of

Rift Valley fever virus in Egypt. (Translated from eng) *The American journal of tropical medicine and hygiene* 29(6):1405-1410 (in eng).
28. Turell MJ & Kay BH (1998) Susceptibility of selected strains of Australian mosquitoes (Diptera: Culicidae) to Rift Valley fever virus. (Translated from eng) *J Med Entomol* 35(2):132-135 (in eng).
29. Meegan JM (1979) The Rift Valley fever epizootic in Egypt 1977-78. 1. Description of the epizzotic and virological studies. *Trans R Soc Trop Med Hyg* 73(6):618-623.
30. Meegan JM & Bailey CL (1988) Rift Valley Fever. *Arboviruses epidemiology and ecology*, ed Monath TP (CRC Press, Boca Raton), Vol 4, pp 51-76.
31. Philippe B, *et al.* (1989) Hemorrhagic forms of Rift Valley fever in Mauritania. *Bull Soc Pathol Exot Filiales* 82(5):611-619.
32. Meegan JM, Hoogstraal H, & Moussa MI (1979) An epizootic of Rift Valley fever in Egypt in 1977. *Vet Rec* 105(6):124-125.
33. Hoogstraal H, Meegan JM, Khalil GM, & Adham FK (1979) The Rift Valley fever epizootic in Egypt 1977-78. 2. Ecological and entomological studies. (Translated from eng) *Trans R Soc Trop Med Hyg* 73(6):624-629 (in eng).
34. Schmaljohn CS & Hooper JW (2001) Bunyaviridae: the viruses and their replication. *Fields Virology*, eds Fields BN, Knipe DM, Howley PM, & Griffin DE (Lippincott, Williams & Wilkins, Philadelphia, PA), 4th Ed, pp 1581-1602.
35. Nichol ST (2001) Bunyaviruses. *Fields Virology*, eds Fields BN, Knipe DM, Howley PM, & Griffin DE (Lippincott, Williams & Wilkins, Philadelphia, PA), 4th Ed, pp 1603-1633.
36. Bouloy M & Flick R (2009) Reverse genetics technology for Rift Valley fever virus: current and future applications for the development of therapeutics and vaccines. (Translated from eng) *Antiviral Res* 84(2):101-118 (in eng).
37. Abdel-Wahab KS, *et al.* (1978) Rift Valley Fever virus infections in Egypt: Pathological and virological findings in man. (Translated from eng) *Trans R Soc Trop Med Hyg* 72(4):392-396 (in eng).
38. Daubney R, Hudson JR, & Garnham PC (1931) Enzootic hepatitis or Rift Valley fever: An undescribed disease of sheep, cattle and man from East Africa. *Journal of Pathology and Bacteriology* 34:545-579.
39. Bray M & Huggins J (1998) Antiviral therapy of haemorrhagic fevers and arbovirus infections. *Antiviral Therapy* 3:53-79.
40. Schmaljohn CS & Nichol ST (2007) Bunyaviridae. *Fields Virology*, eds Knipe DM & Howley PM (Walters Kluwer-Lippincott Williams and Wilkins, Philadelphia), Fifth Ed Vol 2, pp 1741-1789.
41. Gauliard N, Billecocq A, Flick R, & Bouloy M (2006) Rift Valley fever virus noncoding regions of L, M and S segments regulate RNA synthesis. (Translated from eng) *Virology* 351(1):170-179 (in eng).
42. Ikegami T, Won S, Peters CJ, & Makino S (2007) Characterization of Rift Valley fever virus transcriptional terminations. (Translated from eng) *J Virol* 81(16):8421-8438 (in eng).
43. Won S, Ikegami T, Peters CJ, & Makino S (2007) NSm protein of Rift Valley fever virus suppresses virus-induced apoptosis. (Translated from eng) *J Virol* 81(24):13335-13345 (in eng).

44. Le May N, *et al.* (2004) TFIIH transcription factor, a target for the Rift Valley hemorrhagic fever virus. (Translated from eng) *Cell* 116(4):541-550 (in eng).
45. Le May N, *et al.* (2008) A SAP30 complex inhibits IFN-beta expression in Rift Valley fever virus infected cells. (Translated from eng) *PLoS Pathog* 4(1):e13 (in eng).
46. Ikegami T, *et al.* (2009) Rift Valley fever virus NSs protein promotes post-transcriptional downregulation of protein kinase PKR and inhibits eIF2alpha phosphorylation. *PLoS pathogens* 5(2):e1000287.
47. Ikegami T, Won S, Peters CJ, & Makino S (2006) Rescue of infectious rift valley fever virus entirely from cDNA, analysis of virus lacking the NSs gene, and expression of a foreign gene. (Translated from eng) *J Virol* 80(6):2933-2940 (in eng).
48. Won S, Ikegami T, Peters CJ, & Makino S (2006) NSm and 78-kilodalton proteins of Rift Valley fever virus are nonessential for viral replication in cell culture. (Translated from eng) *J Virol* 80(16):8274-8278 (in eng).
49. Gerrard SR & Nichol ST (2007) Synthesis, proteolytic processing and complex formation of N-terminally nested precursor proteins of the Rift Valley fever virus glycoproteins. (Translated from eng) *Virology* 357(2):124-133 (in eng).
50. Gerrard SR & Nichol ST (2002) Characterization of the Golgi retention motif of Rift Valley fever virus G_N glycoprotein. (Translated from eng) *J Virol* 76(23):12200-12210 (in eng).
51. Jupp PG, *et al.* (2002) The 2000 epidemic of Rift Valley fever in Saudi Arabia: mosquito vector studies. *Med Vet Entomol* 16(3):245-252.
52. Shoemaker T, *et al.* (2002) Genetic analysis of viruses associated with emergence of Rift Valley fever in Saudi Arabia and Yemen, 2000-01. (Translated from eng) *Emerg Infect Dis* 8(12):1415-1420 (in eng).
53. Madani TA, *et al.* (2003) Rift Valley fever epidemic in Saudi Arabia: epidemiological, clinical, and laboratory characteristics. *Clinical infectious diseases : an official publication of the Infectious Diseases Society of America* 37(8):1084-1092.
54. Gerrard SR, Bird BH, Albarino CG, & Nichol ST (2007) The NSm proteins of Rift Valley fever virus are dispensable for maturation, replication and infection. (Translated from eng) *Virology* 359(2):459-465 (in eng).
55. Kohl A, Lowen AC, Leonard VH, & Elliott RM (2006) Genetic elements regulating packaging of the Bunyamwera orthobunyavirus genome. (Translated from eng) *J Gen Virol* 87(Pt 1):177-187 (in eng).
56. Flick K, *et al.* (2004) Functional analysis of the noncoding regions of the Uukuniemi virus (Bunyaviridae) RNA segments. (Translated from eng) *J Virol* 78(21):11726-11738 (in eng).
57. Lopez N, Muller R, Prehaud C, & Bouloy M (1995) The L protein of Rift Valley fever virus can rescue viral ribonucleoproteins and transcribe synthetic genome-like RNA molecules. (Translated from eng) *J Virol* 69(7):3972-3979 (in eng).
58. Wasmoen TL, Kakach LT, & Collett MS (1988) Rift Valley fever virus M segment: cellular localization of M segment-encoded proteins. (Translated from eng) *Virology* 166(1):275-280 (in eng).

59. Keegan K & Collett MS (1986) Use of bacterial expression cloning to define the amino acid sequences of antigenic determinants on the G2 glycoprotein of Rift Valley fever virus. (Translated from eng) *J Virol* 58(2):263-270 (in eng).
60. Kirsi JJ, *et al.* (1983) Broad-spectrum antiviral activity of 2-beta-D-ribofuranosylselenazole-4-carboxamide, a new antiviral agent. (Translated from eng) *Antimicrob Agents Chemother* 24(3):353-361 (in eng).
61. Peters CJ, Reynolds JA, Slone TW, Jones DE, & Stephen EL (1986) Prophylaxis of Rift Valley fever with antiviral drugs, immune serum, an interferon inducer, and a macrophage activator. (Translated from eng) *Antiviral Res* 6(5):285-297 (in eng).
62. Canonico PG (1985) Efficacy, toxicology and clinical applications of ribavirin against virulent RNA viral infections. (Translated from eng) *Antiviral Res* Suppl 1:75-81 (in eng).
63. Canonico PG, Kende M, Luscri BJ, & Huggins JW (1984) In-vivo activity of antivirals against exotic RNA viral infections. (Translated from eng) *J Antimicrob Chemother* 14 Suppl A:27-41 (in eng).
64. Habjan M, *et al.* (2009) NSs protein of Rift Valley Fever Virus induces the specific degradation of the double-stranded RNA-dependent protein kinase (PKR). *J Virol* (Journal Article).
65. Leyssen P, Balzarini J, De Clercq E, & Neyts J (2005) The predominant mechanism by which ribavirin exerts its antiviral activity in vitro against flaviviruses and paramyxoviruses is mediated by inhibition of IMP dehydrogenase. (Translated from eng) *J Virol* 79(3):1943-1947 (in eng).
66. Graci JD & Cameron CE (2006) Mechanisms of action of ribavirin against distinct viruses. *Reviews in medical virology* 16(1):37-48.
67. Crotty S, Cameron C, & Andino R (2002) Ribavirin's antiviral mechanism of action: lethal mutagenesis? (Translated from eng) *J Mol Med* 80(2):86-95 (in eng).
68. Sobell HM (1985) Actinomycin and DNA transcription. *Proceedings of the National Academy of Sciences of the United States of America* 82(16):5328-5331.
69. Caliguri LA & Tamm I (1973) Guanidine and 2-(a-hydroxybenzyl)-benzimidazole (HBB): Selective inhibitors of picornavirus multiplication. *Selective inhibitors of viral functions*, ed Carter WA (CRC Press, Cleveland), pp 257--293.
70. Murray KE & Nibert ML (2007) Guanidine hydrochloride inhibits mammalian orthoreovirus growth by reversibly blocking the synthesis of double-stranded RNA. *J Virol* 81(9):4572-4584.
71. Allison AC & Eugui EM (2000) Mycophenolate mofetil and its mechanisms of action. *Immunopharmacology* 47(2-3):85-118.
72. Ausubel FM (1994) *Current protocols in molecular biology* (John Wiley & Sons, New York).
73. Liu L, Celma CC, & Roy P (2008) Rift Valley fever virus structural proteins: expression, characterization and assembly of recombinant proteins. (Translated from eng) *Virol J* 5:82 (in eng).

74. Filone CM, Heise M, Doms RW, & Bertolotti-Ciarlet A (2006) Development and characterization of a Rift Valley fever virus cell-cell fusion assay using alphavirus replicon vectors. (Translated from eng) *Virology* 356(1-2):155-164 (in eng).
75. Flint SJ, Enquist LW, Racaniello VR, & Skalka AM (2004) Structure. *Principles of virology : molecular biology, pathogenesis, and control of animal viruses*, (ASM Press, Washington, D.C.), 2 Ed, pp 83-125.
76. Mohl BP & Barr JN (2009) Investigating the specificity and stoichiometry of RNA binding by the nucleocapsid protein of Bunyamwera virus. (Translated from eng) *RNA* 15(3):391-399 (in eng).
77. Gott P, Stohwasser R, Schnitzler P, Darai G, & Bautz EK (1993) RNA binding of recombinant nucleocapsid proteins of hantaviruses. *Virology* 194(1):332-337.
78. Osborne JC & Elliott RM (2000) RNA binding properties of bunyamwera virus nucleocapsid protein and selective binding to an element in the 5' terminus of the negative-sense S segment. (Translated from eng) *J Virol* 74(21):9946-9952 (in eng).
79. Mir MA, Brown B, Hjelle B, Duran WA, & Panganiban AT (2006) Hantavirus N protein exhibits genus-specific recognition of the viral RNA panhandle. (Translated from eng) *J Virol* 80(22):11283-11292 (in eng).
80. Severson W, Partin L, Schmaljohn CS, & Jonsson CB (1999) Characterization of the Hantaan nucleocapsid protein-ribonucleic acid interaction. *J Biol Chem* 274(47):33732-33739.
81. Severson WE, Xu X, & Jonsson CB (2001) cis-Acting signals in encapsidation of Hantaan virus S-segment viral genomic RNA by its N protein. *J Virol* 75(6):2646-2652.
82. Ogg MM & Patterson JL (2007) RNA binding domain of Jamestown Canyon virus S segment RNAs. *J Virol* 81(24):13754-13760.
83. Mir MA & Panganiban AT (2005) The hantavirus nucleocapsid protein recognizes specific features of the viral RNA panhandle and is altered in conformation upon RNA binding. *J Virol* 79(3):1824-1835.
84. Falk BW & Tsai JH (1998) Biology and molecular biology of viruses in the genus Tenuivirus. *Annual Review of Phytopathology* 36(Journal Article):139-163.
85. Jin H & Elliott RM (1993) Characterization of Bunyamwera virus S RNA that is transcribed and replicated by the L protein expressed from recombinant vaccinia virus. (Translated from eng) *J Virol* 67(3):1396-1404 (in eng).
86. Overby AK, Pettersson RF, & Neve EP (2007) The glycoprotein cytoplasmic tail of Uukuniemi virus (Bunyaviridae) interacts with ribonucleoproteins and is critical for genome packaging. (Translated from eng) *J Virol* 81(7):3198-3205 (in eng).
87. Ye Q, Krug RM, & Tao YJ (2006) The mechanism by which influenza A virus nucleoprotein forms oligomers and binds RNA. (Translated from eng) *Nature* 444(7122):1078-1082 (in eng).
88. Albertini AA, *et al.* (2006) Crystal structure of the rabies virus nucleoprotein-RNA complex. (Translated from eng) *Science (New York, N.Y* 313(5785):360-363 (in eng).

89. Tawar RG, *et al.* (2009) Crystal Structure of a Nucleocapsid-Like Nucleoprotein-RNA Complex of Respiratory Syncytial Virus. *Science (New York, N.Y* 326(5957):1279-1283.
90. Green TJ, Zhang X, Wertz GW, & Luo M (2006) Structure of the vesicular stomatitis virus nucleoprotein-RNA complex. (Translated from eng) *Science (New York, N.Y* 313(5785):357-360 (in eng).
91. Rudolph MG, *et al.* (2003) Crystal structure of the borna disease virus nucleoprotein. (Translated from eng) *Structure* 11(10):1219-1226 (in eng).
92. Coloma R, *et al.* (2009) The structure of a biologically active influenza virus ribonucleoprotein complex. (Translated from eng) *PLoS Pathog* 5(6):e1000491 (in eng).
93. von Bonsdorff CH, Saikku P, & Oker-Blom N (1969) The inner structure of Uukuniemi and two Bunyamwera supergroup arboviruses. (Translated from eng) *Virology* 39(2):342-344 (in eng).
94. Pettersson RF & von Bonsdorff CH (1975) Ribonucleoproteins of Uukuniemi virus are circular. (Translated from eng) *J Virol* 15(2):386-392 (in eng).
95. Marenchino M, Armbruster DW, & Hennig M (2009) Rapid and efficient purification of RNA-binding proteins: application to HIV-1 Rev. (Translated from eng) *Protein Expr Purif* 63(2):112-119 (in eng).
96. Holm L & Sander C (1995) Dali: a network tool for protein structure comparison. (Translated from eng) *Trends Biochem Sci* 20(11):478-480 (in eng).
97. Gibrat JF, Madej T, & Bryant SH (1996) Surprising similarities in structure comparison. (Translated from eng) *Curr Opin Struct Biol* 6(3):377-385 (in eng).
98. Le May N, Gauliard N, Billecocq A, & Bouloy M (2005) The N terminus of Rift Valley fever virus nucleoprotein is essential for dimerization. (Translated from eng) *J Virol* 79(18):11974-11980 (in eng).
99. Raju R & Kolakofsky D (1989) The ends of La Crosse virus genome and antigenome RNAs within nucleocapsids are base paired. (Translated from eng) *J Virol* 63(1):122-128 (in eng).
100. Pettersson RF & Melin L (1996) Synthesis, assembly, and intracellular transport of Bunyaviridae membrane proteins. *The Bunyaviridae*, ed Elliott RMPlenum, New York), pp 159-188.
101. Kuismanen E, Hedman K, Saraste J, & Pettersson RF (1982) Uukuniemi virus maturation: accumulation of virus particles and viral antigens in the Golgi complex. (Translated from eng) *Mol Cell Biol* 2(11):1444-1458 (in eng).
102. Overby AK, Popov VL, Pettersson RF, & Neve EP (2007) The cytoplasmic tails of Uukuniemi Virus (Bunyaviridae) G_N and G_C glycoproteins are important for intracellular targeting and the budding of virus-like particles. (Translated from eng) *J Virol* 81(20):11381-11391 (in eng).
103. Rubach JK, *et al.* (2009) Characterization of purified Sindbis virus nsP4 RNA-dependent RNA polymerase activity in vitro. (Translated from eng) *Virology* 384(1):201-208 (in eng).
104. Reverter D & Lima CD (2004) A basis for SUMO protease specificity provided by analysis of human Senp2 and a Senp2-SUMO complex. (Translated from eng) *Structure* 12(8):1519-1531 (in eng).

105. Otwinowski Z & Minor W (1997) Processing of X-ray diffraction data collected in oscillation mode. (Translated from English) *Meth Enzymol* 276:307-326 (in English).
106. Leslie AG (2006) The integration of macromolecular diffraction data. (Translated from eng) *Acta Crystallogr D Biol Crystallogr* 62(Pt 1):48-57 (in eng).
107. Terwilliger TC & Berendzen J (1999) Automated MAD and MIR structure solution. (Translated from eng) *Acta Crystallogr D Biol Crystallogr* 55(Pt 4):849-861 (in eng).
108. Terwilliger TC (2003) Automated main-chain model building by template matching and iterative fragment extension. (Translated from eng) *Acta Crystallogr D Biol Crystallogr* 59(Pt 1):38-44 (in eng).
109. Adams PD, *et al.* (2002) PHENIX: building new software for automated crystallographic structure determination. (Translated from eng) *Acta Crystallogr D Biol Crystallogr* 58(Pt 11):1948-1954 (in eng).
110. Emsley P & Cowtan K (2004) Coot: model-building tools for molecular graphics. (Translated from eng) *Acta Crystallogr D Biol Crystallogr* 60(Pt 12 Pt 1):2126-2132 (in eng).
111. Murshudov GN, Vagin AA, & Dodson EJ (1997) Refinement of macromolecular structures by the maximum-likelihood method. (Translated from eng) *Acta Crystallogr D Biol Crystallogr* 53(Pt 3):240-255 (in eng).
112. Collaborative Computational Project N (1994) The CCP4 suite: programs for protein crystallography. (Translated from eng) *Acta Crystallogr D Biol Crystallogr* 50(Pt 5):760-763 (in eng).
113. Davis IW, *et al.* (2007) MolProbity: all-atom contacts and structure validation for proteins and nucleic acids. (Translated from eng) *Nucleic Acids Res* 35(Web Server issue):W375-383 (in eng).
114. Delano WL (2007) The PyMOL Molecular Graphics System (DeLano Scientific LLC, USA).
115. Thompson JD, Gibson TJ, & Higgins DG (2002) Multiple sequence alignment using ClustalW and ClustalX. (Translated from eng) *Curr Protoc Bioinformatics* Chapter 2:Unit 2 3 (in eng).
116. Baker NA, Sept D, Joseph S, Holst MJ, & McCammon JA (2001) Electrostatics of nanosystems: application to microtubules and the ribosome. (Translated from eng) *Proc Natl Acad Sci U S A* 98(18):10037-10041 (in eng).
117. Gouet P, Robert X, & Courcelle E (2003) ESPript/ENDscript: Extracting and rendering sequence and 3D information from atomic structures of proteins. (Translated from eng) *Nucleic Acids Res* 31(13):3320-3323 (in eng).
118. Rai BK & Fiser A (2006) Multiple mapping method: a novel approach to the sequence-to-structure alignment problem in comparative protein structure modeling. (Translated from eng) *Proteins* 63(3):644-661 (in eng).
119. Landau M, *et al.* (2005) ConSurf 2005: the projection of evolutionary conservation scores of residues on protein structures. (Translated from eng) *Nucleic Acids Res* 33(Web Server issue):W299-302 (in eng).
120. Philippe B, *et al.* (1989) [Hemorrhagic forms of Rift Valley fever in Mauritania]. (Translated from fre) *Bull Soc Pathol Exot Filiales* 82(5):611-619 (in fre).

121. Bird BH, Albarino CG, & Nichol ST (2007) Rift Valley fever virus lacking NSm proteins retains high virulence in vivo and may provide a model of human delayed onset neurologic disease. (Translated from eng) *Virology* 362(1):10-15 (in eng).
122. Schmaljohn CS & Hooper JW (2001) Bunyaviridae: The Viruses and Their Replication. *Fields Virology*, eds Knipe DM & Howley PM (Lippincoott Williams and Wilkins, Philadelphia), Fourth Ed Vol 2, pp 1581-1602.
123. Gerrard SR & Nichol ST (2002) Characterization of the Golgi retention motif of Rift Valley fever virus G(N) glycoprotein. (Translated from eng) *J Virol* 76(23):12200-12210 (in eng).
124. Kakach LT, Suzich JA, & Collett MS (1989) Rift Valley fever virus M segment: phlebovirus expression strategy and protein glycosylation. (Translated from eng) *Virology* 170(2):505-510 (in eng).
125. Suzich JA, Kakach LT, & Collett MS (1990) Expression strategy of a phlebovirus: biogenesis of proteins from the Rift Valley fever virus M segment. (Translated from eng) *J Virol* 64(4):1549-1555 (in eng).
126. Jin H & Elliott RM (1992) Mutagenesis of the L protein encoded by Bunyamwera virus and production of monospecific antibodies. (Translated from eng) *J Gen Virol* 73 (Pt 9):2235-2244 (in eng).
127. Ribeiro D, Borst JW, Goldbach R, & Kormelink R (2009) Tomato spotted wilt virus nucleocapsid protein interacts with both viral glycoproteins Gn and Gc in planta. (Translated from eng) *Virology* 383(1):121-130 (in eng).
128. Frese M, Kochs G, Feldmann H, Hertkorn C, & Haller O (1996) Inhibition of bunyaviruses, phleboviruses, and hantaviruses by human MxA protein. (Translated from eng) *J Virol* 70(2):915-923 (in eng).
129. Ravkov EV & Compans RW (2001) Hantavirus nucleocapsid protein is expressed as a membrane-associated protein in the perinuclear region. (Translated from eng) *J Virol* 75(4):1808-1815 (in eng).
130. Ramanathan HN, *et al.* (2007) Dynein-dependent transport of the hantaan virus nucleocapsid protein to the endoplasmic reticulum-Golgi intermediate compartment. (Translated from eng) *J Virol* 81(16):8634-8647 (in eng).
131. Shi X, Brauburger K, & Elliott RM (2005) Role of N-linked glycans on bunyamwera virus glycoproteins in intracellular trafficking, protein folding, and virus infectivity. (Translated from eng) *J Virol* 79(21):13725-13734 (in eng).
132. Shi X, Kohl A, Li P, & Elliott RM (2007) Role of the cytoplasmic tail domains of Bunyamwera orthobunyavirus glycoproteins Gn and Gc in virus assembly and morphogenesis. (Translated from eng) *J Virol* 81(18):10151-10160 (in eng).
133. Habjan M, *et al.* (2009) Efficient production of Rift Valley fever virus-like particles: The antiviral protein MxA can inhibit primary transcription of bunyaviruses. (Translated from eng) *Virology* 385(2):400-408 (in eng).
134. Deng MY, Day SP, & Cliver DO (1994) Detection of hepatitis A virus in environmental samples by antigen-capture PCR. (Translated from eng) *Appl Environ Microbiol* 60(6):1927-1933 (in eng).
135. Mohamadzadeh M, *et al.* (2006) Activation of triggering receptor expressed on myeloid cells-1 on human neutrophils by marburg and ebola viruses. (Translated from eng) *J Virol* 80(14):7235-7244 (in eng).

136. Wengler G (1989) Cell-associated West Nile flavivirus is covered with E+pre-M protein heterodimers which are destroyed and reorganized by proteolytic cleavage during virus release. (Translated from eng) *J Virol* 63(6):2521-2526 (in eng).
137. Flint SJ EL, Racaniello VR, Skalka AM (2004) *Principles of virology : molecular biology, pathogenesis, and control of animal viruses* (ASM Press, Washington, D.C.) 2 Ed.
138. Lowen AC, Boyd A, Fazakerley JK, & Elliott RM (2005) Attenuation of bunyavirus replication by rearrangement of viral coding and noncoding sequences. (Translated from eng) *J Virol* 79(11):6940-6946 (in eng).
139. Pantua HD, McGinnes LW, Peeples ME, & Morrison TG (2006) Requirements for the assembly and release of Newcastle disease virus-like particles. (Translated from eng) *J Virol* 80(22):11062-11073 (in eng).
140. Noda T, *et al.* (2006) Assembly and budding of Ebolavirus. (Translated from eng) *PLoS Pathog* 2(9):e99 (in eng).
141. Gomez-Puertas P, Albo C, Perez-Pastrana E, Vivo A, & Portela A (2000) Influenza virus matrix protein is the major driving force in virus budding. (Translated from eng) *J Virol* 74(24):11538-11547 (in eng).
142. Nayak DP, Hui EK, & Barman S (2004) Assembly and budding of influenza virus. (Translated from eng) *Virus research* 106(2):147-165 (in eng).
143. Sugahara F, *et al.* (2004) Paramyxovirus Sendai virus-like particle formation by expression of multiple viral proteins and acceleration of its release by C protein. (Translated from eng) *Virology* 325(1):1-10 (in eng).
144. Irie T, Shimazu Y, Yoshida T, & Sakaguchi T (2007) The YLDL sequence within Sendai virus M protein is critical for budding of virus-like particles and interacts with Alix/AIP1 independently of C protein. (Translated from eng) *J Virol* 81(5):2263-2273 (in eng).
145. Coronel EC, Murti KG, Takimoto T, & Portner A (1999) Human parainfluenza virus type 1 matrix and nucleoprotein genes transiently expressed in mammalian cells induce the release of virus-like particles containing nucleocapsid-like structures. (Translated from eng) *J Virol* 73(8):7035-7038 (in eng).
146. Ciancanelli MJ & Basler CF (2006) Mutation of YMYL in the Nipah virus matrix protein abrogates budding and alters subcellular localization. (Translated from eng) *J Virol* 80(24):12070-12078 (in eng).
147. Pohl C, Duprex WP, Krohne G, Rima BK, & Schneider-Schaulies S (2007) Measles virus M and F proteins associate with detergent-resistant membrane fractions and promote formation of virus-like particles. (Translated from eng) *J Gen Virol* 88(Pt 4):1243-1250 (in eng).
148. Iwasaki M, *et al.* (2009) The matrix protein of measles virus regulates viral RNA synthesis and assembly by interacting with the nucleocapsid protein. (Translated from eng) *J Virol* 83(20):10374-10383 (in eng).
149. Li M, *et al.* (2009) Mumps virus matrix, fusion, and nucleocapsid proteins cooperate for efficient production of virus-like particles. (Translated from eng) *J Virol* 83(14):7261-7272 (in eng).
150. Jayakar HR, Jeetendra E, & Whitt MA (2004) Rhabdovirus assembly and budding. (Translated from eng) *Virus Res* 106(2):117-132 (in eng).

151. Hartlieb B & Weissenhorn W (2006) Filovirus assembly and budding. (Translated from eng) *Virology* 344(1):64-70 (in eng).
152. Swenson DL, *et al.* (2004) Generation of Marburg virus-like particles by co-expression of glycoprotein and matrix protein. (Translated from eng) *FEMS Immunol Med Microbiol* 40(1):27-31 (in eng).
153. Kukkonen SK, Vaheri A, & Plyusnin A (2004) Tula hantavirus L protein is a 250 kDa perinuclear membrane-associated protein. (Translated from eng) *J Gen Virol* 85(Pt 5):1181-1189 (in eng).
154. Besselaar TG & Blackburn NK (1992) The synergistic neutralization of Rift Valley fever virus by monoclonal antibodies to the envelope glycoproteins. (Translated from eng) *Arch Virol* 125(1-4):239-250 (in eng).
155. Garry CE & Garry RF (2004) Proteomics computational analyses suggest that the carboxyl terminal glycoproteins of Bunyaviruses are class II viral fusion protein (beta-penetrenes). (Translated from eng) *Theor Biol Med Model* 1:10 (in eng).
156. Plassmeyer ML, Soldan SS, Stachelek KM, Martin-Garcia J, & Gonzalez-Scarano F (2005) California serogroup Gc (G1) glycoprotein is the principal determinant of pH-dependent cell fusion and entry. (Translated from eng) *Virology* 338(1):121-132 (in eng).
157. Plassmeyer ML, *et al.* (2007) Mutagenesis of the La Crosse Virus glycoprotein supports a role for Gc (1066-1087) as the fusion peptide. (Translated from eng) *Virology* 358(2):273-282 (in eng).
158. Shi X, Goli J, Clark G, Brauburger K, & Elliott RM (2009) Functional analysis of the Bunyamwera orthobunyavirus Gc glycoprotein. (Translated from eng) *J Gen Virol* 90(Pt 10):2483-2492 (in eng).
159. Hoenen T, *et al.* (2006) Infection of naive target cells with virus-like particles: implications for the function of ebola virus VP24. (Translated from eng) *J Virol* 80(14):7260-7264 (in eng).
160. Nugent CI, Johnson KL, Sarnow P, & Kirkegaard K (1999) Functional coupling between replication and packaging of poliovirus replicon RNA. (Translated from eng) *J Virol* 73(1):427-435 (in eng).
161. Venter PA, Krishna NK, & Schneemann A (2005) Capsid protein synthesis from replicating RNA directs specific packaging of the genome of a multipartite, positive-strand RNA virus. (Translated from eng) *J Virol* 79(10):6239-6248 (in eng).
162. Venter PA & Schneemann A (2007) Assembly of two independent populations of flock house virus particles with distinct RNA packaging characteristics in the same cell. (Translated from eng) *J Virol* 81(2):613-619 (in eng).
163. Beaty BJ & Calisher CH (1991) Bunyaviridae--natural history. (Translated from eng) *Curr Top Microbiol Immunol* 169:27-78 (in eng).
164. Accardi L, *et al.* (2001) Activity of Toscana and Rift Valley fever virus transcription complexes on heterologous templates. (Translated from eng) *J Gen Virol* 82(Pt 4):781-785 (in eng).
165. Piper ME & Gerrard SR (2010) A Novel System for Identification of Inhibitors of Rift Valley Fever Virus Replication. *Viruses* 2(3):731-747.

166. Kolakofsky D, Le Mercier P, Iseni F, & Garcin D (2004) Viral DNA polymerase scanning and the gymnastics of Sendai virus RNA synthesis. (Translated from eng) *Virology* 318(2):463-473 (in eng).
167. Curran J & Kolakofsky D (2008) Nonsegmented negative-strand RNA virus RNA synthesis in vivo. (Translated from eng) *Virology* 371(2):227-230 (in eng).
168. Schoehn G, Iseni F, Mavrakis M, Blondel D, & Ruigrok RW (2001) Structure of recombinant rabies virus nucleoprotein-RNA complex and identification of the phosphoprotein binding site. (Translated from eng) *J Virol* 75(1):490-498 (in eng).
169. Murray J, Loney C, Murphy LB, Graham S, & Yeo RP (2001) Characterization of monoclonal antibodies raised against recombinant respiratory syncytial virus nucleocapsid (N) protein: identification of a region in the carboxy terminus of N involved in the interaction with P protein. (Translated from eng) *Virology* 289(2):252-261 (in eng).
170. Ge P, *et al.* (2010) Cryo-EM model of the bullet-shaped vesicular stomatitis virus. (Translated from eng) *Science (New York, N.Y* 327(5966):689-693 (in eng).
171. Lamb RA & Krug RM (2001) Orthomyxoviridae: the viruses and their replication. *Fields Virology*, eds Knipe DM & Howley PM (Lippincott Williams and Wilkins., Philadelphia, PA), Vol 1, pp 1487–1532.
172. Yuan P, *et al.* (2009) Crystal structure of an avian influenza polymerase PA(N) reveals an endonuclease active site. (Translated from eng) *Nature* 458(7240):909-913 (in eng).
173. Poch O, Blumberg BM, Bougueleret L, & Tordo N (1990) Sequence comparison of five polymerases (L proteins) of unsegmented negative-strand RNA viruses: theoretical assignment of functional domains. (Translated from eng) *J Gen Virol* 71 (Pt 5):1153-1162 (in eng).
174. Lenard J (1999) Host cell protein kinases in nonsegmented negative-strand virus (mononegavirales) infection. (Translated from eng) *Pharmacol Ther* 83(1):39-48 (in eng).
175. Portela A & Digard P (2002) The influenza virus nucleoprotein: a multifunctional RNA-binding protein pivotal to virus replication. (Translated from eng) *J Gen Virol* 83(Pt 4):723-734 (in eng).
176. Mir MA, Duran WA, Hjelle BL, Ye C, & Panganiban AT (2008) Storage of cellular 5' mRNA caps in P bodies for viral cap-snatching. (Translated from eng) *Proc Natl Acad Sci U S A* 105(49):19294-19299 (in eng).
177. Kulkarni M, Ozgur S, & Stoecklin G (2010) On track with P-bodies. (Translated from eng) *Biochem Soc Trans* 38(Pt 1):242-251 (in eng).
178. Serman A, *et al.* (2007) GW body disassembly triggered by siRNAs independently of their silencing activity. (Translated from eng) *Nucleic Acids Res* 35(14):4715-4727 (in eng).
179. Mir MA, Sheema S, Haseeb A, & Haque A (2010) Hantavirus nucleocapsid protein has distinct m7G cap and RNA binding sites. (Translated from Eng) *J Biol Chem* (in Eng).
180. Zamoto-Niikura A, Terasaki K, Ikegami T, Peters CJ, & Makino S (2009) Rift valley fever virus L protein forms a biologically active oligomer. (Translated from eng) *J Virol* 83(24):12779-12789 (in eng).

181. Jorba N, Coloma R, & Ortin J (2009) Genetic trans-complementation establishes a new model for influenza virus RNA transcription and replication. (Translated from eng) *PLoS Pathog* 5(5):e1000462 (in eng).
182. Hunter E (2007) Virus Assembly. *Fields Virology*, eds Knipe DM & Howley PM (Lippincott Williams and Wilkins, Philadelphia), Fifth Ed Vol 1, pp 141-168.
183. Lowen AC & Elliott RM (2005) Mutational analyses of the nonconserved sequences in the Bunyamwera Orthobunyavirus S segment untranslated regions. *J Virol* 79(20):12861-12870.
184. Perez M, Craven RC, & de la Torre JC (2003) The small RING finger protein Z drives arenavirus budding: implications for antiviral strategies. (Translated from eng) *Proc Natl Acad Sci U S A* 100(22):12978-12983 (in eng).
185. Overby AK, Popov V, Neve EP, & Pettersson RF (2006) Generation and analysis of infectious virus-like particles of uukuniemi virus (bunyaviridae): a useful system for studying bunyaviral packaging and budding. (Translated from eng) *J Virol* 80(21):10428-10435 (in eng).